

Electronic Thesis and Dissertation Repository

7-20-2017 12:00 AM

Tensile and Impact Behaviour of Shape Memory Alloy Fibre Reinforced Engineered Cementitious Composites

Mohamed Ali El-Sayed Mahmoud Ali
The University of Western Ontario

Supervisor
Moncef L. Nehdi
The University of Western Ontario

Graduate Program in Civil and Environmental Engineering
A thesis submitted in partial fulfillment of the requirements for the degree in Doctor of Philosophy
© Mohamed Ali El-Sayed Mahmoud Ali 2017

Follow this and additional works at: <https://ir.lib.uwo.ca/etd>



Part of the [Civil Engineering Commons](#)

Recommended Citation

Ali, Mohamed Ali El-Sayed Mahmoud, "Tensile and Impact Behaviour of Shape Memory Alloy Fibre Reinforced Engineered Cementitious Composites" (2017). *Electronic Thesis and Dissertation Repository*. 4650.

<https://ir.lib.uwo.ca/etd/4650>

This Dissertation/Thesis is brought to you for free and open access by Scholarship@Western. It has been accepted for inclusion in Electronic Thesis and Dissertation Repository by an authorized administrator of Scholarship@Western. For more information, please contact wlsadmin@uwo.ca.

Abstract

Extreme loading events such as impact, blast, and earthquakes have often led to partial or total collapse of structures, associated with economic and human life loss. Therefore, civil engineers have been seeking innovative materials and systems that would allow designing resilient and smart structures which can withstand such catastrophic events. Recently, engineered cementitious composites (ECC) and shape memory alloys (SMA) have emerged as strong contenders in the production of smart and resilient structural systems.

The aims of this study are to explore possible synergy between ECC and SMA for developing a novel hybrid fibre-reinforced ECC incorporating randomly dispersed SMA and polyvinyl-alcohol short fibres (HECC-SMAF) with possible strain recovery and superior impact resistance. The mechanical properties of the composite, including uniaxial tensile and strain recovery performance were examined. Moreover, the behaviour of the composite under impact loading was explored using a drop weight impact test. Test specimens were also heat-treated to investigate possible pre-stressing effects of SMA fibres on the impact resistance of the ECC. A two-parameter Weibull distribution was used to analyze variations in experimental results in terms of reliability function. Furthermore, numerical simulation was developed to predict the behaviour of the composite under impact loading.

Results indicate that SMA fibres significantly enhanced the performance of the composite both under static and dynamic loading. Adding fibres beyond a certain dosage led to fibre clustering, thus, no further gain in tensile and impact performance was measured. The impact resistance of HECC-SMAF specimens was further improved after exposure to heat treatment. This highlights the significant contribution imparted by the local pre-stressing effect of SMA fibres to the impact resistance of the composite. The Weibull distribution was adequate to predict the impact failure strength of the new composite, allowing to avert additional costly experiments. Also, numerical simulation predictions of the impact behaviour of the hybrid composite were in good agreement with experimental findings, thus offering a suitable predictive tool and allowing to preclude costly and time-consuming experiments.

This research underscores the potential to engineer new cementitious composites with superior tensile properties and impact resistance for the protection of critical infrastructure in the event of explosive or impact loading.

Keywords

Engineered cementitious composite; fibres; heat treatment; impact loading; numerical simulation; shape memory alloy; strain recovery; toughness; Weibull distribution.

Co-Authorship Statement

This thesis was prepared per the integrated-article layout designated by the Faculty of Graduate Studies at Western University, London, Ontario, Canada. All the work stated in this thesis including experimental testing, data analysis, numerical modeling, and writing draft manuscripts for publication was carried out by the candidate under the supervision and guidance of Dr. Moncef L. Nehdi. Any other co-author (if applicable) assisted in conducting the experimental program and/or revision of the initial draft of the manuscript. The following publications have been either accepted or submitted to peer-reviewed technical journals and international conferences:

- 1) **M.A.E.M. Ali**, A.M. Soliman, and M.L. Nehdi, “Hybrid-Fiber Reinforced Engineered Cementitious Composite under Tensile and Impact Loading.” *Materials and Design*, 117, 2017, pp. 139-149.
- 2) **M.A.E.M. Ali** and M.L. Nehdi, “Innovative Crack-Healing Hybrid Fiber Reinforced Engineered Cementitious Composite.” *Construction and Building Materials*, 150, 2017, 689-702.
- 3) **M.A.E.M. Ali** and M.L. Nehdi, “Exploring Synergy of Engineered Cementitious Composites and Shape Memory Alloys in Creating Resilient Civil Infrastructure.” *Magazine of Concrete Research*, accepted.
- 4) **M.A.E.M. Ali** and M.L. Nehdi, “Tensile and Flexural Behavior of Hybrid Fiber Reinforced Engineered Cementitious Composite with Strain Recovery.” *Composites Part B*, submitted.
- 5) **M.A.E.M. Ali** and M.L. Nehdi, “Experimental and Numerical Investigation on Novel SMA-PVA Hybrid Fiber Reinforced Engineered Cementitious Composite under Impact Loading.” *Cement and Concrete Composites*, submitted.
- 6) **M.A.E.M. Ali** and M.L. Nehdi, “Experimental Investigation on Mechanical Properties of Shape Memory Alloy Fibre-Reinforced ECC Composite.” *Proceedings of the 11th International Conference on Civil and Architecture Engineering*, Cairo, Egypt, 19-21 April, 2016, 11 p.
- 7) **M.A.E.M. Ali**, A.M. Soliman, and M.L. Nehdi, “Behaviour of Hybrid Fibre-Reinforced ECC Composite Incorporating SMA Short Fibres under Effect of Impact

Load.” *Proceedings of the 11th International Conference on Civil and Architecture Engineering*, Cairo, Egypt, 19-21 April, 2016, 11 p.

- 8) **M.A.E.M. Ali** and M.L. Nehdi, “Mechanical Performance of Hybrid Fibre-Reinforced Engineered Cementitious Composite Incorporating NiTi-SMA Short Fibres.” *Resilient Infrastructure, Proceedings of the 5th International Conference of the Canadian Society for Civil Engineering*, London, ON, Canada, 1-4 June, 2016, 8 p.
- 9) **M.A.E.M. Ali**, A.M. Soliman, and M.L. Nehdi, “Impact Behaviour of Shape Memory Alloy Hybrid Fibre-Reinforced Engineered Cementitious Composite.” *Resilient Infrastructure, Proceedings of the 5th International Conference of the Canadian Society for Civil Engineering*, London, ON, Canada, 1-4 June, 2016, 8 p.
- 10) **M.A.E.M. Ali** and M.L. Nehdi, “Effect of Fire Exposure on Impact Resistance of Hybrid Fiber-Reinforced Engineered Cementitious Composites.” *Resilient Infrastructure, Proceedings of the 6th International Conference of the Canadian Society for Civil Engineering*, Vancouver, BC, Canada, 31 May-3 June, 2017, 7 p.

Dedication

To: My Father: Ali Elsayed Mahmoud Ali

My Mother: Sabria Ameen

My Sisters: Neveen, Eman and Rehab

My beloved Wife: Hebatallah

My beloved Children: Malek, Anas, Besan and Elias

Acknowledgments

All thanks are first due to God for providing me such opportunities and capabilities that led me towards the completion of this dissertation.

I would like to state my sincere appreciation and humble thankfulness to my worthy research advisor Prof. Moncef L. Nehdi, for his invaluable guidance, supervision, encouragement, and support throughout this study.

The role of the University Machine Shop in fabricating the impact loading frames is appreciated.

I also would like to thank Mr. Wilbert Logan, supervisor of the Concrete and Structures Laboratory at Western University, for his help and suggestions during the various stages of the experimental work.

Special thanks are due to my friend and fellow researcher Assistant Professor Ahmed M. Soliman for his valuable guidance, and suggestions.

Finally, I would like to thank my father and mother whose prayers paved the way to my success. I would also like to express my deep gratitude and appreciation to my sisters. Furthermore, I would like to acknowledge my wife's support, encouragement, and patience, which played a vital role towards the completion of this study.

Table of Contents

Abstract.....	i
Co-Authorship Statement.....	iii
Dedication.....	v
Acknowledgments.....	vi
Table of Contents.....	vii
List of Tables.....	xii
List of Figures.....	xiv
List of Appendices.....	xxiii
Chapter 1.....	1
1 INTRODUCTION.....	1
1.1 GENERAL.....	1
1.2 RESEARCH SIGNIFICANCE.....	3
1.3 SPECIFIC RESEARCH OBJECTIVES.....	3
1.4 RESEARCH CONTRIBUTIONS.....	4
1.5 THESIS OUTLINE.....	5
1.6 REFERENCES.....	6
Chapter 2.....	8
2 EXPLORING SYNERGY OF ENGINEERED CEMENTITIOUS COMPOSITES AND SHAPE MEMORY ALLOYS IN CREATING RESILIENT CIVIL INFRASTRUCTURE.....	8
2.1 INTRODUCTION.....	8
2.2 GLOBAL MARKET FOR SMART MATERIALS.....	11
2.3 ENGINEERED CEMENTITIOUS COMPOSITES (ECCs).....	12
2.3.1 ECC Production.....	12
2.3.2 Mechanical Properties of ECC.....	13

2.3.3	Engineering Properties of ECC.....	13
2.3.4	Material Modelling of ECC	18
2.3.5	Laboratory Investigations on Small Scale ECC Structural Elements	19
2.3.6	Constraints of Using ECC.....	20
2.4	SHAPE MEMORY ALLOYS (SMA).....	20
2.4.1	SMA Fabrication.....	20
2.4.2	Mechanical Properties of SMA.....	21
2.4.3	Unique Characteristics of SMA	24
2.4.4	Modeling SMA	26
2.4.5	Restrictions on Utilizing SMA.....	28
2.5	FULL SCALE APPLICATIONS OF ECC AND SMA	31
2.6	SMA REINFORCED ECC ELEMENTS	33
2.7	CONCLUSIONS.....	35
2.8	REFERENCES	36
Chapter 3.....		49
3	INNOVATIVE CRACK-HEALING HYBRID FIBRE REINFORCED ENGINEERED CEMENTITIOUS COMPOSITE	49
3.1	INTRODUCTION	49
3.2	EXPERIMENTAL PROGRAM	51
3.2.1	Materials and Mixture Proportions	51
3.2.2	Mixture Preparation, Casting and Curing	52
3.2.3	Test Procedures	53
3.3	RESULTS AND DISCUSSION	56
3.3.1	Workability	56
3.3.2	Compressive Strength	57
3.3.3	Elastic Modulus and Poisson's Ratio.....	58

3.3.4	Splitting Tensile Strength	60
3.3.5	Flexural Behaviour.....	61
3.3.6	Microstructural analysis.....	73
3.4	ANALYSIS OF VARIANCE OF TEST RESULTS	78
3.5	SUMMARY AND CONCLUSIONS	80
3.6	REFERENCES	81
Chapter 4	87
4	TENSILE AND FLEXURAL BEHAVIOUR OF HYBRID FIBRE REINFORCED ENGINEERED CEMENTITIOUS COMPOSITE WITH STRAIN RECOVERY	87
4.1	INTRODUCTION	87
4.2	EXPERIMENTAL PROCEDURES.....	88
4.3	INVERSE ANALYSIS FOR DETERMINING TENSILE PROPERTIES.....	89
4.4	RESULTS AND DISCUSSION	90
4.4.1	Tensile Performance	90
4.4.2	Effect of Porosity	91
4.5	UTT AND FPBT data correlation.....	93
4.6	STATISTICAL ANALYSIS	95
4.6.1	Analysis of Variance of Test Results.....	95
4.6.2	Analysis of fibre dispersion	95
4.7	CONCLUSIONS.....	100
4.8	REFERENCES	100
Chapter 5	104
5	EXPLORING BEHAVIOUR OF NOVEL HYBRID-FIBRE REINFORCED ENGINEERED CEMENTITIOUS COMPOSITE UNDER IMPACT LOADING ..	104
5.1	INTRODUCTION	104
5.2	TESTING METHOD.....	107
5.2.1	Drop-Weight Impact Test	107

5.3 RESULTS AND DISCUSSION	110
5.3.1 Impact Behaviour.....	110
5.3.2 Fracture Performance.....	114
5.3.3 Behaviour Subsequent to Fire Exposure.....	117
5.3.4 Mode of Failure.....	118
5.3.5 Statistical Analysis of Test Results.....	120
5.4 CONCLUSIONS.....	126
5.5 REFERENCES	127
Chapter 6.....	132
6 EXPERIMENTAL AND NUMERICAL INVESTIGATION ON NOVEL SMA-PVA HYBRID FIBRE REINFORCED ENGINEERED CEMENTITIOUS COMPOSITE UNDER IMPACT LOADING.....	132
6.1 INTRODUCTION	132
6.2 FINITE ELEMENT MODELLING OF ECC.....	134
6.2.1 Plasticity Models.....	135
6.2.2 Defining Tensile and Compressive Behaviour	136
6.2.3 Defining Modeling Parameters.....	137
6.2.4 Simulation Technique.....	138
6.2.5 Damage Criterion.....	139
6.2.6 Initial and Boundary Conditions.....	139
6.3 ANALYSIS OF RESULTS AND DISCUSSION	140
6.3.1 Effect of Mesh Density on Model Accuracy	140
6.3.2 Energy-Penetration Behaviour.....	141
6.3.3 Impact Load-Time History	147
6.4 FAILURE CRITERION	149
6.5 VALIDATION OF NUMERICAL MODELS	152
6.6 CONCLUSIONS.....	154

6.7 REFERENCES.....	155
Chapter 7.....	157
7 SUMMARY, CONCLUSIONS AND RECOMMENDATIONS.....	157
7.1 SUMMARY AND CONCLUSIONS.....	157
7.2 RECOMMENDATIONS FOR FUTURE WORK.....	159
Appendices.....	161
Curriculum Vitae	166

List of Tables

Table 2-1: Findings of recent research work on mechanical properties of ECC	14
Table 2-2: Unique characteristics of ECC	15
Table 2-3: Mechanical properties of various SMAs	22
Table 2-4: Mechanical and physical properties of Ni-Ti alloy	22
Table 2-5: Utilizing SMA in new structural applications	30
Table 2-6: Full-scale structural applications of ECC and SMA	32
Table 3-1: Chemical analysis of cement, fly ash, and silica sand.....	51
Table 3-2: Mechanical properties of SMA and PVA fibres	52
Table 3-3: Mixture proportions of ECC mixtures.....	52
Table 3-4: Flexural strength and corresponding deflection of HECC-SMAF at different ages	62
Table 3-5: Toughness ranges for different concrete materials.....	68
Table 4-1: Cumulative mercury intrusion volume of ECC specimens (mL/g).....	92
Table 4-2: Tensile and flexural behaviour of ECC specimens at 90 days	93
Table 5-1: Statistical analysis of test results (N_1/N_2)	114
Table 5-2: Shape, scale parameters and coefficient of determination of ECC specimens ...	122
Table 5-3: Weibull distribution for first crack impact energy of ECC specimens	122
Table 5-4: Weibull distribution for impact energy at failure of ECC specimens	123
Table 5-5: Weibull distribution for impact energy of ECC specimens at failure	124
Table 5-6: Relationship between N_2 and N_1 of ECC specimens	125

Table 6-1: Input parameters of plasticity models.	138
Table 6-2: Mechanical properties of different ECC specimens.....	139
Table 6-3: Sensitivity analysis on mesh density	141
Table 6-4: Experimental and numerical impact test results.....	143

List of Figures

Figure 2-1: Four-point bending load-deformation behaviour of PVA-ECC.	9
Figure 2-2: Typical tensile stress-strain curve NC and ECC.	9
Figure 2-3: Schematic diagram of electric heating effect on RC element incorporating SMA wire.	10
Figure 2-4: Global market forecast for smart materials for 2013-2019 (modified after McWilliams, 2014).	12
Figure 2-5: Typical stress-strain curve of SMA under tension/compression (reprinted from Alam <i>et al.</i> , 2007, with permission from NRC research press).	23
Figure 2-6: Typical stress-strain curve of super-elastic SMA at different temperatures (reprinted from Dolce and Cardone 2001, with permission from Elsevier).	24
Figure 3-1: Particle size distribution of cement, fly ash, and silica sand.	51
Figure 3-2: Crack monitoring optical microscope.	55
Figure 3-3: Heat treatment gun.	55
Figure 3-4: Relative reduction in flow diameter due to fibre addition.	56
Figure 3-5: Compressive strength of ECC mixtures at different testing ages.	57
Figure 3-6: Elastic modulus of various ECC mixtures.	58
Figure 3-7: Poisson's ratio of different ECC mixtures.	59
Figure 3-8: Correlation between measured and calculated elastic modulus of ECC mixtures.	60
Figure 3-9: Splitting tensile strength of ECC specimens.	61

Figure 3-10: Load-deflection curves of ECC specimens at different ages: a) 3 days, b) 28 days, and c) 90 days.	64
Figure 3-11: Load-deflection curves of non-heated and heated ECC specimens.	65
Figure 3-12: Effect of fibre volume fraction on toughness index of ECC specimens at different ages: a) 3 days, b) 28 days, and c) 90 days.	66
Figure 3-13: Effect of fibre volume fraction on post-cracking strength of ECC specimens. .	67
Figure 3-14: Relative enhancement in toughness index of ECC2-1.	68
Figure 3-15: Flexural deflection of ECC prisms at different ages.	69
Figure 3-16: Average number of cracks of ECC prisms at different ages.	70
Figure 3-17: Fibre bridging capability of SMA.	71
Figure 3-18: Surface cracking of ECC specimens due to heat treatment.	72
Figure 3-19: PVA fibre deterioration due to heat treatment effect.	72
Figure 3-20: Percent enhancement in recovery strain of cracked ECC specimens.	73
Figure 3-21: BSE images of ECC0-0 specimen.	74
Figure 3-22: BSE images of ECC2-1.5 specimen.	74
Figure 3-23: SEM for fracture of PVA fibres.	75
Figure 3-24: SEM for pullout of SMA fibres.	75
Figure 3-25: SEM for flexural crack pattern of ECC specimens.	77
Figure 3-26: SEM for crack pattern of ECC specimens without heat treatment.	78
Figure 3-27: SEM for crack pattern of ECC specimens after heat treatment.	78
Figure 4-1: Illustration of ECC coupon specimens: a) schematic, and b) photograph.	88

Figure 4-2: Failure patterns of ECC coupon specimens: a) PVA-ECC, and b) HECC-SMAF.	89
Figure 4-3: Typical tensile stress-strain curve of different ECC specimens.	91
Figure 4-4: Incremental mercury intrusion volume and pore size distribution for ECC specimens.....	92
Figure 4-5: Cumulative mercury intrusion volume and pore size distribution for ECC specimens.....	92
Figure 4-6: Comparison between tensile strain capacity of UTT and FPBT.....	94
Figure 4-7: Predicted tensile strength and MOR relationship with respect to tensile strain capacity of ECC.	94
Figure 4-8: Dispersion of SMA fibres: a) ECC2-0.5, b) ECC2-1, and c) ECC2-1.5.	96
Figure 4-9: Typical statistical K-function of ECC specimens and random dispersion.....	98
Figure 4-10: Typical statistical F-function of ECC specimens and random dispersion.	99
Figure 4-11: Fibre-free areas percentage of ECC specimens with respect to r distance.	99
Figure 5-1: Instron impact loading testing machine setup.....	108
Figure 5-2: Schematic diagram of of the drop weight impact testing system.	109
Figure 5-3: Heating chamber setup.....	110
Figure 5-4: Typical Energy-penetration curves for different ECC mixtures at different drop levels: a) 1st hit, b) 2nd hit, and c) 3rd hit.	111
Figure 5-5: Percent enhancement in energy dissipation capability of ECC specimens.....	112
Figure 5-6: Accumulated penetration depth in ECC specimens.	112
Figure 5-7: Impact load-time history curves for different ECC specimens at different drop levels: a) 1st hit, b) 2nd hit, and c) 3rd hit.	113

Figure 5-8: Impact energy sustained by ECC specimens up to failure.	115
Figure 5-9: Impact failure energy of ECC specimens with and without heat treatment.	116
Figure 5-10: Impact failure energy of ECC specimens with and without fire exposure.	117
Figure 5-11: Failure patterns of ECC disc specimens: a) ECC0-0, b) ECC2-0, c) ECC2-0.5, d) ECC2-1, e) ECC2-1.5, and f) SMA fibre bridging.....	119
Figure 5-12: Weibull distribution of first crack impact energy of ECC specimens.	121
Figure 5-13: Weibull distribution of impact energy at failure of ECC specimens.	121
Figure 5-14: Weibull distribution for impact energy of ECC specimens at failure after fire exposure.	123
Figure 5-15: Relationship between N2 and N1 of ECC specimens.....	124
Figure 6-1: Concrete behaviour under uniaxial tensile loading (ABAQUS Analysis User's Manual, 2012).	135
Figure 6-2: Concrete behaviour under compression loading (ABAQUS Analysis User's Manual, 2012).	136
Figure 6-3: Tension stiffening variables (ABAQUS Analysis User's Manual, 2012).	137
Figure 6-4: Compression hardening variables (ABAQUS Analysis User's Manual, 2012).	137
Figure 6-5: Finite element modelling of drop weight impact test.	138
Figure 6-6: a) initial conditions and b) boundary conditions.....	139
Figure 6-7: Effect of different mesh densities on numerical results: a) load-time history, and b) applied energy-penetration depth.	140
Figure 6-8: Applied energy-penetration depth curves for ECC specimens at different drop levels; a) 1st hit, b) 2nd hit, and c) 3rd hit.	142

Figure 6-9: Strain energy magnitude in ECC specimens due to impact at: a) 2.5 ms, b) 5 ms, c) 7.5 ms, and d) 10 ms. 144

Figure 6-10: Accumulated dissipated energy of different ECC specimens due to multiple impacts: a) experimental, b) CDP, and c) DP. 145

Figure 6-11: Accumulated penetration depth for various ECC specimens due to multiple impacts: a) experimental, b) CDP, and c) DP. 146

Figure 6-12: Penetration depth for ECC specimens due to multiple impacts using the CDP model: a) ECC2-0, b) ECC2-0.5, c) ECC2-1, and d) ECC2-1.5. 146

Figure 6-13: Penetration depth for ECC specimens due to multiple impacts using the DP model: a) ECC2-0, b) ECC2-0.5, c) ECC2-1, and d) ECC2-1.5. 147

Figure 6-14: Typical impact load-time history curves for ECC specimens at different impact levels: a) 1st hit, b) 2nd hit, and c) 3rd hit. 148

Figure 6-15: Applied impact load of different ECC specimens due to multiple impacts: a) experimental, b) CDP, and c) DP. 149

Figure 6-16: Upper surface stress distribution of ECC specimens due to impact at: a) 1 ms, b) 2 ms, c) 3 ms, and d) 4 ms. 150

Figure 6-17: Distal face stress distribution of ECC specimens due to impact at: a) 1 ms, b) 2 ms, c) 3 ms, and d) 4 ms. 150

Figure 6-18: Experimental failure criterion of ECC specimens due to impact: a) ECC2-0, b) ECC2-0.5, c) ECC2-1, and d) ECC2-1.5. 151

Figure 6-19: Numerical failure criterion of ECC specimens due to impact: a) ECC2-0, b) ECC2-0.5, c) ECC2-1, and d) ECC2-1.5. 152

Figure 6-20: Impact energy sustained by ECC specimens: a) 1st crack, and b) failure. 153

List of Symbols

A_R	observed central area of specimen
C	Constant that represents fibre clustering
$F_N(n)$	cumulative distribution function
$F(r)$	complete spatial randomness F-function
F_o	distribution density function
F	function that measures the fibre-free area
f	constant with a value of 9.806×10^{-3}
$f(n)$	Weibull distribution function
g	acceleration due to gravity with a value of $9810 \text{ (mm/s}^2\text{)}$
h	falling height of the steel mass (mm)
IE	impact energy (joule)
i	failure order number
$K(r)$	complete spatial randomness K-function
K	function that represents the tendency of fibres to clump
k	number of data points
L_N	probability of survivorship function
N_1	numbers of impacts to induce the first visible crack
N_2	numbers of impacts to induce the failure
N_i	number of blows

n	specific value of a random variable N
R^2	coefficient of determination
r	distance from fibre (mm)
t	time required for the steel mass to fall from the 457 mm height (s)
u	scale parameter
V_f	fibre volume fraction in ECC mixture (%)
V	impact velocity (m/s)
w	mass of the steel hammer (kg)
λ	fibre density
α	shape parameter
α_1	significance level
a	number of treatments (variables)
B	beam width (mm)
D	beam depth (mm)
d	diameter of cylinder (mm)
E	elastic modulus (GPa)
I_n	toughness index
L	beam span (mm)
l	length of cylinder (mm)
MOR	modulus of rupture (MPa)

MS_E	mean square due to error
$MS_{Treatment}$	mean square due to treatments
N	total number of observations
n	number of observations (specimens)
P	maximum applied load indicated by testing machine (N)
Q_1	stress corresponding to a longitudinal strain of 50 millionths (MPa)
Q_2	stress corresponding to 40 % of the ultimate compressive load (MPa)
SS_E	sum of squares due to error (due to using replicates rather than testing only one specimen)
SS_T	total corrected sum of squares
$SS_{Treatments}$	sum of squares due to reinforcing the specimens
T	splitting tensile strength (MPa)
y_{ij}	j^{th} observations taken under factor level of treatment i
μ	Poisson's ratio of ECC
\mathcal{E}_2	longitudinal strains produced by stress Q_2
\mathcal{E}_{t1}	transverse strain at mid-height of the cylinder produced by stress Q_1
\mathcal{E}_{t2}	transverse strain at mid-height of the cylinder produced by stress Q_2
ρ	density of specimen (kg/m^3)
f_c	compressive strength of ECC (MPa)
δ	flexural deflection value at first crack (mm)

d	fibres' diameter
Ln	natural logarithm
PD	Predicted deviation for tensile strain capacity (%)
SD	standard deviation of the deflection capacity (mm)
σ_{tl}	lower limits of predicted effective tensile strength (MPa)
σ_{tu}	upper limits of predicted effective tensile strength (MPa)
β	dispersion coefficient
η	fibres' orientation factor
\mathcal{E}_{tu}	Predicted average tensile strain capacity (%)
δ_u	δ_u average deflection capacity of FPBT (mm)

List of Appendices

Appendix A: Sample calculations using inverse analysis of ECC2-1.....	161
Appendix B: Sample calculations using ANOVA of ECC2-1.5.....	162
Appendix C: Sample calculations of fibre dispersion of ECC2-0.5.....	164
Appendix D: Sample calculations of Weibull distribution of ECC2-0.....	165

Chapter 1

1 INTRODUCTION

1.1 GENERAL

Concrete is the most utilized construction material in the world. Although it primarily carries compressive loads, concrete is also subjected to tensile stresses under the complex combination of dead and live loads, shrinkage and thermal deformation, and other mechanical and environmental loads in field exposure. Concrete is also often exposed to impact and dynamic loading. Recent explosions have caused extensive economic and human losses around the world due to the poor performance of reinforced concrete (RC) structures. The impact resistance of conventional RC frame structures largely depends on the energy dissipation ability of key structural components such as beams, columns, and their connection zones. Extreme loading events such as blast, impact, and earthquake events have shown that failure of these structural elements often led to partial or total collapse of buildings (Alemdar and Sezen, 2010). Such a hazardous failure mechanism is unacceptable and must be prevented in design. After a strong impact or explosion, if the structure experiences excessive deformation, although the structural elements may remain functional, it will not be able to fully recover its original shape. Thus, the occupants/users of that structure will not feel safe to use it.

Furthermore, the study of the impact resistance of structures, especially military and defense facilities and those with strategic importance against explosive waves and penetration of fragments has attracted great research interest in recent years. One of the ballistic impact loads against which these structures should be protected is the localized impact from high-velocity projectiles caused by small arms or blast-induced fragments.

Therefore, civil engineers have been seeking innovative materials and solutions to design structural members and smart systems that possess enhanced deformation capacity and ductility, higher damage tolerance, better concrete confinement, decreased or minimized residual crack sizes and recovered or reduced permanent deformations (Parra-Montesinos *et al.*, 2005). If such RC elements can be tailored, this would allow the design of structures having enhanced ductility, exhibiting little damage, thus minimizing concrete repair. This goal could be achieved for instance using shape memory alloy (SMA) bars in structural elements as full or partial replacement for traditional steel reinforcement. This was explored for example by Saiidi *et al.* (2007), Xiaopeng *et al.* (2015), and Choi *et al.* (2015). It is also possible to use SMA bars as reinforcement in joints of RC frames while the other structural elements are reinforced with regular steel (Nehdi *et al.*, 2010).

Another alternative would be using hybrid polyvinyl alcohol-engineered cementitious composites (PVA-ECCs) incorporating randomly dispersed nickel titanium (NiTi) SMA short fibres as a replacement for traditional RC, which has not yet been fully investigated. The main drawback of using large-diameter SMA bars is that it reduces the hysteretic area of the SMA, thus impacting its ability to dissipate energy compared to small-diameter wires. This is due to the accumulation of more distorted martensite crystalline structure and inherent deficiencies that exist in larger-diameter SMA rods as compared to smaller-diameter wires. From a technical standpoint, the larger the diameter of SMA rods, the more distortion and inconsistency are observed at the microstructural level, which impacts the hysteretic behaviour of the SMA (Zafar and Andrawes, 2014). Moreover, short fibres have advantages over continuous wires in that the distribution of fibres is more uniform; thus, they enable crack closing in any direction. Also, if SMA fibres could be used instead of straight tendons or continuous wires, then thin or curved shaped SMA-reinforced structural members could be easily constructed.

The rapid progress in missile and explosives technology coupled with the poor behaviour of structures against such events emphasize the need for dedicated research to develop smart and novel structural materials with superior resistance against impact loading.

The concept of smart structures and adaptive systems has gained global importance. Smart systems can automatically adjust their structural characteristics in response to unexpected severe loading and/or disturbance towards enhancing structural safety and serviceability. In particular, smart materials can be integrated into structures to provide functions such as sensing, self-adapting and self-healing (Song *et al.*, 2006). An example of such smart materials is shape memory alloys (SMAs).

1.2 RESEARCH SIGNIFICANCE

In response to substantial economic and human life loss incurred due to blast, impact and earthquakes inflicted on civil infrastructure, there has been substantial research attempting to develop resilient, smart and sustainable systems that can withstand such extreme loading events. Yet, this research remains scattered. This dissertation is an attempt to create synergy between two emerging materials: engineered cementitious composites and shape memory alloys. It is believed that when these two materials are combined, smart systems that are sustainable and resilient under extreme loading events could be developed with endowed self-centering and self-healing capability.

1.3 SPECIFIC RESEARCH OBJECTIVES

This dissertation aims at exploring the fundamental characteristics of hybrid PVA-ECC incorporating short, randomly dispersed NiTi-SMA fibres with consideration of possibly using this novel composite in structural applications with vulnerability to impact hazards. The specific objectives of this research are:

- 1) Examining the effects of incorporating NiTi-SMA fibres having 0.625 mm in diameter and 16 mm in length at 0.5%, 1.0% and 1.5 % volume fraction on the compressive, tensile and flexural strength of PVA-ECC composites.
- 2) Exploring the effect of SMA fibre addition on the fracture toughness of the ECC material and how it affects the ductile behaviour of the composite.

- 3) Providing a correlation between the tensile properties and flexural characteristics of the composite in order to overcome the problems associated with complicated tensile tests.
- 4) Experimentally investigating strain recovery as a self-healing mechanism in flexural damaged HECC-SMAF prisms exposed to controlled high temperature stimuli and evaluating its performance under re-loading.
- 5) Acquiring superior capability to recover large deformations in ECC elements to enhance structural safety and service life performance.
- 6) Achieving large energy dissipation and crack control capability utilizing NiTi-SMA fibres.
- 7) Experimentally investigating the impact resistance of cylinders made with mono and hybrid fibre-reinforced ECC mixtures.
- 8) Exploring the impact behaviour of the new composite after exposure to high temperatures.
- 9) Developing a numerical model using finite elements (FE) to evaluate the performance of HECC-SMAF cylinders under impact loading in terms of extent of damage, load-time history, and energy absorption capacity, and verifying its results versus that acquired from the experimental investigation.

1.4 RESEARCH CONTRIBUTIONS

This research is considered the first study that provides a novel investigation on the synergy of utilizing two emerging materials in developing damage resilient infrastructures, ECC and SMA fibres. Evaluating the behaviour of the novel hybrid fibre-reinforced composite subjected to static and dynamic loading under normal exposure and subsequent to both heat-treatment and fire exposure provides a new contribution to the state-of-the-art. The new composite is endowed with strain recovery and superior impact resistance. Moreover, this study provides a numerical investigation demonstrating that the finite element modeling technique can be used to successfully simulate the response of the novel composite exposed to impact loading.

1.5 THESIS OUTLINE

This dissertation has been prepared according to the integrated-article format predefined by the Faculty of Graduate Studies at Western University, London, Ontario, Canada. It was organized in seven chapters covering the scope of the study: Tensile and impact resistance of shape memory alloy fibre reinforced engineered cementitious composite.

The current chapter 1 provides a brief introduction along with the research significance and objectives.

Chapter 2 presents a critical literature review of research on ECC, its composition, specifications and design procedures. It also provides a brief discussion on SMA with specific background of NiTi-SMA. The shape memory effect as well as the super-elastic and super-plastic characteristics of NiTi-SMA are explained at a micro-structural level. The chapter concludes with a summary of the research conducted on ECC and how it is being used in civil engineering applications. In addition, a brief review of current structural applications of NiTi-SMA, focusing on beams, columns and their connection zones, is also provided.

Chapter 3 presents an experimental program covering the fabrication and analysis of the mechanical performance of hybrid PVA-ECC incorporating randomly dispersed NiTi-SMA fibres (HECC-SMAF) at 0.5%, 1% and 1.5% by volume fraction having 16 mm in length. The compressive strength, tensile properties, and flexural performance of the new composite are examined and discussed.

Chapter 4 provides a proposed tool based on experimental results to predict the uniaxial tensile characteristics of the ECC composite using simple flexural test results in order to overcome the problems associated with complicated direct tensile testing.

Chapter 5 reports the performance of the new composite under impact loading and its impact behaviour after exposure to a high temperature stimuli in terms of energy dissipation capability, pre-stressing effect, first crack strength, and fracture energy.

Chapter 6 presents the proposed numerical models using a commercial Finite Element (FE) software (ABAQUS/Explicit) to simulate the behaviour of the new composite under drop weight impact loading in terms of energy absorption capacity, applied impact loading-time history, and extent of damage.

Chapter 7 summarizes the results of the study, draws conclusions and discusses needed future research.

1.6 REFERENCES

- Alemdar, F., and Sezen, H., “Shear behavior of exterior reinforced concrete beam-column joints.” *Structural Engineering and Mechanics*, 35(1), 2010, pp. 123-126.
- Choi, E., Hu, J., Lee, J., and Cho, B., “Recovery stress of shape memory alloy wires induced by hydration heat of concrete in reinforced concrete beams.” *Journal of Intelligent Material Systems and Structures*, 26(1), 2015, pp. 29–37.
- Nehdi, M., Shahria, A., and Youssef, M. (2010). “Development of corrosion-free concrete beam-column joint with adequate seismic energy dissipation.” *Engineering Structures*, 32 (9), 2518-2528.
- Parra-Montesinos, G. J., Peterfreund, S. W., and Chao, S., “Highly damage-tolerant beam-column joints through use of high-performance fiber-reinforced cement composites.” *ACI Structural Journal*, 102(3), 2005, pp. 487-495.
- Saiidi, M., Zadeh, M., Ayoub, C., and Itani, A., “A pilot study of behavior of concrete beams reinforced with shape memory alloys.” *Journal of Materials in Civil Engineering*, 19(6), 2007, pp. 454–461.
- Song, G., Ma, N., and Li, N., “Applications of shape memory alloys in civil structures.” *Engineering Structures*, 28(9), 2006, pp. 1266–1274.

Xiaopeng L., Mo L., and Song, G., “Energy-dissipating and self-repairing SMA-ECC composite material system.” *Smart Materials and Structures*, 24(2), 2015.

Zafar, A., and Andrawes, B., “Fabrication and cyclic behavior of highly ductile super-elastic shape memory composites.” *Journal of Materials in Civil Engineering*, 26(4), 2014, pp. 622-632.

Chapter 2

2 EXPLORING SYNERGY OF ENGINEERED CEMENTITIOUS COMPOSITES AND SHAPE MEMORY ALLOYS IN CREATING RESILIENT CIVIL INFRASTRUCTURE¹

2.1 INTRODUCTION

ECC was developed in 1993 by Li (Li, 2003) at the University of Michigan. It is made of a cementitious binder, small particle size sand, fillers, and high-modulus, short random fibres micro-mechanically designed to achieve high damage tolerance under severe loading and high durability in normal service conditions (Sahmaran and Li, 2010). Furthermore, supplementary cementitious materials are used as partial replacement for cement in ECC production to improve its sustainability and durability in aggressive environments (Suleiman and Nehdi, 2017). ECC is categorized as a sustainable high-performance cementitious material, with growing efforts to incorporate in it increasing contents of recycled by-products and mineral admixtures. It has been produced in ready-mix concrete plants and transported to construction sites using conventional transit trucks. The ECC mixture can be placed without need for vibration due to its self-consolidating ability. The relatively low fibre content (2% by volume fraction) has also made ECC shotcrete viable. Moreover, the costliest component of the composite, fibres, is minimized resulting in ECC that is more acceptable to the cost-sensitive construction industry. Under flexure, normal concrete (NC) fractures in a brittle manner. In contrast, due to presence of fibres, very high curvature can be achieved by ECC at increasingly higher loads, much like the yielding of a ductile metal plate, as shown in **Fig. 2-1**.

¹ A version of this chapter was accepted for publication in the *Magazine of Concrete Research Journal* (2017).

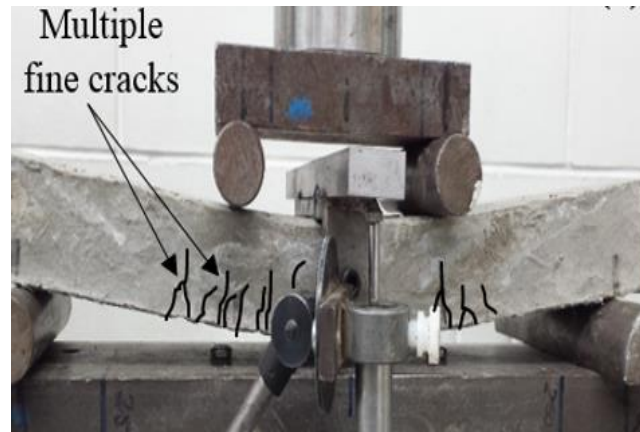


Figure 2-1: Four-point bending load-deformation behaviour of PVA-ECC.

Extensive inelastic deformation in ECC is achieved via multiple micro-cracks having a width of usually less than $60\ \mu\text{m}$ (about half the diameter of a human hair). This inelastic deformation of ECC is similar to plastic yielding in ductile metals in which the material undergoes distributed damage throughout the yielding zone (Dhawale and Joshi, 2013).

Figure 2-2 displays the typical tensile stress-strain behaviour of ECC compared to that of NC.

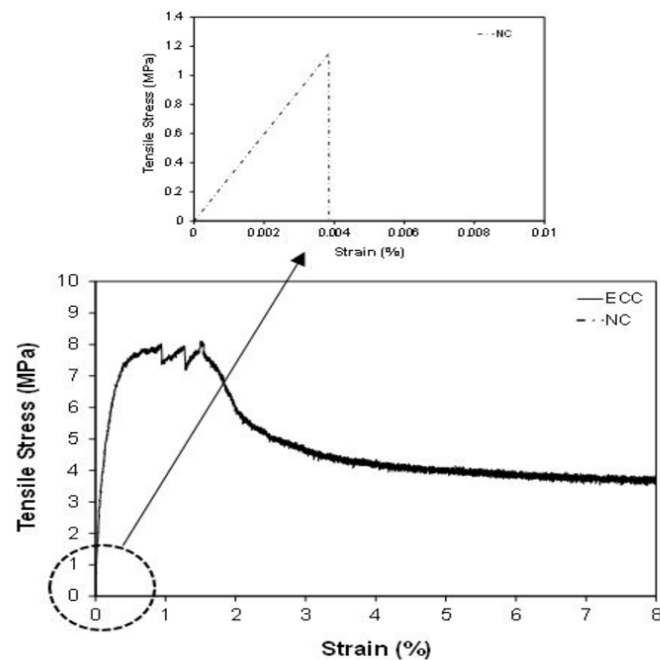


Figure 2-2: Typical tensile stress-strain curve NC and ECC.

Recently, the concept of smart structures and adaptive systems has gained global importance. Smart systems can automatically adjust their structural characteristics in response to unexpected severe loading or disturbance towards enhancing structural safety and serviceability. In particular, smart materials can be integrated into structures to provide functions such as sensing, actuation and information processing essential to monitoring (Song *et al.*, 2006). Also, using such materials in concrete structures can help achieving autogenous-healing. Smart materials have recently found numerous applications in many civil engineering areas, especially shape memory alloys (SMAs).

SMAs are a class of metallic alloys that "remember" their original shapes, with unique ability to undergo large inelastic deformation and regain its un-deformed shape when subjected to stimulus such as radiations, thermo-mechanical or magnetic variations, and electric heating. The properties of SMAs were discovered by accident (Buehler and Wang, 1968). Anecdotally, samples of the alloy were being subjected to strength tests by being pounded with hammers to see how much force was necessary to deform them. After several dents were created, the researchers left the samples on a windowsill and went for lunch. Upon their return, they discovered that the dents had "repaired" themselves. The main types of SMAs include copper-zinc-aluminum, copper-aluminum-nickel, iron-manganese-silicon and nickel titanium (NiTi) alloys.

A concrete structure can be considered intelligent if it has the ability to sense and self-rehabilitate itself. There are fertile opportunities for exploiting SMA in engineering smart and resilient structures. For instance, Song and Mo (2003) proposed the concept of intelligent reinforced concrete (IRC) whereby in the presence of cracks due to explosions or earthquakes, by electrically heating SMA wires, the wire strands contract and reduce the crack width, as shown in **Fig. 2-3**.

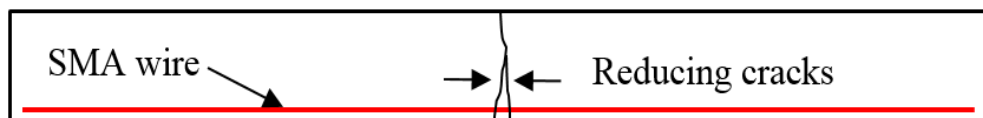


Figure 2-3: Schematic diagram of electric heating effect on RC element incorporating SMA wire.

The present chapter first examines ECC and NiTi-SMA production techniques and their mechanical properties. The shape memory effect as well as the super-elastic characteristics of NiTi-SMA are broken down and explained at a micro-structural level. A general description of modelling aspects of ECCs and SMAs with information on built-in ECC and SMA models available in some finite element (FE) packages is provided. In addition, current structural applications of these materials, such as beams, columns and their connection zones, are critically discussed. Furthermore, the impact resistance of ECC structural elements reinforced by traditional steel and/or SMA is highlighted with a proposed view on further research needed on the applicability of such promising materials in structural applications. It is demonstrated that ECC and SMA possess a substantial potential to replace or complement conventional structural materials, while achieving great gains in terms of performance, resilience and safety.

2.2 GLOBAL MARKET FOR SMART MATERIALS

Research (e.g. McWilliams, 2014) reported that the global market for smart materials was about USD 19.6 billion in 2010, USD 22 billion in 2011 and estimated to reach over USD 40 billion by 2016 with a compound annual growth rate (CAGR) of 12.8% between 2011 and 2016. The largest application segment (55% of the total market) is motors and actuators, with sales of nearly USD 10.8 billion in 2010, expected to reach USD 25.4 billion (approximately 64% of the market) by 2016 with CAGR of 15.4% between 2011 and 2016, as shown in **Fig. 2-4**. It was reported that the global market for these materials totaled about \$26.0 billion in 2014 and is forecasted to reach \$42.2 billion in 2019, registering a CAGR of 10.2% for the period of 2014-2019. More recently, Transparency Market Research (2016) estimated that this market will reach USD 63.2 billion by 2020, with rising demand for piezoelectric devices to drive the growth. It is believed that smart materials will find growing applications in civil infrastructure systems. Thus, researchers ought to explore this potential and pursue opportunities offered by such intelligent materials and systems to yield, smart, resilient and sustainable infrastructure with superior performance and lower service life cost, maintenance and repair requirements.

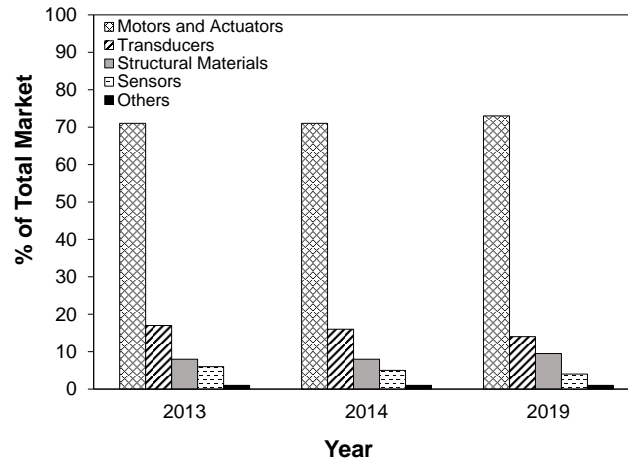


Figure 2-4: Global market forecast for smart materials for 2013-2019 (modified after McWilliams, 2014).

2.3 ENGINEERED CEMENTITIOUS COMPOSITES (ECCs)

2.3.1 ECC Production

ECC utilizes similar ingredients to that of FRC. However, coarse aggregates are not used in ECC because they tend to adversely affect the unique ductile behaviour of the composite. A typical ECC mixture composition employs cement and supplementary cementitious materials of nano to millimeter scale, micro-silica sand or limestone powder of 300 μm particle size diameter or less, water, water reducing admixtures and about 2% by volume of discrete fibres. Typically, fibres are of the order of a few millimeters in length and tens of micrometers in diameter, along with a nano-scale surface coating. A variety of fibres have been used in ECC production, such as polyvinyl alcohol (PVA) (Said *et al.*, 2015), polypropylene (PP) (Zhang *et al.*, 2015), polyethylene (PE) (Qudah and Maalej, 2014), and steel fibres (SE) (e.g. Soe *et al.*, 2013). Recently, Ali *et al.* (2017) have pioneered the use of short shape memory alloy (SMA) fibers in ECC production. Because of the relatively small amount of fibres and its chopped nature, the mixing process of ECC is similar to that of normal concrete.

2.3.2 Mechanical Properties of ECC

The mechanical properties of ECC depend mainly on various mixture design parameters and the type of fibres used (Pan *et al.*, 2015). ECCs have two inherent characteristics: ability of multiple micro-cracking in the matrix instead of one large crack formation before failure, along with strain hardening capability (i.e. rise in tensile deformation accompanied by a rise in load carrying capacity after first cracking), as shown in **Fig. 2-2**. What makes ECC different from normal concrete and other fibre-reinforced concretes is the unique properties associated with its specially tailored composite nature. As portrayed in **Fig. 2-2**, these properties include smaller crack width, metal-like ability to carry higher load after first cracking while undergoing further deformation, significantly higher ductility, self-healing ability, and relatively low fibre volume fraction (Sahmaran and Li, 2010). Such properties contribute to improving the safety, mechanical strength and sustainability of structures made with ECC. It was reported that ECC has a typical moderate tensile strength of 4 to 12 MPa, compressive strength of 20 to 95 MPa, flexure strength of 10 to 30 MPa and a high ductility of more than 1%, which is hundred times that of normal concrete. These properties can be tailored depending on the demands of a particular structure. **Table 2-1** summarizes some of the mechanical properties of ECC retrieved from recent research works.

2.3.3 Engineering Properties of ECC

For the sake of the aforementioned superior behaviour of ECC, several researchers have been motivated to further explore its performance, for instance under impact and blast loading, its sustainability, self-healing capability, etc. **Table 2-2** summarizes some of these unique characteristics retrieved from various studies.

2.3.3.1 Impact Resistance of ECC

Military facilities, mountainous rock sheds and protective walls of nuclear power plants must be designed to resist severe loading conditions such as impact and blast loads imparted by missiles, falling rocks, crushing vehicles and aircrafts (Alhadid *et al.*, 2014). Impact testing is an effective way for determining the impact responses of RC structural members (Adhikary *et al.*, 2015, 2016).

Table 2-1: Findings of recent research work on mechanical properties of ECC

Mechanical property	Achievement	Reference
Compressive strength and elastic modulus	<ul style="list-style-type: none"> • Increasing fly ash (FA) partial replacement of cement (C) by 50%, 100 and 150% decreased the compressive strength by 19%, 33% and 52%, respectively. Increasing water/binder (w/b) ratio (0.28 control) by 7% and 14%, decreased compressive strength by 22.2% and 26.67%, respectively. Increasing sand/binder ratio (0.3 control) by 20% and 40%, increased compressive strength by 7.7% and 65.4%, respectively. • Increasing the fibre volume fraction (1.2 control) by 8.3% and 16.6%, decreased the compressive strength by 12.5% and 25%, respectively. • Partial or total replacement of silica sand by limestone powder increased the ECC compressive strength. • Incorporation of 10% tire rubber as partial replacement for fine aggregate in ECC mixtures significantly reduced compressive strength and elastic modulus of the composite by more than 50%. 	<p>Pan <i>et al.</i> (2015), Huang <i>et al.</i> (2013), Turk and Demirhan (2013)</p>
Tensile strength	<ul style="list-style-type: none"> • The higher the fibre dispersion, the higher was the tensile ductility and ultimate tensile strength of ECC. • Highly inclined fibres by more than 20 degrees with respect to the tensile load axis, reduced the fibre bridging efficiency by up to 64%, and consequently reduced the tensile ductility of ECC specimens. • Incorporating tire rubber in ECC mixtures can achieve tensile strain capacity of 2-3% at 28 days. • The first cracking strength of ECC significantly decreased with existence of tire rubber in ECC mixtures. • The incorporation of tire rubber in ECC mixtures substantially reduced the tensile capacity of the composite by about 50% compared to that of the ECC mixtures not including tire rubber. 	<p>Tosun-Felekoglu <i>et al.</i> (2014), Huang <i>et al.</i> (2013)</p>
Flexural strength	<ul style="list-style-type: none"> • Producing ECC mixtures with low-modulus fibres such as PP and nylon 66, achieved high flexural strength. However, PVA-ECC mixtures still acquire higher flexural strength compared to that of low-modulus fibres. • Generally, the first crack strength of the composite decreased with increasing FA/C and/or w/b ratio. • Increasing the FA/C and/or w/b ratio by more than 1.2 and 0.28, respectively, generally decreased the ECC's flexural strength. Also, flexural capacity slightly increased with increasing the sand/b ratio by more than 0.3. • The flexural deflection capacity tended to increase with an increase in both the w/b and FA/C ratios. • The number of cracks in ECC increased as the FA/C and/or w/b ratios increased. Additionally, higher FA content tended to reduce the flexural crack width. 	<p>Pan <i>et al.</i> (2015), Halvaei <i>et al.</i> (2014)</p>
Shear strength	<ul style="list-style-type: none"> • ECC specimens had a reserve capacity against shear failure ranging between 14% and 27% relative to similar specimens made with normal 45 MPa concrete. • The failure process of ECC beams was less brittle than that of normal concrete beams. Also, critical cracks were propagated in ECC beams when the shear test progressed beyond the peak load. • The shear capacity of beams produced with and without stirrups increased by 20.6% and 107.6%, respectively, when replacing normal concrete with ECC. 	<p>Zhang <i>et al.</i> (2015) Qudah and Maalej (2014)</p>

Table 2-2: Unique characteristics of ECC

Property	Main Findings	Reference
Behaviour under reversed cycling loading	<ul style="list-style-type: none"> • The use of ECC in RC structural elements as replacement for traditional concrete and/or transverse reinforcement, enhanced the seismic energy dissipation ability of the element and the shear resistance and cracking response, and reduced reinforcement congestion and construction complexity. • Replacing conventional concrete with ECC allowed developing spalling-free concrete elements with adequate seismic energy dissipation even when stirrups reinforcement was not used. • ECC/reinforcement bond was not degraded under the effect of reverse loading cycles, consequently, delaying the failure of key structural elements such as columns, beams and their connection zones. 	Qudah and Maalej (2014), Yuan <i>et al.</i> (2014), Gencturk <i>et al.</i> (2013)
Drying shrinkage, frost and corrosion resistance	<ul style="list-style-type: none"> • Drying shrinkage of ECC was higher than that of normal concrete due to the absence of coarse aggregates. Using tire rubber in ECC mixtures can accommodate shrinkage deformations without localized fracture failure. • ECC provides excellent frost protection compared to that of fibreless ECC matrices. • The development of multiple fine cracks in ECC specimens compared to large cracks in normal concrete can reduce corrosion damage. 	Huang <i>et al.</i> (2013), Zhu <i>et al.</i> (2012), Mihashi <i>et al.</i> (2011)
Behaviour under different curing conditions	<ul style="list-style-type: none"> • The tensile strength of ECC specimens achieved under accelerated curing at high temperature was higher than that acquired at normal curing, while a reverse trend was observed for the tensile strain capacity. • The tensile strain capacity of ECC specimens generally decreased when the curing age was prolonged. • The tensile crack width in ECC enlarged with curing age compared to that in specimens tested at earlier age. 	Qian and Zhang (2012), Zhu <i>et al.</i> (2012)
Self-healing capability	<ul style="list-style-type: none"> • The unique micro-crack property and tight crack-width behaviour of ECC along with its relatively high dosage of cementitious materials and lower w/b ratio compared with that in conventional concrete endowed ECC with a high of self-healing capability. • Preloaded ECC specimens showed negligible recovery of strain when the crack width was larger than 150 μm, partial recovery was observed when the crack width was between 50 and 150 μm, and full recovery occurred when the crack width was lower than 50 μm. • The healing ability of cracked ECC specimens, in terms of stiffness recovery, was found to be less at early age compared to that for more mature specimens. 	Wu <i>et al.</i> (2012), Sahmaran <i>et al.</i> (2007)

The response of a structure subjected to impact loading is complex (Naik and Doshi, 2008), depending on its geometry, material properties, along with the characteristics of the projectile or explosive load. When a projectile strikes a target, stress waves inducing considerable energy are produced at the surfaces of the target, resulting in time-dependent zones of tensile stress. When the tensile stresses exceed the dynamic tensile strength of the target material, tensile failure occurs. To resist such vigorous loads, the structural material must possess sufficient strength at high strain rate and adequate energy absorption capacity to maintain its integrity without shattering and failing. Incorporating fibres in structural elements, even in those pre-damaged by static loads was found to have significant positive effect on their response under impact loading (Mindess *et al.*, 1986).

Research on ductile materials and smart systems that exhibit excellent resistance to low and high velocity impacts has attracted major interest. For instance, Maalej *et al.* (2005) studied the behaviour of hybrid-fibre ECC panels incorporating 1.5% PE and 0.5% steel fibres under high velocity projectile impact from a small-mass projectile (15 g). The ECC panels were 300 x 170 mm [12 x 6.8 in] prismatic specimens with thicknesses of 55, 75, 100, 120, and 150 mm that were subjected to various impact velocities ranging from 300 to 750 m/s. The test results indicated the potential of utilizing ECC panels as a protective material in various applications, such as enhancing shatter resistance with minimized scabbing and spalling associated with distributed micro-cracking. Zhang *et al.* (2007) further explored the damage pattern and failure mode under drop weight impact loading of full-scale 2000 x 1000 x 50 mm hybrid- fibre ECC panels made with similar constituents to that tested by Maalej *et al.* (2005). Their hybrid-fibre ECC panels had enhanced impact resistance against multiple impacts, high ductility and energy absorption capability compared to that of both RC and FRC counterparts. Furthermore, Yang and Li (2012) carried out a series of drop weight impact tests on hybrid-fibre ECC panels and beams reinforced by PVA and steel fibres. The 305 x 305 x 25.4 mm panels and 305 x 76 x 51 mm beams were subjected to drop mass of 12 kg. Results demonstrated that the load carrying capacity and energy dissipation ability of the ECC panels were improved.

Li and Zhang (2011) developed a numerical model for the impact behaviour of hybrid-fibre ECC panels using the LS-DYNA software. The results were in good agreement with experimental data obtained by Maalej *et al.* (2005). Moreover, Soe *et al.* (2013) investigated the impact resistance of hybrid-fibre ECC panels incorporating a combination of 1.75% PVA and 0.58% steel fibres. The 300 x 170 x 50 mm ECC panels were subjected to high velocity projectile impact ranging from 300 to 657 m/s. The ECC panels achieved superior behaviour and absorbed higher energy than that of its normal concrete counterpart. The ECC panels withstood multiple impacts at velocity of 460 m/s, reflecting superior performance under impact loading. More recently, Zhuge *et al.* (2014) developed a lightweight ECC via replacing a volume fraction of cement by lightweight hollow glass additives. They tested the 30 mm x 9.6-14.7 mm cylindrical specimens under pressurized impact loading produced using Split Hopkinson Bar (SHB). Results showed that the dynamic compressive strength increased with increasing strain rate, while it decreased with higher replacement level of hollow microspheres compared to that of normal ECC specimens produced without hollow glass additives. Considering the aforementioned studies, ECC has become as promising engineering material for the construction of impact protective structures.

2.3.3.2 Sustainability of ECC

Every ton of cement produced generates around one ton of CO₂ released into the atmosphere, which is responsible for about 7% of global greenhouse gas emissions (Black and Purnell, 2016). When structures such as roads are built using pure portland cement, they often need to be repaired more frequently, thus consuming more cement and releasing additional greenhouse gas. During road repair, traffic crowding in the area leads to increased fuel use and emissions (Li *et al.*, 2004). Using ECC in such applications can help decrease this environmental impact, thus improving the sustainability of the project. Li *et al.* (2004) investigated the effects of using ECC, concrete made with portland cement, and hot mixed asphalt (HMA) on important environmental parameters. It was concluded that the energy required to produce ECC is less than that utilized for regular concrete and HMA by about 21% and 72%, respectively. Also, the CO₂ emission due to ECC is less than that of regular concrete and HMA by about 33% and 38%, respectively. Yet most proposed

ECC mixtures include a considerable amount of cement. By partially substituting cement with industrial by-products such as cement kiln dust and fly ash, the environmental footprint of ECC could be reduced, while also disposing of waste. Moreover, by-products such as fly ash could facilitate self-healing reactions in ECC. Building sustainability features such as the ability to reduce negative environmental impacts, increased life-span of structures via decreasing resources needed for maintenance and repair, all seem to indicate that ECC is a sustainable strong contender against conventional concrete.

2.3.4 Material Modelling of ECC

Many research works attempted to develop models that can predict the structural performance of ECC without need for costly and time-consuming experimental investigations. Models could for instance help in determining the structural response of ECC under missile attack or explosion, which are difficult to test in laboratories. A numerical model was developed by Li and Zhang (2011) to simulate the impact behaviour of hybrid fibre ECC panels incorporating SE and PE fibres using the LS-DYNA commercial software. The panels were similar to that tested by Maalej *et al.* (2005), thus the numerical model was validated against these experimental results. It was concluded that the numerical model was effective in modelling the impact response of hybrid-fibre ECC panels. Following similar concept, Zhang *et al.*, (2007) also analyzed the global performance and energy absorption capacity of RC and hybrid fibre ECC panels using a Single Degree of Freedom (SDOF) concept. The high ultimate resistance and maximum allowable deflection of the ECC panels appeared to be the main factors contributing to its superior energy absorption capacity and overall improved global resistance compared to that of its RC counterpart.

Moreover, the high ductility of ECC motivated investigating the effects of using this composite in wall elements. For instance, Kesner and Billington (2005) performed a two-dimensional finite element simulation following that proposed by Han *et al.* (2003) to identify adequate infill geometries under fully reversed cyclic loading. They reported that rectangular ECC wall panels outperformed ordinary rectangular RC wall panels in terms of peak load and energy dissipation. An infill wall system has been developed for use in steel framed structures using precast panels made of ECC. A series of finite element

analyses were performed to determine panel sizes and geometries. The infill system was developed specifically for use as a retrofit strategy to improve the seismic performance of critical facilities such as hospitals and emergency response structures. The experimental and simulation results demonstrated the potential of the infill system as a retrofit.

Moreover, Artificial Neural Network (ANN) models have been developed as tools for predicting the mechanical and durability properties of concrete (e.g. Sadrumontazi *et al.*, 2013, Shahriar and Nehdi, 2011, Hewayde *et al.*, 2007, El-Chabib and Nehdi, 2005). ANN models identify the patterns between an input and its output. Recently, Hossain and Samani (2015) used the Levenberg Marquardt back propagation method to develop models for predicting the 28-days compressive strength of ECC based on 134 ECC mixtures retrieved from the literature. It was found that the degree of agreement (ξ) and ratio between model and experimental outputs for the testing and validating data of the ANN model was very close to 1. It was concluded that the model can be used as a tool for the design of ECC mixtures based on desired strength or for predicting the compressive strength of a given ECC mixture.

2.3.5 Laboratory Investigations on Small Scale ECC Structural Elements

Research has been conducted over the last few decades to optimize ECC constituents and explore the applicability of using ECC in full-scale structural elements. For instance, Pan *et al.* (2015), Soe *et al.* (2013), and Tosun-Felekoglu *et al.* (2014) attempted to optimize the fly ash, silica sand, fibres, and water reducing agent contents in ECC. Also, Turk and Demirhan (2013) and Halvaei *et al.* (2014) explored the feasibility of replacing silica sand by limestone powder and using different types of fibres on the mechanical properties of ECC. Using ECC in full-scale structural elements, such as beams (Yuan *et al.*, 2014), columns (Gencturk *et al.*, 2013), beam-connection zones (Qudah and Maalej, 2014), slabs (Soe *et al.*, 2013) and walls (Maalej *et al.*, 2010) and retrofitting/repairing of existing ones (Huang *et al.*, 2013) was investigated. Moreover, Zhang *et al.* (2013) studied the potential applications of low drying shrinkage ECC (LSECC) in strips placed between traditional concrete slabs for forming joint-less concrete pavement systems and accommodating temperature and shrinkage deformations. It was found that a composite slab containing

both plain concrete and LSECC, using steel bars at the LSECC/concrete interface, could localize tensile cracks into the LSECC strip instead of cracking in adjacent concrete slabs, which reduces the cost and time of maintenance needed for such elements.

2.3.6 Constraints of Using ECC

A cost comparison of ECC and regular concrete should not only consider their manufacturing costs, but also account for the structure's lifetime costs. Regular concrete has an initial cost roughly about three times less than that of ECC, but this can come at the expense of quality (Dhawale and Joshi, 2013). Initial costs are in favor of regular concrete, but long-term benefits are sufficient to favor ECC. To lower the cost of ECC, lower cost and more sustainable cementitious materials can be used as partial replacement for cement. Also, smaller ECC structural member size, reduced or eliminated reinforcement, and faster construction offered by self-compacting ECC can further reduce costs (Dhawale and Joshi, 2013).

Using ECC can have further long-term benefits on the reduction of maintenance costs compared to that of regular concrete. Being more sturdy, less brittle, more flexible, and self-healing, it normally requires less maintenance and repair, which is particularly desirable for large-scale infrastructure such as highways and tunnels that need to be in continuous service. Under such circumstances, automatic repair, or self-healing, of cracks without onerous labor and capital requirements could be very attractive. Repair work may also be difficult or impossible because of existing conditions such as difficult access to damage in the affected structure (Wu *et al.*, 2012). When long-term costs and environmental benefits are accounted for, the advantages offered by ECC over conventional concrete become more prominent.

2.4 SHAPE MEMORY ALLOYS (SMA)

2.4.1 SMA Fabrication

Several SMAs having different compositions have been developed (Choi *et al.*, 2015, Debbarma and Saha, 2012, Nehdi *et al.*, 2010, and Maruyama *et al.*, 2008), including Cu-Al-Ni, Cu-Zn-Al, Cu-Al-Be, Cu-Sn, Cu-Zn, Fe-Mn-Al-Ni, Fe-Mn-Si-Cr, Fe-Ni-Nb, Fe-

Cr-Ni-Mn-Si, Fe-Ni-Co-Al-Ta-B, Mn-Cu, Ti-Ni-Hf, Ni-Ti-Fe, Ni-Ti-Nb, Ni-Ti-Al, Ni-Ti-Cu and Ni-Ti. Most popular amongst SMAs are Ni-Ti alloys, known as a ‘Nitinol’. There are various ways to manufacture Nitinol. Current techniques of producing NiTi alloys include vacuum melting techniques such as electron-beam melting, vacuum arc melting or vacuum induction melting. The alloys are then hot or cold worked to the desired shape (e.g. wire, ribbon, tube, sheet, or bar). Carbide and diamond dies are used to produce wires ranging from 0.075 to 1.25 mm in diameter (Gupta *et al.*, 2012). The final stage of the fabrication process is the shape memory treatment that characterizes SMA distinctively from other structural metals, in which alloys undergo appropriate thermomechanical processing to exhibit shape memory effect and super-elasticity. Cold working of Nitinol causes marked changes in the mechanical and physical properties of the alloy than the hot working technique (Alam *et al.*, 2007). This results in a finished shape with enhanced mechanical properties.

2.4.2 Mechanical Properties of SMA

Tables 2-3 and 2-4 provide mechanical and physical properties of various SMAs, pointing to the superiority of NiTi versus other alloys. The NiTi alloy has higher yield and ultimate strengths as well as better failure elongation and recoverable strain. Yet, the properties of NiTi SMAs can vary greatly. A slight shift in the Ni/Ti ratio or minor modifications to the manufacturing process can make great variations, even for the same alloy. For instance, the addition of a third metal to NiTi to compose a threefold alloy can result in desirable properties for specific applications. For example, Copper based alloy (NiTiCu) has lower hysteresis associated with phase transformations, which makes it a better choice for actuator applications. Likewise, Niobium based alloy (NiTiNb) has wider thermal hysteresis, associated with minimal response to large temperature changes and is preferred for coupling applications. It is possible to obtain SMAs for applications operating at high temperatures by adding to NiTi a third element such as palladium, platinum, hafnium, and gold (Ozbulut *et al.*, 2011). This sensitivity makes careful planning necessary to choose SMA that is optimal for a given application.

Table 2-3: Mechanical properties of various SMAs

Type	E_y (GPa)	f_y (MPa)	f_u (MPa)	\mathcal{E}_u (%)	\mathcal{E}_{PI} (%)	f_{PI} (MPa)	Source
NiTiNb	21	-	1270	10.6	-	-	Kim <i>et al.</i> (2015)
NiTiFe	-	688	1443	10	8	-	Memry Corp. (2015)
TiNiCu	15-16	300	-	-	4.5-7.5	280-700	Liu (2003)
FeMnSiCr	140-170	200	650	8-29	3.4:5	-	Maruyama <i>et al.</i> (2008), Janke <i>et al.</i> (2005)
CuZnAl	70-100	150-350	400-900	10-15	3.5	-	Janke <i>et al.</i> (2005)
FeMnAlNi	-	-	1200	-	13	-	
CuAlNi	80-100	150-300	500-1200	8-10	2	-	
CuAlBe	25	110-210	-	-	8-10	220	Rejzner <i>et al.</i> (2002)

Table 2-4: Mechanical and physical properties of Ni-Ti alloy

Property	Phase	Range	Unit	Source
Young's modulus, E_y	Austenite	30-98	GPa	Kim <i>et al.</i> (2015), Hung and Yen (2014), Tang and Lui (2014), Alam <i>et al.</i> (2007), Janke <i>et al.</i> (2005)
	Martensite	14-52		
Yield strength, f_y	Austenite	100-800	MPa	
	Martensite	50-300		
Ultimate tensile strength, f_u	Austenite	800-1900	MPa	
	Martensite	800-2000		
Elongation at failure, \mathcal{E}_u	Austenite	5-50	%	
	Martensite	20-60		
Recovered pseudoelastic strain, \mathcal{E}_{PI}	Austenite	8 or less		
Maximum recovery stress, f_{PI}	Austenite	600-800	MPa	
Density	-	6.45	g/cm^3	
Coefficient of thermal expansion	Austenite	11×10^{-6}	$\text{cm/cm/}^\circ\text{C}$	
	Martensite	6.6×10^{-6}		
Resistivity	-	80-100	$\mu\Omega \text{ cm}$	Sharma <i>et al.</i> (2015)

In addition, **Fig. 2-5** exhibits typical stress-strain relationship of SMA (austenite or martensite) under tensile and compressive stresses (Alam *et al.*, 2007). The curve is composed of four linear branches that are connected by smooth curves. For simplicity, the linear branches are assumed to intersect by broken lines. The first line represents the elastic behaviour of the alloy at the start of the test, with a modulus of elasticity E_y until it reaches the pseudo-yield stress, f_y . A significant reduction in stiffness occurs after crossing f_y , where the modulus of elasticity, E_{PI} , decreases to about 10%–15% of E_y . Such stiffness is maintained up to a stress of f_{PI} and strain of \mathcal{E}_{PI} . As soon as it passes \mathcal{E}_{PI} , the specimen

becomes stiffer and its modulus of elasticity E_{P2} reaches about 50%-60% of E_y . Another pseudo-yield point, f_{P2} , occurs at a strain of ϵ_{P2} , which is followed by a pseudo-yield plateau with a modulus of elasticity E_u (3-8% of E_y) until failure occurs by reaching the ultimate stress, f_u , at a strain of ϵ_u . The stress-strain curve of SMA under shear and torsion follows a similar pattern to that of the stress-strain curve under tension/compression.

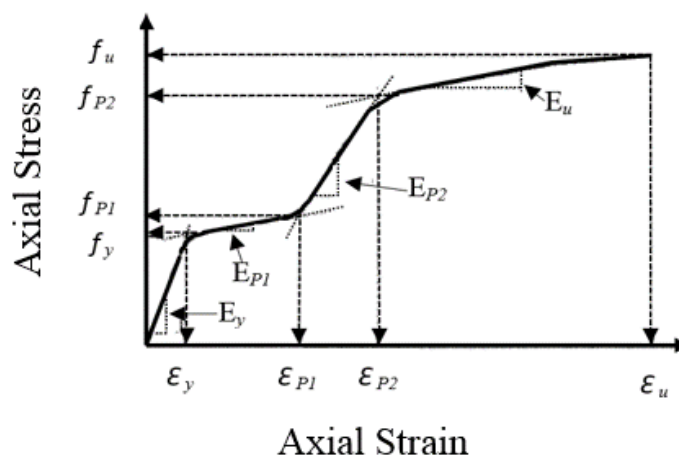


Figure 2-5: Typical stress-strain curve of SMA under tension/compression (reprinted from Alam *et al.*, 2007, with permission from NRC research press).

SMA's are mostly known for their ability to revert to their initial shape upon heating from their low temperature state, or martensite, to the high temperature phase, or austenite. Depending on the crystal orientation direction, martensite can exist in two forms; twinned (TM) or de-twinned (DM). These two phases have different mechanical properties and can be transformed into each other under different stress and thermal conditions. **Figure 2-6** shows a stress-strain curve of SMA's at different temperatures. In the parent phase, austenite occurs at high temperature and its crystal structure has a high order of symmetry. In the martensitic phase, it is stable at low temperatures and under high stresses. The unique ability of SMA's to recover its shape is due to the ordered crystalline structure between the austenitic and martensitic phases. SMA's could be transformed from austenite to martensite either by reducing the temperature or by applying a mechanical stress and vice versa. The four temperatures that define the SMA's transformation from one phase to the other (**Fig. 2-6**) are: austenite start temperature (A_s), where the austenite starts to develop in the alloy;

austenite finish temperature (A_f), where the development of austenite is 100% complete; martensite start temperature (M_s), where the development of martensite starts; and martensite finish temperature (M_f), where the development of martensite is 100% complete.

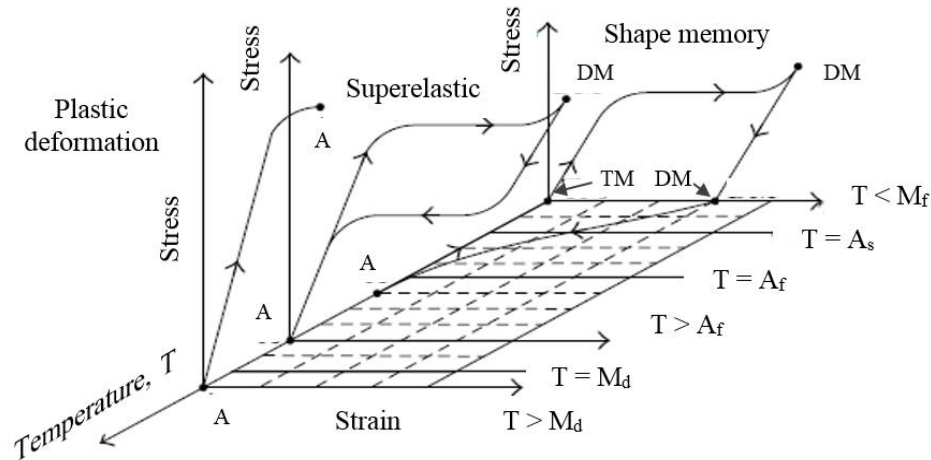


Figure 2-6: Typical stress-strain curve of super-elastic SMA at different temperatures (reprinted from Dolce and Cardone 2001, with permission from Elsevier).

2.4.3 Unique Characteristics of SMA

SMA has two unparalleled characteristics, which grant this material superior behaviour: the shape memory effect (SME) and super-elasticity (SE). SME or super-plasticity is a characteristic that shows thermo-elastic phase transformation. It is defined as the ability of the alloy to recover its original shape after being deformed via thermal cycling. Through shape training (ability to change the alloy into a desired shape), the material has the ability to memorize a very specific physical configuration or shape in either the martensite or austenite phase. The key to the SME is the build-up of residual stress fields within the SMA by deforming the material plastically, and then these stress fields control the phase transformation. The magnitude of the temperature-induced strains depends on the applied stress. If martensite SMAs are strained beyond their elastic point, a residual strain results when the stress is removed. Upon raising the temperature of the alloy above the A_f , this strain is recovered. This phenomenon is known as the one-way effect and can be used to recover, with negligible residual deformation, strains of up to 8%. Some alloys such as

NiTi-SMA can show two-way effect (Jani *et al.*, 2014), which is the ability of the alloy to remember a shape at low temperature and a different shape at high temperature and can repeatedly transition between the two when heated or cooled. However, two-way shape memory effect is less applied commercially due to the training requirements and to the fact that it usually produces about half of the recovery strain provided by the one-way shape memory effect and its strain recovery tends to deteriorate, especially at high temperatures.

On the other hand, PE is the ability of the alloy to accommodate large strains (up to 8%) due to stress-induced phase change at a sufficiently high temperature and recover its initial shape upon unloading. If a sufficiently high stress is applied to the alloy when it is in the austenite phase or by other meaning when the temperature is higher than A_f , the SMA transforms into the de-twinned (DM) form. When the load is released, a reverse transformation to the austenite state takes place, which results in complete shape recovery and a substantial hysteretic loop. The typical flag shaped hysteresis of super-elastic SMAs is shown in **Fig. 2-6**. Furthermore, if the temperature is below the A_f , but above its start temperature, there will only be partial shape recovery. Also, if the temperature in the austenite phase exceeds the maximum temperature at which martensite occurs, M_d , the alloy is stabilized in the austenite phase and the martensitic transformations cannot be induced by loading, thus the PE of SMA is completely lost, as shown in **Fig. 2-6**.

In recent years, SMA has been used for the seismic retrofit of buildings owing to its unique shape memory effect and super-elastic behaviour. When a SMA specimen is subjected to a cycle of deformation within its SE strain range, it dissipates a certain amount of energy without permanent deformation. This results from the phase transformation from austenite to martensite during loading and the reverse transformation during unloading, showing a net release of energy. When SMA is loaded in the martensite phase, it yields at a nearly constant stress after initial elastic deformation and displays strain hardening at larger strains. Upon unloading, there remains some residual strain at zero stress. This martensitic composition of SMA generates a full hysteresis loop. Thus, martensite SMA dissipates a much higher amount of energy compared to that of the austenite phase due to its larger hysteresis loop.

2.4.4 Modeling SMA

Several constitutive models that simulate the behaviour of SMA have been proposed. Such models can be characterized as: (i) Phenomenological macroscopic constitutive models in terms of stress, strain, temperature with assumed phase transformation kinetics described by pre-established simple mathematical functions proposed for instance by Sun and Rajapakse (2003); (ii) One-dimensional polynomial models which allow super-elasticity and SME description, presented by Falk and Konopka (1990); (iii) Thermodynamic models based on the free energy and dissipation potential developed by Huang and Brinson (1998); and (iv) Plastic flow models based on dislocation theories of solid state physics presented by Zhang and Zhu (2007).

2.4.4.1 Phenomenological and Thermo-Dynamical Models of SMA

Although three dimensional (3D) constitutive models are available, 1D models are more common since they are able to characterize the behaviour of SMAs in their most predominant form, which is the wire form. In recent years, the modeling of SME and PE behaviour has been an active area of research. The constitutive models of SMAs are more commonly represented by phenomenological or thermos-dynamical approaches.

The phenomenological modeling is essentially a macroscopic approach, which attempts to capture the SMA's response at the macroscopic level using phenomenology. In these models, the material's parameters are defined based on SMA experimental tests and vary in number with the complexity of the model. Phenomenological models of SMA have been utilized in several finite element software packages such as ANSYS (Moradi and Alam, 2015), Opensees (Zafar and Andrawes, 2015), VecTor2 (Abdulridha *et al.*, 2013), ABAQUS (Ghassemieh *et al.*, 2012), and SeismoStruct (Billah and Alam, 2012). In the field of civil engineering, SMAs are mostly used as bars and wires. Several phenomenological models have been proposed to capture the response of SMA due to their relative simplicity and accuracy.

On the other hand, thermomechanical models have been developed based on the micromechanics theory and crystallographic data used to estimate the evolution of martensitic transformation (Alam *et al.*, 2007). One of the first thermomechanical models

of SMAs was developed by Muller (1979). This model was based on potential energy principles. Tanaka and Nagaki (1982) expanded this model by considering the temperature and stress effect on the potential energy. Following the same concepts, several models have been proposed, some of which are presented by Patoor *et al.* (1996) and Huang and Brinson (1998). Unfortunately, these models proved to be impractical for design because they were based on thermomechanical parameters that are extremely difficult to obtain. SMA thermomechanical-models used in SMA composites were studied by Zak *et al.* (2003) who compared the uniaxial version of several models. This study found that the Brinson's model performed well and is recommended for modeling super-elastic SMAs in composites. Generally, micromechanical constitutive models are more complex and computationally intensive than phenomenological models because they present a highly sensible technique to derive accurate three-dimensional constitutive law. Consequently, one-dimensional phenomenological models are often considered suitable.

2.4.4.2 Modelling of SMA in Civil Structures

Several researchers have conducted series of experiments on SMAs and developed several related models. For instance, Moradi and Alam (2015) generated and analyzed 3D models for beam-column connection using the FE software ANSYS to capture the SE behaviour. The SE behaviour of SMA was simulated using Auricchio's (2001) model where the material undergoes large strain without showing permanent deformation under isothermal conditions. The FE model was verified by comparing the cyclic behaviour of the steel beam-column connection model with previous experimental results. Moreover, Zafar and Andrawes (2015) modeled a 2-D three-story one-bay RC moment resisting frame (MRF) using the OpenSees software to investigate the behaviour of steel and SMA-FRP composite reinforcement under the effect of sequential ground motions. SMA uniaxial material model "Pinching4" available in the OpenSees library was used to represent the behaviour of SMA wire. Parallel material command was employed to link the epoxy and SMA/glass fibre material models in which the strains are equal, while stresses and stiffness are additive. It was concluded that the proposed model incorporating SMA-based wires was simple and effective in estimating the response of a building frame under the effect of sequential ground motions.

Furthermore, a numerical model presented by Abdulridha *et al.* (2013) utilizing the VecTor2 program was developed to assess cyclically loaded SMA reinforced beams. Rectangular plane stress elements were used to represent the concrete; truss bar elements were used to model the longitudinal reinforcement and the transverse shear reinforcement was smeared within the concrete elements. The results obtained from the numerical investigation were compared to that experimentally acquired. It was concluded that the proposed preliminary model consisting of a series of linear segments provided reasonable simulations, indicating its applicability to SMA reinforced members. Also, the behaviour of shear walls subjected to seismic excitations was investigated numerically by Ghassemieh *et al.* (2012). They introduced two ordinary and coupled shear walls modeled by the finite element (ABAQUS) software as reference structures. The SMA material was defined in ABAQUS via a FORTRAN subroutine material model attached to the main program. The dynamic response of the shear walls subjected to seismic loading was investigated through time history analyses under El-Centro and Koyna earthquake records. It was concluded that the model was successful in estimating the increased displacement capacity of the tested shear walls, especially the one reinforced with SMA.

On the other hand, Billah and Alam (2012) conducted an analytical investigation on the effects of seismic loading on the plastic hinge region at the base of columns using a finite element (FE) program (SeismoStruct). The fibre modeling approach was employed to represent the distribution of material nonlinearity along the length and cross-sectional area of the member. SMA was modeled per the model of Auricchio and Sacco (1997) as in Alam *et al.* (2009). They tailored the columns such that SMA or stainless steel bars are used at the base and FRP or stainless steel rebar are located in the rest of the structural member. They found that the model could consider both geometric nonlinearities and material inelasticity and can predict large displacements.

2.4.5 Restrictions on Utilizing SMA

SMA reinforced elements could allow structural engineers to design RC members displaying little damage and mitigating structural repairs. In recent years, there have been substantial research on the applicability of SMAs as partial/total replacement of conventional steel in new structural applications such as dampers, bearings, beams,

columns, and connections. **Table 2-5** summarizes some of these applications. However, there are certain hurdles currently hindering the usage of smart materials generally and SMAs specifically in structural applications. These include cost, lack of knowledge of mechanical properties, and difficulties in joining technology.

The cost of SMAs is perceived to be high, which is a major reason for the relatively slow development of its civil engineering applications. This is particularly true for NiTi, which is one of the costliest SMAs. Consequently, low cost Cu and Fe based SMAs have attracted interest, despite their inferior performance. Considering commodity prices for metals and comparing the cost of Ni and Ti versus that of Fe, Mn, Si, and Cr on the other hand, the ratio is about 8 to 12. This means that the cost of an iron-based SMA could be a fraction of that of the high-performance Ni-Ti system. Nevertheless, the use of SMA composites could lead to economically viable solutions. One could achieve a great effect on the behaviour of structures even if the unique properties of NiTi are utilized only in small devices or selected regions of the structure (Nehdi *et al.*, 2010). SMA dampers, isolation devices and bracings have proven to be of the same order of cost as that of conventional steel devices. With increased demand and streamlined production, the cost of SMAs has and will continue to drop, which will continue to increase its applications. Furthermore, providing buildings with re-centering properties can prevent damage in other structural systems. That is, SMA applications can reduce economic losses and minimize human risks associated with natural disasters such as earthquakes. Li *et al.* (2013) contended that developing low-cost Fe-based SMAs with improved properties can lead to significant reduction in the fabrication and final cost of SMA. SMA devices have been desirable because they do not require additional maintenance or replacement costs. Therefore, there has been growing research interest over the past decade on utilizing SMA in civil engineering applications.

Table 2-5: Utilizing SMA in new structural applications

Application	Main Findings	Reference
Partial/total replacement of steel reinforcement	<ul style="list-style-type: none"> The performance of moment resisting frames reinforced with hybrid steel-SMA was better than that reinforced with steel or SMA alone by about 30% in terms of spectral acceleration and effective damping. SMA-reinforced beams could fail under cyclic loading due to fracture of the SMA-steel connection. Beam-column connections reinforced with SMA bars had adequate energy dissipation under earthquake loading and could carry 89% of its load capacity beyond the collapse limit. 	Bajoria and Kaduskar (2015), Hung and Yen (2014), Nehdi <i>et al.</i> (2010)
Active confinement for columns	<ul style="list-style-type: none"> SMA confined-columns had enhanced strength and ductility due to the ability of the SMA spirals to apply active confining pressure on the damaged region of the columns and increasing its ultimate strain. Using a simple method for heating SMA wires (flame torch), activated the alloy to apply the confinement pressure on damaged columns similar to that of the wires heated utilizing thermal changers. SMA wire jackets can be installed manually (low cost) and introduce active confinement via heating, avoiding both corrosion problems of steel jackets and FRP jackets failure problems. 	Shin and Andrawes (2011), Choi <i>et al.</i> (2010)
Dampers	<ul style="list-style-type: none"> The damping capability of SMA could be used to improve the seismic behaviour of cable-stayed bridges. The synergistic effect of SMA can significantly reduce both the peak and residual story drifts of RC frames and has potential to bring the frame back to its original configuration upon frequent earthquakes. SMA dampers were able to reduce RC bridge base shear, bending moment, and maximum displacement by about 65%, 69%, and 65%, respectively, compared to that of bridges made without SMA dampers. 	Tang and Lui (2014), Mortazavi <i>et al.</i> (2013)
Bearings	<ul style="list-style-type: none"> Utilizing a combination of SMA and ECC in bridge bearings could keep the bridge in service after exposure to the maximum design earthquake, therefore minimizing economic losses due to earthquakes. SMA-bridge bearings have base shear lower than that of traditional steel-reinforced bearings by about 59%. SMA rubber bearing could recover up to 95% of its original shape and decrease deck-pier relative displacement. 	Noguez <i>et al.</i> (2013), Khodaverdian <i>et al.</i> (2012)
Bracings	<ul style="list-style-type: none"> Steel frames braced with SMA can reduce storey drifts and eliminate residual drift. Steel frames equipped with SMA braces could substantially reduce the peak relative displacements and peak accelerations of the frame. SMA-braces could enhance seismic performance of frames similar to that of steel braces, while having an additional self-centering feature. 	Boroschek <i>et al.</i> (2007), Zhu (2007b)
Actuators and restrainers	<ul style="list-style-type: none"> SMA restrainers could significantly reduce the relative hinge displacements compared to steel restrainers. SMA could transfer larger force to bridge frames than that transferred by traditional steel cable restrainers. SMA restrainer was effective in limiting movements of bridge decks subjected to near-field ground motion. 	Cho <i>et al.</i> (2005), DesRochs and Delemont (2002)

There are several other problems preventing wider usage of SMAs in structural applications. For instance, SMA can be heated using electric current for actuation. But short activation times in the range of seconds are not yet possible for large cross-sections. A high capacity power supply with a current of several hundred Amperes is needed to considerably reduce activation times (Janke *et al.*, 2005), which would not be practical and can cause greater costs for setting up the actuator and keeping up the high temperature state for long time. Another difficulty regarding the application of SMA is the machining of large diameter bars using conventional equipment, due to the SMA high hardness.

Designing civil engineering structures requires proper knowledge of the engineering properties of the material to be used. The mechanical properties of SMA largely depend on the heat-treatment temperature, where a slight variation can cause significant changes in properties. To implement wider use of SMA in the construction industry, manufacturers are required to produce SMAs in mass scale with proper control of its properties and transformation temperatures. The poor ductility of Cu-based alloys, poor shape recovery and lower shape recovery stress of Fe-based alloys are two major problems which prevent such alloys from wider use in civil engineering applications (Alam *et al.*, 2007). Other problems include difficulty in welding and machining. There is a lack of welding technology for joining SMA bars to each other or to steel. Zhou *et al.* (2012) reported on the joining of Fe-based SMA using crossflow laser welding. At this point, an effective SMA welding technology is not readily available.

2.5 FULL SCALE APPLICATIONS OF ECC AND SMA

ECC was originally developed for earthquake resistant structures. It has since been applied in full-scale buildings, transportation, water and energy infrastructure, and for enhanced safety, durability and sustainability (Zhang and Li, 2014) owing to its unique characteristics. Some ECC and SMA structural applications are outlined in **Table 2-6**. There are more than 10,000 SMA related patents proposed in many sectors (Jani *et al.*, 2014), such as biomedical (artificial muscles, toxic free SMAs and SMA implants), micro-electromechanical systems (rotary robotics, fast and accurate actuators), automotive and aerospace (dampers, high temperature actuators, smart tire and airbags). SMAs have also

been applied in medicine, for example, as fixation devices for osteotomies in orthopedic surgery and in dental braces to exert constant tooth-moving forces on the teeth.

Table 2-6: Full-scale structural applications of ECC and SMA

Material	Application	Reference
ECC	<ul style="list-style-type: none"> • Precasting of R/ECC coupling beams in the core of Glorio Roppongi high-rise R/C residential building in central Tokyo. • Precasting of ECC beams in the 41 storey Yokohama tower in Japan. • ECC permanent formwork. • Utilizing ECC material as a binder in radioactive waste treatment. • Cast-in-place ECC link slabs in bridge decks in the United States. • ECC covering layers in Mihara Bridge, Hokkaido, Japan. • Repairing of Mitaka Dam and irrigation channel in Hiroshima, Japan. • Repairing a damaged earth retaining wall in Gifu, Japan. • Utilizing ECC in tunnel linings in South Korea, and for prototype pipe extrusion in Australia. • Retrofitting of existing bridge-deck link slab in Michigan, USA. • Patching railway viaducts in Shizuoka, Japan. 	Lepech and Li (2009), Li <i>et al.</i> (2009), CCEH (2008), Wu <i>et al.</i> (1996)
SMA	<ul style="list-style-type: none"> • Earthquake resistant retrofit of 17 m tall masonry San Giorgio Church Bell-Tower, Italy. • Enhancing shear resistance of a cracked region of RC bridge girder in Michigan, USA. • Hydraulic line couplings for jet fighters in the 1970's. • Earthquake resistant retrofit of Basilica San Francesco at Assisi, Italy. 	Ingalkar (2014), Motavalli <i>et al.</i> (2009), Song <i>et al.</i> (2006), Janke <i>et al.</i> (2005)

Furthermore, SMA was proposed for safety devices. Anti-scalding devices and fire-sprinklers utilizing SMAs are already commercialized. Anti-scalding valves can be used in water faucets and shower heads. Beyond a certain temperature, the device automatically shuts off the water flow. Aircraft companies, such as Boeing and General Electric Aircraft Engines, developed the “Variable Geometry Chevron” using SMA to reduce the aircraft engine noise (Wang and Wu, 2012). Also, the military has been using NiTi couplers in F-14 fighter jets since the late 1960s (Gupta *et al.*, 2012). These couplers join hydraulic lines tightly and easily. SMAs are not only used in the engineering community, but also in the arts field. SMAs have been used as actuation materials to move sculptress. Thin SMA wire rises and falls upon heating and power cutoff respectively in artificial mimosa. Similarly, very thin SMA wire can be used to design artificial wigs (Sharma *et al.*, 2015), which are capable to suddenly change styles, e.g., from straight to curly.

2.6 SMA REINFORCED ECC ELEMENTS

Over the last few decades, substantial research has explored the materials science and possible uses of SMAs in structural applications, most of which focused on the applicability of utilizing SMA as bars and wires. Reinforcing ECC structural elements with SMA bars has been explored by several researchers. For instance, Noguez *et al.* (2010) produced a numerical model to evaluate the performance of ECC bridge pier reinforced by SMA bars as compared to traditional RC and SMA-RC piers based on earlier investigation by Saiidi *et al.* (2009). To validate their results, Noguez and Saiidi (2013) developed full-scale details for three unconventional plastic hinge regions of bridge columns subjected to seismic loads. They used post-tensioned columns and elastomeric bearings in three different piers made with ECC reinforced by SMA bars to improve the seismic performance of the bridge in terms of minimizing damage and reducing residual displacements. The columns were subjected to a series of biaxial earthquake excitations with increasing amplitudes. The experimental results showed that a combination of SMA and ECC or built-in shimmed elastomeric pads with de-bonded bars could keep the bridge in service after exposure to the maximum design earthquake, thus minimizing economic losses due to earthquakes.

Utilizing SMA bars as reinforcement for structural elements exhibits extraordinary performance in energy dissipation, ductility, strain recovery, and minimizing damage and residual displacement. However, it was observed that using SMA wires is more practical and efficient than using SMA bars for the following reasons; (i) Producing small-size SMA wires is easier and more cost-effective compared to producing large-size SMA bars. (ii) The hysteretic damping capability of SMAs decreases significantly with the increase in bar diameter. (iii) Threading large diameter bars for connections reduces the strength of SMA due to its sensitivity to notches (Zafar and Andrawes, 2014; Wierschem and Andrawes, 2010).

By taking into consideration the aforementioned drawbacks, a new technique of smart self-repairing concrete beams with damage self-repairing performance was proposed by Sakai *et al.* (2003). They used SMA wires as main reinforcement for the concrete beams to enable large cracks propagated during loading to be mechanically closed after unloading. The

same concept was followed by Kuang and Ou (2008). They embedded SMA wires and brittle fibres into concrete during fabrication to form a smart self-repairing concrete. To obtain sufficient adhesive for repairing cracks, the fibres were connected with a vessel by rubber pipes containing a repairing adhesive that can be supplied. In the presence of damage and cracks due to earthquakes, fibres around the cracked areas rupture. Once the loads are removed, the super-elasticity of SMA wires can recover deflections and deformations of the structural member. At the same time, the switch of the repairing vessel containing the adhesive is turned on and repairing adhesives flow out from the broken open fibres to fill/repair cracks. Moreover, Li *et al.* (2015) conducted a series of cyclic loading tests on small scale flexure beams made of ECC reinforced by SMA wires, RC, ECC, and SMA-RC. The SMA-ECC beam achieved superior energy dissipation capability, reduced residual deformation, enhanced strain capacity, minimized micro-crack width, and full self-repairing compared to its counterparts. The unique ductile feature of ECC in synergy with the super-elasticity characteristic of SMA wires exhibited great promise in enhancing the resilience of structural members under extreme loading events without relying on steel reinforcement.

Although numerous researchers have reported the usefulness of utilizing SMA wires in concrete, only a few have reported the use of SMA fibres for crack repairing. Short fibres have advantages over continuous wires in that the distribution of fibres is more uniform; thus, they enable local crack closing in any direction. Also, if SMA fibres could be used instead of straight tendons or wires, then thin or curved shaped SMA reinforced structural members could be easily constructed. Incorporation of SMA fibres in composite systems was introduced by Birman *et al.* (1996). Thereafter, Moser *et al.* (2005) explored the pre-stressing ability of loop- and star-shaped SMA fibres imbedded in cement mortar specimens. They found that a major prestress (about 7 MPa) was obtained in the paste specimens at the age of 7 days stimulating the alloy fibres via heating. Following a similar concept, Freed and Aboudi (2008) developed thermos-micromechanical framework to simulate the pre-stressing ability of SMA-fibre-reinforced matrix (SMAF-M) specimens. It was observed that the proposed framework could capture the tensile and compressive responses of the prestressed composite with adequate accuracy. Likewise, Shajil *et al.* (2013) investigated the self-centering capability of SMAF-M beams under cyclic loading.

The test specimens achieved a self-centering factor of 0.7 compared to only 0.1 acquired by its counterpart made with steel fibres. Recently, Kim *et al.* (2016) performed uniaxial tensile tests on prestressed SMAF-M coupon specimens. It was observed that the used prestressing technique enhanced the tensile elastic modulus of the composite while it decreased its tensile capacity compared to that of normal SMAF-M specimens.

The investigations above provide valuable information for implementing SMA fibres in real concrete structures. However, further work needs to be carried out on other aspects such as utilizing micro-short SMA fibres in structural elements and how that could affect the overall structural performance under static and dynamic stimulus such as explosions and impact loads (Ali and Nehdi, 2017; Ali *et al.*, 2017). Producing hybrid-ECC elements incorporating micro SMA and PVA short fibres could be a promising alternative for mono-PVA-ECC and traditional RC elements. Also, producing numerical models capable of capturing the performance of such innovative composite under extreme events such as explosions, seismic and impact loading, is needed to minimize the cost and complications involved in purely experimental investigations.

2.7 CONCLUSIONS

This chapter discussed the engineering properties and potential civil infrastructure applications of engineered cementitious composites and shape memory alloys, with particular focus on creating possible synergy between these two materials to coin resilient structures that can withstand extreme load events under explosive, seismic or impact excitation. Based on this discussion, the following conclusions are drawn:

- Owing to its superior impact resistance compared to that of conventional concrete, ECC is a promising material for the construction of protective civilian and defense structures.
- ECC can be a sustainable construction option requiring less energy consumption and generating less CO₂ emissions, particularly when it uses recycled by-products. It would also need less maintenance, repair and replacement.

- Ductile ECC structural elements could be produced with self-centering capability by incorporating SMA as partial or total replacement for traditional steel reinforcement.
- SMA was utilized in several structural applications in the form of bars or wires. However, the usage of SMA fibres in structural applications still needs further investigation.
- The material cost, activation technique, difficulty of welding and strength degradation due to threading are chief problems preventing wider usage of SMA in structural applications.
- Further investigations are required on using SMA fibres in structural elements. Incorporation of SMA short fibres in the production of hybrid-fibre-reinforced ECC elements has not been duly investigated. Such composite could achieve unique behaviour under static and dynamic loadings, possibly achieving major gains in structural performance and safety.

2.8 REFERENCES

- Abdulridha, A., Palermo, D., Foo, S., and Vecchio, F.J., "Behavior and modeling of superelastic shape memory alloy reinforced concrete beams." *Engineering Structures*, 49(2013), pp. 893-904.
- Adhikary SD., Li, B., and Fujikake, K., "Residual resistance of impact-damaged reinforced concrete beams." *Magazine of Concrete Research*, 67(7), 2015, pp. 364-378.
- Adhikary SD., Li, B., and Fujikake, K., "State-of-the-art review on low-velocity impact response of reinforced concrete beams." *Magazine of Concrete Research*, 68(14), 2016, pp. 701-723.
- Alam, M.S., Nehdi, M., and Youssef, M.A., "Seismic performance of concrete frame structures reinforced with super-elastic shape memory alloys." *Smart Structures and Systems*, 5(5), 2009, pp. 565-585.

- Alam, M.S., Youssef, M.A., and Nehdi, M., "Utilizing shape memory alloys to enhance the performance and safety of civil infrastructure: a review." *Canadian Jr. of Civ. Eng.*, 34(9), 2007, pp. 1075-1086.
- Alhadid, M.M.A., Soliman, A.M., Nehdi, M.L., and Youssef, M.A., "Critical overview of blast resistance of different concrete types." *Magazine of concrete research*, 66(2), 2014, pp. 72-81.
- Ali, M.A.E.M. and Nehdi, M.L., "Innovative self-healing hybrid fiber reinforced engineered cementitious composite." *Construction and Building Materials*, 150, 2017, pp. 689-702.
- Ali, M.A.E.M., Nehdi, M.L., and Soliman, A.M., "Exploring behavior of novel hybrid-fiber reinforced engineered cementitious composite under impact loading." *Materials and Design*, 117, 2017, pp. 139-149.
- Auricchio, F., "A robust integration-algorithm for a finite-strain shape-memory-alloy." *International Journal of Plasticity*, 17(7), 2001, pp. 971-990.
- Auricchio, F., and Sacco, E., "A Superelastic shape-memory-alloy beam model." *Journal of Intelligent Material Systems and Structures*, 8(6), 1997, pp. 489-501.
- Bajoria, K.M., and Kaduskar, S.S., "Improvement in performance of reinforced concrete structures using shape memory alloys." *Active and Passive Smart Structures and Integrated Systems*, 9431(2015), 7 p.
- Billah, A.H.M.M., and Alam, M.S., "Seismic performance of concrete columns reinforced with hybrid shape memory alloy (SMA) and fibre reinforced polymer (FRP) bars." *Construction and Building Materials*, 28(1), 2012, pp. 730-742.
- Birman, V., Saravanis, D.A., and Hopkins, D.A., "Micromechanics of composites with shape memory alloy fibers in uniform thermal fields." *Inst. of Aeronautics & Astronautics Jr*, 34(9), 1996, pp. 1905-1912.

- Black, L. and Purnell, P., "Is carbon dioxide pricing a driver in concrete mix design?" *Magazine of Concrete Research*, 68(11), 2016, pp. 561-567.
- Boroschek, R.L., Farias, G., Moroni, O., and Sarrazin, M., "Effect of SMA braces in a steel frame building." *Journal of Earthquake Engineering*, 11(3), 2007, pp. 326-342.
- Buehler, W.J., and Wang, F.E., "A summary of recent research on the nitinol alloys and their potential application in ocean engineering." *Journal of Ocean Engineering*, 1(1), 1968, pp.105-120.
- Cho, J.W., Kim, J.W., Jung, Y.C., and Goo, N.S., "Electroactive shape-memory polyurethane composites incorporating carbon nanotubes." *Macromolecular Rapid Communications*, 26(5), 2005, pp. 412-416.
- Choi, E., Cho, S-C., Hu, J.W., Park, T., and Chung, Y-S., "Recovery and residual stress of SMA wires and applications for concrete structures." *Smart Materials and Structures*, 19(2010), 10 p.
- Choi, E., Hu, J.W., Lee, J-H., and Cho, B-S., "Recovery stress of shape memory alloy wires induced by hydration heat of concrete in reinforced concrete beams." *Journal of Intelligent Material Systems and Structures*, 26(1), 2015, pp. 29-37.
- Concrete Construction Engineering Handbook (CCEH), "Engineered cementitious composite (ECC): material, structural, and durability performance," Li, V., Taylor, and Francis, 2008.
- Debbarma, S.R, and Saha, S., "Review of Shape Memory Alloys applications in civil structures, and analysis for its potential as reinforcement in concrete flexural members." *International Journal of Civil and Structural Engineering*, 2(3), 2012, pp. 924-942.
- Dhawale, A.W., and Joshi, V.P., "Engineered cementitious composites for structural applications." *Application or Innovation in Engineering and Management*, 2(4), 2013, pp. 198-205.

- Dolce, M. and Cardone, D., “Mechanical behaviour of shape memory alloys for seismic applications 1. Martensite and austenite Ni–Ti bars subjected to torsion.” *International Journal of Mechanical Sciences*, 43, 2001, pp. 2631-2656.
- El-Chabib, H. and Nehdi, M., “Neural network modelling of properties of cement-based materials demystified.” *Advances in Cement Research*, 17(3), 2005, pp. 91-102.
- Falk, F., and Konopka, P., “Three-dimensional Landau theory describing the martensitic transformation of shape memory alloys.” *Journal de Physique: Condensed Matter*, 2(1), 1990, pp. 61-77.
- Freed, Y. and Aboudi, J., “Micromechanical investigation of plasticity-damage coupling of concrete reinforced by shape memory alloy fibers.” *Smart Materials and structures*, 17(1), 2008, pp. 1-14.
- Gencturk, B., Elnashai, A.S., Lepech, M.D., and Billington, S., “Behavior of concrete and ECC structures under simulated earthquake motion.” *Journal of Structural Engineering*, 139(3), 2013, pp. 389-399.
- Ghassemieh, M., Bahaari, M.R., Ghodrati, S.M., and Nojoumi, S.A., “Improvement of concrete shear wall structures by smart materials.” *Open Journal of Civil Engineering*, 2(2012), pp. 87-95.
- Gupta, P.K., Seena, P., and Rai, R.N., “Studies on shape memory alloys—a review.” *Intern. Journal of Advanced Engineering Technology*, 3(1), 2012, pp. 378-382.
- Halvaei, M., Jamshidi, M., and Latifi, M., “Application of low modulus polymeric fibers in engineered cementitious composites.” *Journal of industrial textile*, 43(4), 2014, pp. 511-524.
- Han, T-S., Feenstra, P.H., and Billington, S.L., “Simulation of highly ductile fiber-reinforced cement-based composites under cyclic loading.” *ACI Structural Journal*, 100(6), 2003, pp. 749-757.

- Hewayde, E., Nehdi, M., Allouche, E., and Nakhla, G., “Neural network prediction of concrete degradation by sulphuric acid attack”, *Structure and Infrastructure Engineering*, 3(1), 2007, pp. 17-27.
- Hossain, K.M.A., and Samani, S.G., “Prediction of strength properties of engineered cementitious composites using artificial neural network.” *Building on Our Growth Opportunities: Proceedings of Canadian Society for Civil Engineering Annual Conference*, Regina, SK, 27-30 May, 2015, 10 p.
- Hung, C-C., and Yen, W-M., “Experimental evaluation of ductile fiber reinforced cement-based composite beams incorporating shape memory alloy bars.” *Procedia Engineering*, 79(2014), pp. 506-512.
- Huang, M.S., and Brinson, L.C., “A multivariant model for single crystal shape memory alloy behavior.” *Journal of the Mechanics and Physics of Solids*, 46(8), 1998, pp.1379-1409.
- Huang, X., Ranade, R., Ni, W., and Li, V.C., “On the use of recycled tire rubber to develop low E-modulus ECC for durable concrete repairs.” *Construction and Building Materials*, 46(2013), pp. 134-141.
- Ingalkar, R.S., “Rehabilitation of buildings and bridges by using shape memory alloys (SMA).” *International Journal of Civil Engineering Research*, 5(2), 2014, pp. 163-168.
- Jani, J.M., Leary, M., Subic, A., and Gibson, M.A., “A review of shape memory alloy research, applications and opportunities.” *Materials and Design*, 56(2014), pp. 1078-1113.
- Janke, L., Czaderski, C., Motavalli, M., and Ruth, J., “Applications of shape memory alloys in civil engineering structures – Overview limits and new ideas.” *Mat. & Struct.*, 38(279), 2005, pp. 578-592.

- Kesner, K., and Billington, S.L., "Investigation of infill panels made from engineered cementitious composites for seismic strengthening & retrofit." *Structural Eng.*, 131(11), 2005, pp. 1712-1720.
- Khodaverdian, A., Ghorbani-Tanha, A.K., and Rahimian, M., "An innovative base isolation system with Ni-Ti alloy and its application in seismic vibration control of Izadkhasht Bridge." *Journal of Intelligent Material Systems and Structures*, 23(8), 2012, pp. 897-908.
- Kim, D.J., Kim, H.A., Chung, Y-S., and Eunsoo Choi, E., "Pullout resistance of deformed shape memory alloy fibres embedded in cement mortar." *Intelligent Material Systems and Structures*, 2015, 12 p.
- Kim, M.K., Kim, D.J., Chung, Y-S., and Choi, E., "Direct tensile behavior of shape-memory-alloy fiber-reinforced cement composites." *Construction and Building Materials*, 102(2016), pp. 462-470.
- Kuang, Y., and Ou, J., "Self-repairing performance of concrete beams strengthened using superelastic SMA wires in combination with adhesives released from hollow fibers." *Smart Mat. Str.*, 17(2), 2008, 7 p.
- Lepech, M.D., and Li, V.C., "Application of ECC for bridge deck link slabs." *Journal of Materials and Structures*, 42(9), 2009, pp. 1185–1195.
- Li, H., Leung, C.K.Y., Xu, S., and Cao, Q., "Potential use of strain hardening ECC in permanent formwork with small scale flexural beams." *Jr. Wuhan University of Tech., Mat. Sci. Edition*, 24(3), 2009, pp. 482-487.
- Li, J., and Zhang, Y.X., "Evolution and calibration of a numerical model for modelling of hybrid fibre ECC panels under high-velocity impact." *Composite Structures*, 93(11), 2011, pp. 2714-2722.
- Li, K., Dong, Z., Liu, Y., and Zhang, L., "A newly developed Fe-based shape memory alloy suitable for smart civil engineering." *Smart Materials and Structures*, 22(4), 2013, 6 p.

- Li, V., Lepech, M., Wang, S., Weimann, M., and Keoleian, G., "Development of green engineered cementitious composites for sustainable infrastructure systems." *International Workshop on Sustainable Development and Concrete Technology*, 2004, pp. 181-192.
- Li, V.C., "On engineered cementitious composites (ECC): A review of the material and its applications." *Journal of Advanced Concrete Technology*, 1(3), 2003, pp. 215-230.
- Li, X., Li, M., and Song, G., "Energy-dissipating and self-repairing SMA-ECC composite material system." *Smart Materials and Structures*, 24(2), 2015, 15 p.
- Liu, Y., "Mechanical and thermomechanical properties of a $Ti_{50}Ni_{25}Cu_{25}$ melt spun ribbon." *Materials Science and Engineering: A*, 354(1), 2003, pp. 286-291.
- Maalej, M., Lin, V.W.J., Nguyen, M.P., and Quek, S.T., "Engineered cementitious composites for effective strengthening of unreinforced masonry walls." *Engineering Structures*, 32(8), 2010, pp. 2432-2439.
- Maalej, M., Quek, S.T., and Zhang, J., "Behaviour of hybrid-fibre engineered cementitious composites subjected to dynamic tensile loading and projectile impact." *Mat. in Civ. Eng.*, 17(2), 2005, pp. 143-152.
- Maruyama, T., Kurita, T., Kozaki, S., Andou, K., Farjami, S., and Kubo, H., "Innovation in producing crane rail fishplate using Fe–Mn–Si–Cr based shape memory alloy", *Materials Science and Technology*, 24(8), 2008, pp. 908-912.
- McWilliams, A., "Smart materials and their applications: technologies and global markets." *BCC Research Advanced Materials Report*, 2014, 140 pp.
- Memry Corporation. 2015. <http://www.memry.com/products-services/melting/nitinol-alloys>, Visited on 11 November, 2016.
- Mihashi, H., Ahmed, S.F.U., and Kobayakawa, A., "Corrosion of reinforcing steel in fiber reinforced cementitious composites." *Journal of Advanced Concrete Technology*, 9(2), 2011, pp. 159-167.

- Mindess, S., Banthia, N., and Benturt, A., "The response of reinforced concrete beams with a fiber concrete matrix to impact loading." *The International Journal of Cement Composites and Lightweight Concrete*, 8(3), 1986, pp. 165-170.
- Moradi, S., and Alam, M.S., "Feasibility study of utilizing superelastic shape memory alloy plates in steel beam-column connections for improved seismic performance." *Journal of Intelligent Material Systems and Structures*, 26(4), 2015, pp. 463-475.
- Mortazavi, S.M.R., Ghassemieh, M., and Motahari, S.A., "Seismic control of steel structures with shape memory alloys." *Automation and Control Engineering*, 2(1), 2013, pp. 28-34.
- Motavalli, M., Czaderski, C., Bergamini, A., and Janke, L., "Shape memory alloys for civil engineering structures-on the way from vision to reality." *Architecture Civil Engineering Environment*, 4(2009), pp. 81-94.
- Moser, K., Bergamini, A., Christen, R., and Czaderski, C., "Feasibility of concrete prestressed by shape memory alloy short fibers." *Materials and Structures*, 38(5), 2005, pp. 563-600.
- Muller, I., "A model for a body with shape-memory." *Arch. Rat. Mech. & Anal.*, 70(1), 1979, pp. 61-77.
- Naik, N.K. and Doshi, A.V., "Ballistic impact behavior of thick composites: parametric studies." *Composite Structures*, 82(3), 2008, pp. 447-464.
- Nehdi, M., Alam, M.S., and Youssef, M.A., "Development of corrosion-free concrete beam-column joint with adequate seismic energy dissipation." *Engineering Structures*, 32(9), 2010, pp. 2518-2528.
- Noguez, C.A.C., and Saiidi, M.S., "Performance of advanced materials during earthquake loading tests of a bridge system." *Journal of Structural Engineering*, 139(1), 2013, pp. 144-154.

- Noguez, C.A.C., Saiidi, M.S., and Hillis, D., “Analytical study of a 4-span bridge with advanced materials.” *4th International Workshop on Reliable Engineering Computing*, 2010, pp. 197-210.
- Qian, S., and Zhang, Z., “Comparison of tensile properties of strain hardening cementitious composite cured in normal and accelerated conditions.” *Journal of Testing and Evaluation*, 40(5), 2012, 6 p.
- Qudah, S., and Maalej, M., “Application of engineered cementitious composites (ECC) in interior beam–column connections for enhanced seismic resistance.” *Engineering Structures*, 69(2014), pp. 235-245.
- Ozbulut, O.E., Hurlbauss, S., and DesRoches, R., “Seismic response control using shape memory alloys: a review.” *Journal of Intelligent Material Systems and Structures*, 22(2011), pp. 1531-1549.
- Pan, Z., Wu, C., Liu, J., Wang, W., and Liu, J., “Study on mechanical properties of cost-effective polyvinyl alcohol engineered cementitious composites (PVA-ECC).” *Const. Build. Mat.*, 78(2015), pp. 397-404.
- Patoor, E., Eberhardt, A., and Berveiller, M., “Micromechanical modelling of superelasticity in shape memory alloys.” *Int. Seminar on Mechanics and Mechanisms of Solid-Solid Phase Transf.*, 6(1), 1996, pp. 277-292.
- Rejzner, J., Lexcellent, C., and Raniecki, B., “Pseudoelastic behaviour of shape memory alloy beams under pure bending: Experiments and modelling.” *Mechanical Sciences*, 44(4), 2002, pp. 665-686.
- Sadrmomtazi, A., Sobhani, J., and Mirgozar, M.A., “Modeling compressive strength of EPS lightweight concrete using regression, neural network and ANFIS.” *Const. & Build. Materials*, 42(2013), pp. 205-216.
- Sahmaran, M., and Li, V., “Engineered cementitious composites: can composites be accepted as crack-free concrete?” *Journal of the Transportation Research Board*, 2164(1), 2010, pp. 1-8.

- Sahmaran, M., Li, M., and Li, V.C., "Transport properties of engineered cementitious composites under chloride exposure." *ACI Materials Journal*, 104(6), 2007, pp. 604-611.
- Said, S.H., Razak, H.A., and Othman, I., "Flexural behavior of engineered cementitious composite (ECC) slabs with polyvinyl alcohol fibers." *Construction and Building Materials*, 75(30), 2015, pp. 176-188.
- Saiidi, M.S., O'Brian, M., and Zadeh, M., "Cyclic response of concrete bridge columns using superelastic nitinol and bendable concrete." *ACI Structural Journal*, 106(1), 2009, pp. 69-77.
- Sakai, Y., Kitagawa, Y., Fukuta, T., and Iiba, M., "Experimental study on enhancement of self-restoration of concrete beams using SMA wire." *Smart Structures and Materials*, 5057, 2003, pp. 178-186.
- Shahriar, A. and Nehdi, M.L., "Modeling rheological properties of oil well cement slurries using artificial neural networks." *Journal of Materials in Civil Engineering*, 23(12), 2011, pp. 1703-1710.
- Shajil, N., Srinivasan, S.M., and Santhanam, M., "Selfcentering of shape memory alloy fiber reinforced cement mortar members subjected to strong cyclic loading." *Mat. & Str.*, 46(4), 2013, pp. 651-661.
- Sharma, N., Raj, T., and Jangra, K.K., "Applications of Nickel-Titanium alloy." *Eng. & Tech.*, 5(1), 2015, 7 p.
- Shin, M., and Andrawes, B., "Lateral cyclic behavior of reinforced concrete columns retrofitted with shape memory spirals and FRP wraps." *Materials in Civil Engineering*, 137(11), 2011, pp. 1282-1290.
- Soe, K.T., Zhang, Y.X., and Zhang, L.C., "Impact resistance of hybrid-fiber engineered cementitious composite Panels." *Composite Structures*, 104(2013), pp. 320-330.

- Song, and Mo, "Increasing concrete structural survivability using smart materials." *a proposal submitted to Grants to Enhance and Advance Research (GEAR)*, University of Houston, January, 2003.
- Song, G., Ma, N., and Li, H.N., "Applications of shape memory alloys in civil structures." *Engineering Structures*, 28(9), 2006, pp. 1266-1274.
- Suleiman, AR. and Nehdi, ML, "Exploring effects of supplementary cementitious materials in concrete exposed to physical salt attack." *Magazine of Concrete research*, 69(11), 2017, pp. 576-585.
- Sun, S., and Rajapakse, R.K.N.D., "Simulation of pseudoelastic behavior of SMA under cyclic loading." *Computational Materials Science*, 28(3), 2003, pp. 663-674.
- Tanaka, K., and Nagaki, S., "A thermomechanical description of materials with internal variables in the process of phase transformation." *Ingenieur-Archiv*, 51(5), 1982, pp. 287-299.
- Tang, W., and Lui, E.M., "Hybrid recentering energy dissipative device for seismic protection." *Structures*, 2014, 17 p.
- Tosun-Felekoglu, K., Felekoglu, B., Ranade, R., Lee, B.Y., and Li, V.C. "The role of flaw size and fiber distribution on tensile ductility of PVA-ECC." *Composites: Part B*, 56(2014), pp. 536-545.
- Transparency Market Research, 2016, <http://www.transparencymarketresearch.com/pressrelease/smart-materials-market.htm>, accessed on January 05, 2017.
- Turk, K. and Demirhan, S., "The mechanical properties of engineered cementitious composites containing limestone powder replaced by microsilica sand." *Can. Jour. Civil Eng.*, 40(2), 2013, pp. 151-157.

- Wang, Q., and Wu, N., “A review on structural enhancement and repair using piezoelectric materials and shape memory alloys.” *Smart Materials and Structures*, 21(1), 2012, 23 p.
- Wierschem, N., and Andrawes, B., “Superelastic SMA-FRP composite reinforcement for concrete structures.” *Smart Materials and Structures*, 19(2), 2010, 13 p.
- Wu, H.C., Li, V.C., Lim, Y.M., Hayes, K.F., and Chen, C.C., “Control of Cs leachability in cementitious binders.” *Journal of Materials Science Letters*, 15(19), 1996, pp. 1736-1739.
- Wu, M., Johannesson, B., and Geiker, M., “A review: Self-healing in cementitious materials and engineered cementitious composite as a self-healing material.” *Constr. & Build. Mat.*, 28(1), 2012, pp. 571-583.
- Yang, E-H and Li, V.C., “Tailoring engineered cementitious composites for impact resistance.” *Cement and Concrete Research*, 42, 2012, pp. 1066-1071.
- Yuan, F., Pan, J., Dong, L., and Leung, C.K.Y., “Mechanical behaviors of steel reinforced ECC or ECC/concrete composite beams under reversed cyclic loading.” *Mat. in Civ. Eng.*, 26(8), 2014, 8 p.
- Zafar, A., and Andrawes, B., “Fabrication and cyclic behavior of highly ductile superelastic shape memory composites.” *Journal of Materials in Civil Engineering*, 26(4), 2014, pp. 622-632.
- Zafar, A., and Andrawes, B., “Seismic behavior of SMA–FRP reinforced concrete frames under sequential seismic hazard.” *Engineering Structures*, 98(2015), pp. 163-173.
- Zak, A.J., Cartmell, M.P., Ostachowicz, W.M., and Wiercigroch, M., “One-dimensional SMA models for use with reinforced composite structures.” *Smart Materials and Structures*, 12(3), 2003, pp. 338-346.

- Zhang, J., Maalej, M., Quek, S.T., “Performance of hybrid-fiber ECC blast/shelter panels subjected to drop weight impact.” *Journal of Materials in Civil Engineering*, 19(10), 2007, pp. 855-863.
- Zhang, J., Wang, Z., and Ju, X., “Application of ductile fiber reinforced cementitious composite in jointless concrete pavements.” *Composites: Part B*, 50(2013), pp. 224-231.
- Zhang, R., Matsumoto, K., Hirata, T., Ishizeki, Y., and Niwa, J., “Application of PP-ECC in beam–column joint connections of rigid-framed railway bridges to reduce transverse reinforcements.” *Engineering Structures*, 86(2015), pp. 146-156.
- Zhang, Y., and Zhu, S., “A shape memory alloy-based reusable hysteretic damper for seismic hazard mitigation.” *Smart Materials and Structures*, 16(5), 2007, pp.1603-1613.
- Zhang, Q. and Li, V.C., “Adhesive bonding of fire-resistive engineered cementitious composites (ECC) to steel” *Const. & Building Materials*, 64(2014), pp. 431–439.
- Zhou, C., Lin, C., and Liu, L., “Study on CO2 laser weldability of Fe-Mn-Si shape memory alloy.” *Third International Conference on Smart Materials and Nanotechnology in Engineering*, 8409(2012), 6 p.
- Zhu, S., and Zhang, Y., “Seismic behaviour of self-centring braced frame buildings with reusable hysteretic damping brace.” *Earthquake Engineering and Structural Dynamics*, 36(10), 2007b, pp. 1329-1346.
- Zhu, Y., Yang, Y., and Yao, Y., “Use of slag to improve mechanical properties of engineered cementitious composites (ECCs) with high volumes of fly ash.” *Constr. & Build. Mat.*, 36(2012), pp. 1076-1081.
- Zhuge, Y., Shen, C.J., Lu, G.X., Hesse, G., Chen, S., and Ruan, D., “Material properties and impact resistance of a new lightweight engineered cementitious composite.” *23rd Australian Conf. on Mechanics of Struc. & Mat, (ACMSM23)*, Byron Bay, Australia, 9-12 December 2014, pp. 77-82.

Chapter 3

3 INNOVATIVE CRACK-HEALING HYBRID FIBRE REINFORCED ENGINEERED CEMENTITIOUS COMPOSITE²

3.1 INTRODUCTION

The concept of using fibres to reinforce brittle materials has been utilized for thousands of years, for instance when sunbaked bricks reinforced with straw were used to build the 57-m high hill of Aqar-Quf near Baghdad (Hannant, 1995). Cement products have also been reinforced with asbestos and cellulose fibres for about 90 years (MacVicar *et al.*, 1999). Glass, polypropylene and steel fibres have also been used in reinforcing cement-based matrices over the past 70 years (Hannant, 1995). Concrete, which is the world's most utilized construction material, is often subjected to various combinations of compressive, tensile and shear stresses via gravity, seismic and wind loads, explosive forces, shrinkage, thermal contraction, etc.

² A version of this chapter was published in the *Construction and Building Materials Journal* (2017). Parts of this chapter were also published in the *11th International conference on Civil and Architecture Engineering*, Cairo, Egypt, (2016) and in the *5th International conference of the CSCE*, London, Canada, (2016).

Past research has primarily focused on the mechanical performance of mono-fibre-reinforced-cement-based materials (Li and Xu, 2009; Song *et al.*, 2005). Since micro-fibres can restrain the growth of micro-cracks, while large fibres inhibit the growth of larger cracks, there is growing interest in using hybrid fibres involving two or more fibre types and sizes that could create synergistic effects through their different elastic properties and/or various sizes and shapes (Almusallam *et al.*, 2015; Soe *et al.*, 2013; Nehdi and Ladanchuk, 2004). Said *et al.* (2015) investigated the flexural behaviour of mono-fibre ECC slabs reinforced with 1%, 2% and 3% PVA fibre under four-point bending. Results indicated the potential of PVA fibres in reinforcing ECC slabs. Increasing the reinforcing index (product of fibre content by its aspect ratio) led to improving the deflection at failure (corresponding deflection at 25% of ultimate load in the descending part of load-deflection curve), flexural capacity, ductility and energy absorption capacity. However, this decreased the compressive strength of the ECC composite by up to 15% at 7 days. Moreover, Yuan *et al.* (2014) explored the mechanical performance of steel-fibre-reinforced ECC beams subjected to reverse cycling loading. It was revealed that ECC beams exhibited 46% higher load carrying capacity and 400% larger energy dissipation ability compared to that of traditional concrete beams. Furthermore, Huang *et al.* (2013) showed that incorporating recycled tire rubber in the production of ECC composites significantly enhanced the cracking resistance, while it generally decreased the tensile and compressive strengths of the ECC composite, thus compromising potential structural applications. Soe *et al.* (2013) observed that the young's modulus of hybrid fibre-reinforced ECC composites is lower than that of conventional concrete having comparable compressive strength at all testing ages. Similar observation was reported by Huang *et al.* (2013) for mono-fibre-reinforced ECC.

Utilizing hybrid ECCs incorporating both randomly dispersed PVA and nickel titanium (NiTi) SMA short fibres as a replacement for traditional RC is yet to be explored. Therefore, in the present chapter, the mechanical performance of novel hybrid fibre-reinforced ECC mixtures incorporating a combination of randomly dispersed polyvinyl alcohol and nickel titanium shape memory alloy (NiTi-SMA) short fibres was investigated. The study aims at ultimately developing a composite with eminent mechanical properties and possibly crack-healing capability, thus minimizing concrete repair.

3.2 EXPERIMENTAL PROGRAM

3.2.1 Materials and Mixture Proportions

ASTM C150 (Standard Specification for Portland Cement) Type I portland cement was used in the production of the ECC mixtures. It has a specific gravity and surface area of 3.15 g/cm^3 and $371 \text{ m}^2/\text{kg}$, respectively. Class-C fly ash (FA) meeting the requirements of ASTM C618 (Standard Specification for Coal Fly Ash and Raw or Calcined Natural Pozzolan for Use in Concrete) with a CaO content of 16% was also used. The chemical compositions of the cement and fly ash are given in **Table 3-1**.

Table 3-1: Chemical analysis of cement, fly ash, and silica sand

Component (%)	Cement	Fly ash	Silica sand
CaO	64.35	16.00	0.01
SiO ₂	20.08	52.19	99.70
Al ₂ O ₃	4.63	17.56	0.14
Fe ₂ O ₃	2.84	3.66	0.016
MgO	2.07	1.57	0.01
SO ₃	2.85	2.40	---
K ₂ O	---	0.90	0.04
Na ₂ O	---	0.70	0.01
Loss of ignition	2.56	1.60	---

Micro-silica sand (SS) with a maximum particle size of $200 \mu\text{m}$ and specific gravity of 2.65 was also utilized. The laser diffraction particle size distribution curves for the OPC, FA and SS are displayed in **Fig. 3-1**.

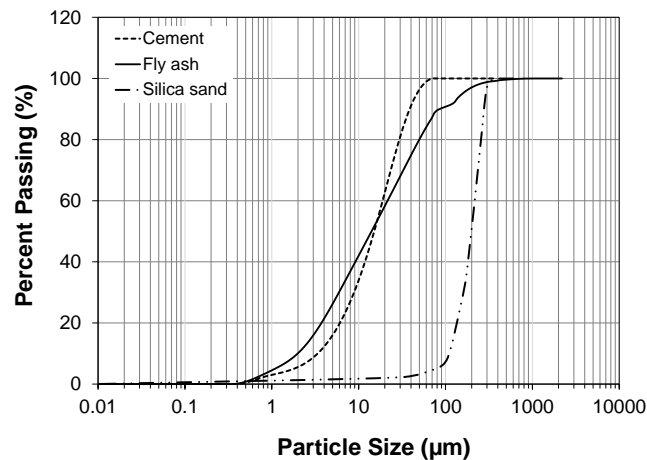


Figure 3-1: Particle size distribution of cement, fly ash, and silica sand.

The ECC mixture was reinforced with NiTi-SMA fibres conforming to ASTM F2063 (Standard Specification for Wrought Nickel-Titanium Shape Memory Alloys for Medical Devices and Surgical Implants), along with PVA short fibres. **Table 3-2** summarizes the mechanical properties of the PVA and SMA fibres. The tensile stress-strain behaviour of the utilized Ni-Ti SMA fibre and its strain recovery performance were tested elsewhere (Nehdi *et al.*, 2010). To control the workability of the different ECC mixtures, a polycarboxylate high-range water reducing admixture (HRWRA) according to ASTM specifications C494 (Standard Specification for Chemical Admixtures for Concrete) was added by percentage of cement weight.

Table 3-2: Mechanical properties of SMA and PVA fibres

Mechanical properties	Ultimate tensile strength (MPa)	Diameter (mm)	Length (mm)	Young's modulus (GPa)	Elongation (%)	Density (kg/m ³)
SMA	869	0.635	16	41	38	6450
PVA	1620	0.039	8	43	6	1300

Table 3-3 displays the proportions of the tested ECC mixtures with a target 28-days compressive strength of 65 MPa. The first number in the mixture label shows the PVA fibre content, while the second indicates the SMA fibre content. For example, ECC2-0.5 refers to an engineered cementitious composite incorporating 2% PVA and 0.5% SMA fibre by volume fraction.

Table 3-3: Mixture proportions of ECC mixtures

Mixture	Cement	Fly ash	Silica sand	w/cm	HRWRA	PVA (%V _f)	SMA (%V _f)
ECC0-0	1.00	1.20	0.80	0.26	0.012	0.00	0.00
ECC2-0	1.00	1.20	0.80	0.26	0.012	2.00	0.00
ECC2-0.5	1.00	1.20	0.80	0.26	0.012	2.00	0.50
ECC2-1	1.00	1.20	0.80	0.26	0.012	2.00	1.00
ECC2-1.5	1.00	1.20	0.80	0.26	0.012	2.00	1.50

3.2.2 Mixture Preparation, Casting and Curing

First, a 20-L rotary mixer was used to dry mix the solid ingredients including the cement, FA, and silica sand for one minute. Then, the mixing water and HRWRA were gradually added to the dry mixture over three minutes until a homogeneous mixture was produced. This was followed by the gradual addition of PVA and SMA fibres and mixing continued

for another three minutes until fibres were uniformly dispersed. Finally, the specimens for testing mechanical properties were prepared by direct pouring of the mixture into molds without compaction. All specimens were demolded after 24 h and cured inside sealed plastic bags for 7-days at laboratory temperature (21 ± 2 °C) without external moisture supply, which is a common curing method for ECC. All reported test results represent average values obtained on identical triplicate specimens.

3.2.3 Test Procedures

Flow table tests were conducted on freshly mixed ECC mixtures to evaluate the effect of SMA and/or PVA fibre addition on the workability of freshly mixed ECC mixtures as per the guidelines of ASTM C230 (Standard Specification for Flow Table for Use in Tests of Hydraulic Cement). For each ECC mixture, nine cubic specimens of 50 mm x 50 mm x 50 mm [2 in x 2 in x 2 in] were made and tested at the ages of 3, 28 and 90 days to determine the compressive strength as per ASTM C39 (Standard Test Method for Compressive Strength of Cylindrical Concrete Specimens), using a standard MTS compression testing machine with a capacity of 2000 kN. The elastic modulus and Poisson's ratio for all ECC mixtures were evaluated according to ASTM C469 (Standard Test Method for Static Modulus of Elasticity and Poisson's Ratio of Concrete in Compression). Three 75 mm in diameter by 150 mm in height [3 in x 6 in] cylindrical specimens from each ECC mixture were tested at the age of 28 days using a standard MTS machine. The elastic modulus and Poisson's ratio for all ECC mixtures were calculated using (Eqs. 3-1 and 3-2):

$$E = \frac{(Q_2 - Q_1)}{(\varepsilon_2 - 0.000050)} \quad \text{(Eq. 3-1)}$$

$$\mu = \frac{(\varepsilon_{t2} - \varepsilon_{t1})}{(\varepsilon_2 - 0.000050)} \quad \text{(Eq. 3-2)}$$

Where E is the elastic modulus in GPa, μ is the Poisson's ratio, Q_2 and Q_1 are stresses in MPa corresponding to 40% of the ultimate compressive load and a longitudinal strain of 50 millionths, respectively. ε_2 , ε_{t2} , and ε_{t1} are the longitudinal strains produced by stress Q_2 , transverse strain at mid-height of the cylinder produced by stress Q_2 , and Q_1 , respectively. From each ECC mixture, nine cylindrical specimens of 75 mm in diameter by 150 mm in height [3 in x 6 in] were tested at the ages of 3, 28 and 90 days to obtain the splitting tensile strength as per ASTM C496 (Standard Test Method for Splitting Tensile

Strength of Cylindrical Concrete Specimens). The splitting tensile strength was calculated as follows (**Eq. 3-3**):

$$T = \frac{2*P}{\pi*l*d} \quad (\text{Eq. 3-3})$$

Where T is the splitting tensile strength in MPa, P is the maximum applied load indicated by the testing machine in Newton, l and d are the length and diameter of the cylinder in mm, respectively. For the determination of flexural capacity (modulus of rupture) of ECC specimens, nine 40 mm x 80 mm x 360 mm [1.6 in x 3.2 in x 14.4 in] prisms were tested as per the guidelines of ASTM C1609 (Standard Test Method for Flexural Performance of Fibre-Reinforced Concrete - Using Beam with Third-Point Loading) at testing ages of 3, 28 and 90 days, using a MTS machine with capacity of 250 kN under a loading rate of 0.05 mm/min. A data acquisition system together with two linear variable displacement transducers (LVDTs) were used in the testing procedure to measure the applied force and mid-span deflection. The number of cracks and their corresponding width were measured after each test using an optical microscope, as exhibited in **Fig. 3-2**. The modulus of rupture (MOR) was calculated as follows (**Eq. 3-4**):

$$MOR = \frac{P*L}{b*d^2} \quad (\text{Eq. 3-4})$$

Where P is the applied load in Newton. L , b , and d are the beam's span, width and depth in mm, respectively. After testing the specimens, heat treatment for 3 minutes was applied using a heat gun fixed at 35 mm away from the specimen's tensile (cracked) side to investigate the strain recovery performance of SMA fibres, as displayed in **Fig. 3-3**. The heat treatment process was similar to that proposed by Kim *et al.* (2016). The gun was able to heat the specimens by up to 150°C. The heat treatment process was used to activate the SMA fibres, which were in the martensite phase before heating, and investigate its strain recovery capability.



Figure 3-2: Crack monitoring optical microscope.



Figure 3-3: Heat treatment gun.

Additionally, in order to estimate the ductility and energy absorption capacity of ECC specimens, ASTM C1018 (Standard Test Method for Flexural Toughness and First-Crack Strength of Fibre-Reinforced Concrete - Using Beam with Third-Point Loading) was deployed. The toughness indices I_5 , I_{10} , I_{20} , I_{30} and I_{40} were determined through calculating the ratio between the area under flexural load-deflection curves up to 3δ , 5.5δ , 10.5δ , 15.5δ and 20.5δ , respectively, and that of δ . Where δ is the flexural deflection at first crack. The first crack deflection was determined for each specimen through estimating the point on the load-deflection curve at which the form of the curve first becomes nonlinear.

These indicators describe the flexural toughness and ability of ECC specimens to absorb energy and achieve high ductility. The higher the toughness, the higher is the ductility and energy absorption capacity. Furthermore, microanalysis was carried out on chips from different ECC specimens to observe the possible effects of utilizing PVA and SMA fibres on the microstructure of ECC, as per the guidelines of ASTM C1723 (Standard Guide for Examination of Hardened Concrete Using Scanning Electron Microscopy). The analysis was conducted both on non-heated and heated ECC specimens to investigate the effects of heat treatment on the ECC's microstructure. The specimen cross-sections were examined using scanning electron microscopy (SEM) coupled with energy dispersive X-ray analysis (EDX) using a Hitachi SU-3500 Field Emission SEM.

3.3 RESULTS AND DISCUSSION

3.3.1 Workability

Figure 3-4 illustrates the relative reduction in flow diameter for the different ECC mixtures compared to that of the control specimen. Flow table tests indicated that the ECC matrix (control) mixture could flow under its self-weight, while fibre addition led to an overall reduction in workability as expected. This is consistent with previous study by Said *et al.* (2015). For example, as shown in **Fig. 3-4**, the flow of the mixture incorporating 2% PVA fibre decreased by 5.6% compared to that of the control ECC0-0 mixture.

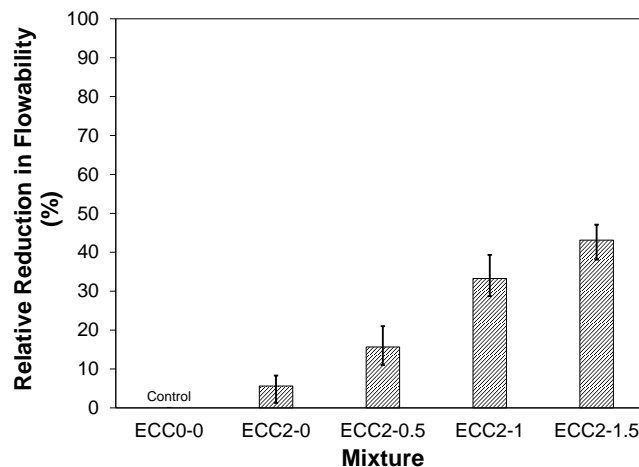


Figure 3-4: Relative reduction in flow diameter due to fibre addition.

Likewise, the flow decreased by about 15.6%, 33.3% and 43.1% due to 0.5%, 1% and 1.5% SMA fibre addition, respectively compared to that of the ECC mixture made with 2% PVA fibre alone. It should be noted that flow reduction can affect the compactness of the composite, acting as an exogenous parameter, which can affect the mechanical performance. Attempts of using higher superplasticizer dosage were not effective at increasing the flow since it may lead to bleeding of the matrix. Although, SMA and/or PVA fibre addition had led to general reduction in workability, all tested mixtures flowed and effectively filled the moulds without need for external compaction.

3.3.2 Compressive Strength

Figure 3-5 displays the variation in compressive strength for the different ECC mixtures at testing ages of 3, 28 and 90 days. As expected, the compressive strength of the different ECC specimens increased with age. The compressive strength of ECC specimens at 3, 28 and 90 days ranged from 37 to 41, 60 to 66 and 66 to 71 MPa, respectively, depending on the fibre content. Generally, SMA and PVA fibre addition induced a slight decrease in the ECC's compressive strength at all testing ages. This can be ascribed to the increased porosity (as shown later) induced by the lower compactness, which emanates from increasing the fibre dosage, thus resulting in reduced compressive strength.

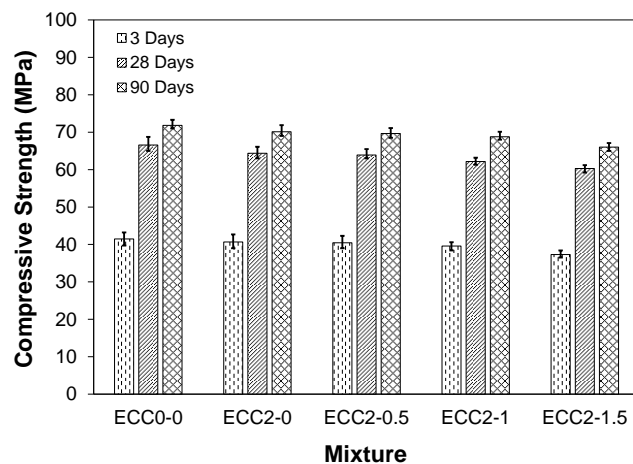


Figure 3-5: Compressive strength of ECC mixtures at different testing ages.

3.3.3 Elastic Modulus and Poisson's Ratio

The elastic modulus and Poisson's ratio test results of ECC mixtures at 28-days are displayed in **Figs. 3-6 and 3-7**, respectively. The elastic modulus of the various ECC mixtures was generally lower than that of comparable strength conventional concrete. This is ascribed to the absence of coarse aggregates in ECC mixtures. The elastic modulus and Poisson's ratio of ECC incorporating SMA and/or PVA fibres ranged from 18.8 to 22.7 GPa and 0.14 to 0.21, respectively depending on the fibre content.

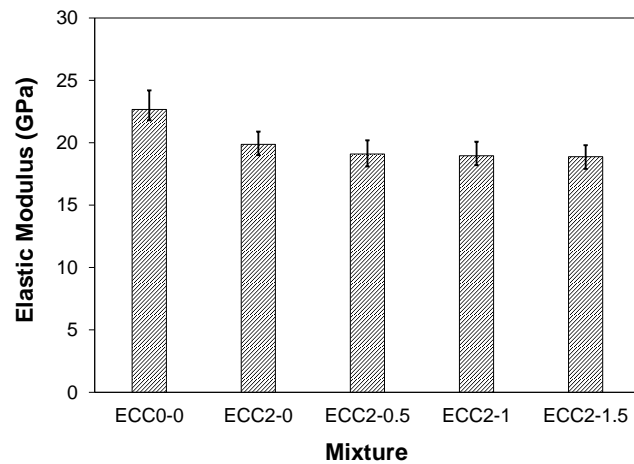


Figure 3-6: Elastic modulus of various ECC mixtures.

The incorporation of 2% PVA in the ECC mixture led to 12% and 13% reduction in the elastic modulus and Poisson's ratio, respectively, compared to that of the control mixture. Similar performance was observed due to SMA fibre addition. For instance, 0.5%, 1%, and 1.5% SMA fibre addition led to a reduction in elastic modulus by about 15.9%, 16.5%, and 16.8%, respectively compared to that of the control fibreless mixture.

Similar trend was observed for the Poisson's ratio. For example, specimens ECC2-0.5, ECC2-1, and ECC2-1.5 had Poisson's ratio of 14%, 20.2%, and 34.3% lower than that of the control ECC0-0 specimens, respectively. The overall reduction in elastic modulus of the ECC mixtures can be attributed to the reduced compressive strength caused by increased porosity due to fibre addition as a result of the reduced workability and possibly

fibre clustering. The reduction in Poisson's ratio imparted by fibres is due to the fibre restriction on lateral strain.

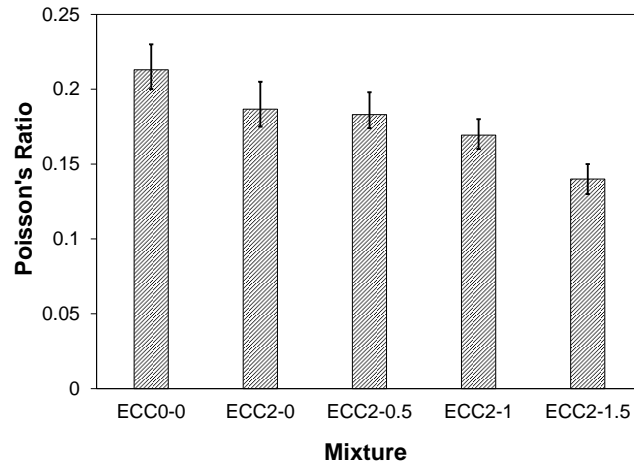


Figure 3-7: Poisson's ratio of different ECC mixtures.

According to ACI 318-11 (Building Code Requirements for Structural Concrete and Commentary), the elastic modulus of concrete with density ranging from 1440 to 2560 kg/m³ can be calculated using **Eq. 3-5**. Since, in this study, the density of the various ECC mixtures ranged from 1736 to 1960 kg/m³, **Eq. 3-5** was used to estimate the elastic modulus of ECC mixtures.

$$E = 0.043 * \rho^{1.5} * \sqrt{f_c} \quad (\text{Eq. 3-5})$$

Where E is the elastic modulus in MPa, ρ is the density in kg/m³, and f_c is the compressive strength in MPa at 28 days. **Figure 3-8** exhibits the correlation between the average elastic modulus measured at 28 days (shown as solid line) and that calculated using the empirical relation of **Eq. 3-5** (represented by a dashed line). It can be observed that the calculated elastic modulus values followed similar trend to that of the experimentally measured values with maximum tolerance of 25%, which reflects the dependency of the elastic modulus of ECC on its compressive strength and density, similar to other concrete types.

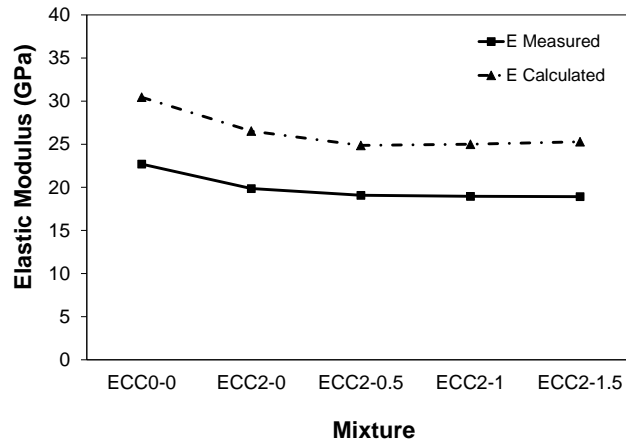


Figure 3-8: Correlation between measured and calculated elastic modulus of ECC mixtures.

3.3.4 Splitting Tensile Strength

Figure 3-9 displays the variation in splitting tensile strength of the different ECC mixtures at testing ages of 3, 28 and 90 days, which ranged from 1.5 to 12.1 MPa, depending on the fibre dosage and maturity of specimens. It can be observed that the splitting tensile capacity of the different ECC specimens increased with age, as expected. Furthermore, the tensile capacity of the composite was enhanced due to fibre addition. For example, the tensile capacity at 3, 28 and 90 days of the mixture incorporating 2% PVA fibre increased by about 84.8%, 42.9% and 41.6%, respectively compared to that of the fibreless ECC mixture. Likewise, SMA fibre addition exhibited similar behaviour at all testing ages. For instance, the tensile capacity of the hybrid-ECC mixtures incorporating 2% PVA and 0.5%, 1% or 1.5% SMA fibre was enhanced by about 153.9%, 193.8% and 158.4% compared to that of the fibreless matrix mixture at 3 days; by 85.9%, 98.7% and 87.7%, at 28-days; and by 71%, 81% and 76% at 90 days, respectively. This enhancement in tensile capacity can be ascribed to the fibre-matrix interfacial bond (both chemical and frictional) which enhanced the load transfer across cracks with increasing fibre content, consequently improving the overall tensile load carrying capacity of the composite.

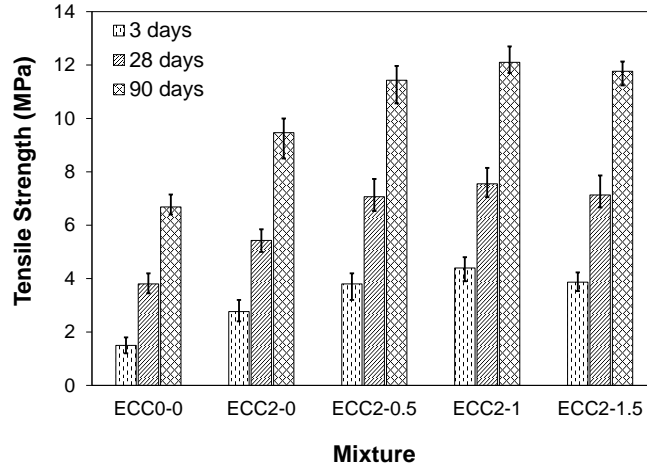


Figure 3-9: Splitting tensile strength of ECC specimens.

3.3.5 Flexural Behaviour

3.3.5.1 Flexural strength

Table 3-4 summarizes the four-point bending test results for specimens from all tested ECC mixtures at 3, 28 and 90 days. As expected, the flexural strength of ECC specimens generally increased with fibre addition. The ultimate flexural strength (MOR) of ECC specimens varied from 2.3 to 12.5 MPa, depending on the curing age and fibre dosage. For instance, at 3 days, the ECC mixture incorporating 2% PVA fibre achieved first crack and ultimate flexural strengths of about 90.1% and 130% higher than that of the control fibreless ECC mixture at the same testing age, respectively. Similar performance was observed at later age whereby the first crack and ultimate flexural strength of the ECC2-0 specimens were 56% and 131% higher than that of the control ECC0-0 specimens at 28-days, and by about 30.3% and 153.7% at 90 days, respectively, confirming the well documented beneficial effect of PVA fibres in ECC composites (Said *et al.*, 2015; Pan *et al.*, 2015).

Table 3-4: Flexural strength and corresponding deflection of HECC-SMAF at different ages

Specimen	3 days			28 days			90 days		
	First crack strength (MPa)	MOR (MPa)	Deflection at failure (mm)	First crack strength (MPa)	MOR (MPa)	Deflection at failure (mm)	First crack strength (MPa)	MOR (MPa)	Deflection at failure (mm)
ECC0-0	2.33	2.33	0.25	2.68	2.68	0.22	2.81	2.81	0.21
ECC2-0	4.43	5.36	4.76	4.18	6.19	2.66	3.66	7.13	2.93
ECC2-0.5	4.23	5.49	8.55	3.92	6.49	3.49	3.53	8.11	3.66
ECC2-1	5.67	8.15	12.07	5.28	12.22	6.46	4.25	12.52	6.17
ECC2-1.5	5.31	7.76	13.18	5.05	10.40	6.07	4.92	10.54	4.24

Similarly, the flexural strength of ECC specimens significantly increased with increasing SMA fibre addition at all testing ages. For instance, the ECC2-0.5, ECC2-1 and ECC2-1.5 specimens achieved 135.6%, 249.8% and 233% higher flexural capacity than that of the ECC0-0 specimen, respectively at 3-days. Similar behaviour was observed later; for example, the ECC2-0.5, ECC2-1 and ECC2-1.5 specimens acquired flexural strength of 142.2%, 356% and 288% higher than that of ECC0-0 at 28-days, respectively and about 188.6%, 345.6% and 275% higher at 90-days, respectively. Furthermore, using 2% PVA and 1% SMA fibres by volume fraction in ECC achieved the highest flexural capacity among all tested mixtures. This is consistent with other investigations by Said *et al.* (2015) and Hirata *et al.* (2009) who also observed that higher fibre dosage led to enhanced higher flexural strength ECC. However, increasing the fibre dosage beyond this threshold value led to general reduction in flexural capacity of the composite. This is attributed to fibre clustering and the associated increased porosity.

Figures 3-10a, b and c illustrate the load-deflection curves of specimens from the different ECC mixtures tested under four-point bending at 3, 28 and 90 days, respectively. The fibreless ECC specimens exhibited brittle failure under flexural testing. Conversely, adding SMA and/or PVA fibres enhanced the composite's behaviour under bending and yielded ductile performance. For example, the ECC2-0, ECC2-0.5, ECC2-1, and ECC2-1.5 specimens sustained flexural loading about 138.3%, 155.5%, 317%, and 265.4% higher than that of the control ECC0-0 specimens. Furthermore, the recovery of ultimate flexural strength of ECC specimens was investigated through conducting post-cracking heat treatment, immediately after removing the cracked ECC specimens from the flexural bending test. Both heat-treated and non-heat treated cracked ECC specimens were re-tested under flexural loading.

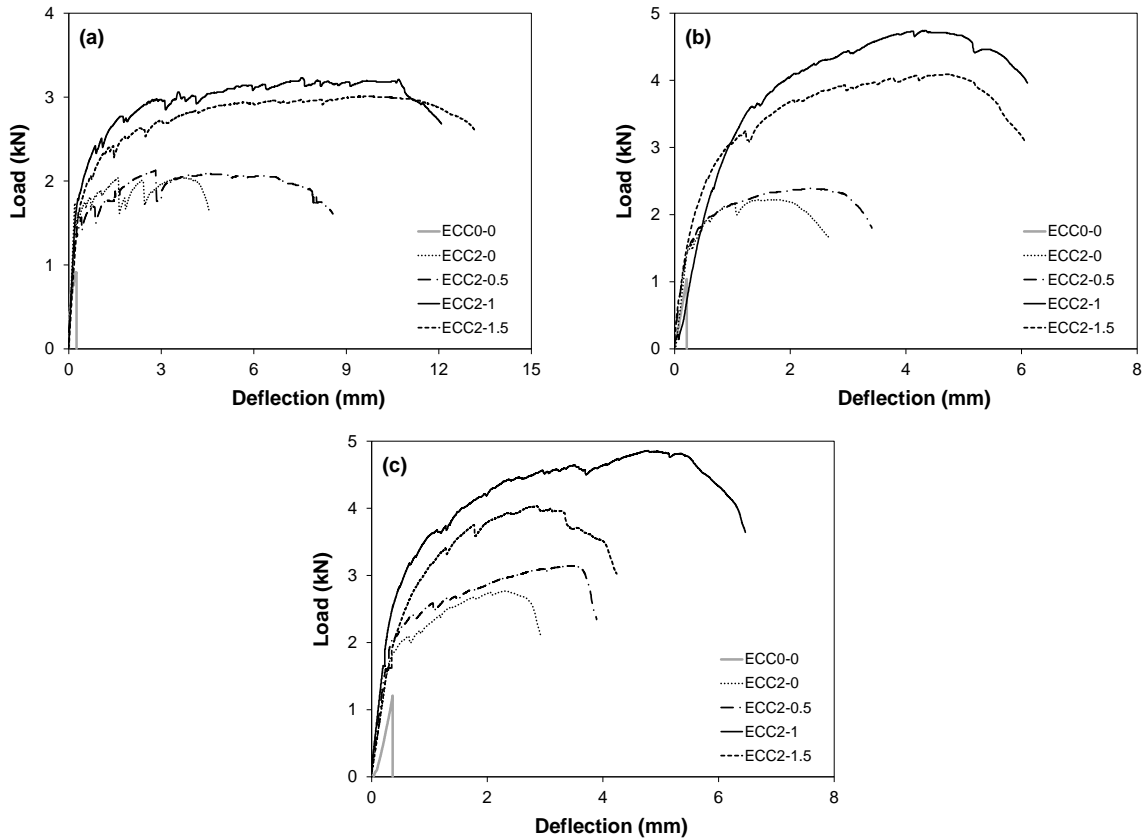


Figure 3-10: Load-deflection curves of ECC specimens at different ages: a) 3 days, b) 28 days, and c) 90 days.

Figure 3-11 portrays the load-deflection curve of ECC cracked specimens with and without heat treatment. It can be observed that the heat-treated PVA-ECC specimens did not achieve any recovered ultimate strength, but rather exhibited a deterioration of about 24.7% compared to its non-heat treated counterpart. This can be attributed to the deterioration of PVA fibres due to the heating process. Conversely, the heat treated HECC-SMAF specimens showed superior performance under flexural loading compared to its non-heated counterparts. For instance, the ultimate strength of the heated ECC2-0.5, ECC2-1 and ECC2-1.5 specimens increased by about 90.8%, 163.8% and 131.6% compared to that of the non-heated HECC-SMAF specimens, respectively. This can be attributed to the shape memory effect of SMA fibres, which applied a local pre-stressing effect upon heat treatment, leading to superior performance of the heat-treated HECC-SMAF specimens.

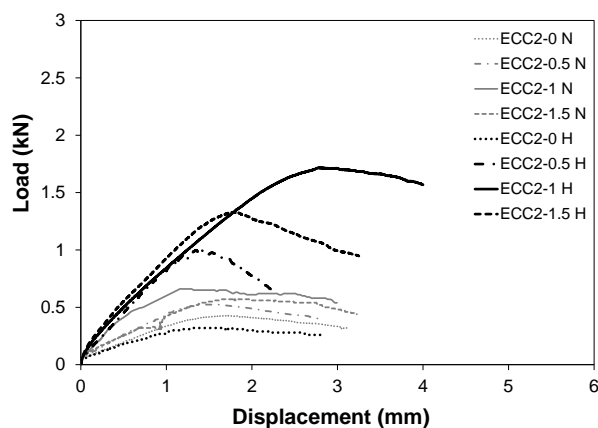


Figure 3-11: Load-deflection curves of non-heated and heated ECC specimens.

3.3.5.2 Flexural toughness

The toughness characteristics of ECC specimens were estimated through evaluating toughness indices as per the ASTM C1018 standard, which describes the method of determination of toughness indices I_5 , I_{10} and I_{20} and allows for higher indices as well. In the present study, due to the high deflection results achieved for ECC specimens (**Fig. 3-10**), I_5 , I_{10} , I_{20} , I_{30} and I_{40} were estimated through calculating the area under load-deflection curves up to δ (deflection value at first crack), 3δ , 5.5δ , 10.5δ , 15.5δ and 20.5δ , respectively.

Figure 3-12a, b and c illustrates the correlation between the toughness indices and total fibre volume fraction incorporated in the different ECC specimens at different ages. A total volume fraction (V_f , %) of fibres refers to the addition of PVA and SMA fibres in each ECC mixture. For example, a total V_f of 2% represents ECC2-0 specimens which incorporate 2% PVA and 0% SMA fibres, while a total V_f of 2.5% denotes ECC2-0.5 specimens, which incorporate 2% PVA and 0.5% SMA fibres, and so on. It can be observed that all toughness indices increased with increasing SMA fibre addition at all testing ages. The fit lines for toughness indices at all ages were found to be linear with a coefficient of determination (R^2) of 0.7024 or higher. According to Rahmani *et al.* (2012), a coefficient of determination of 0.7 or higher is sufficient for a reasonable reliability model.

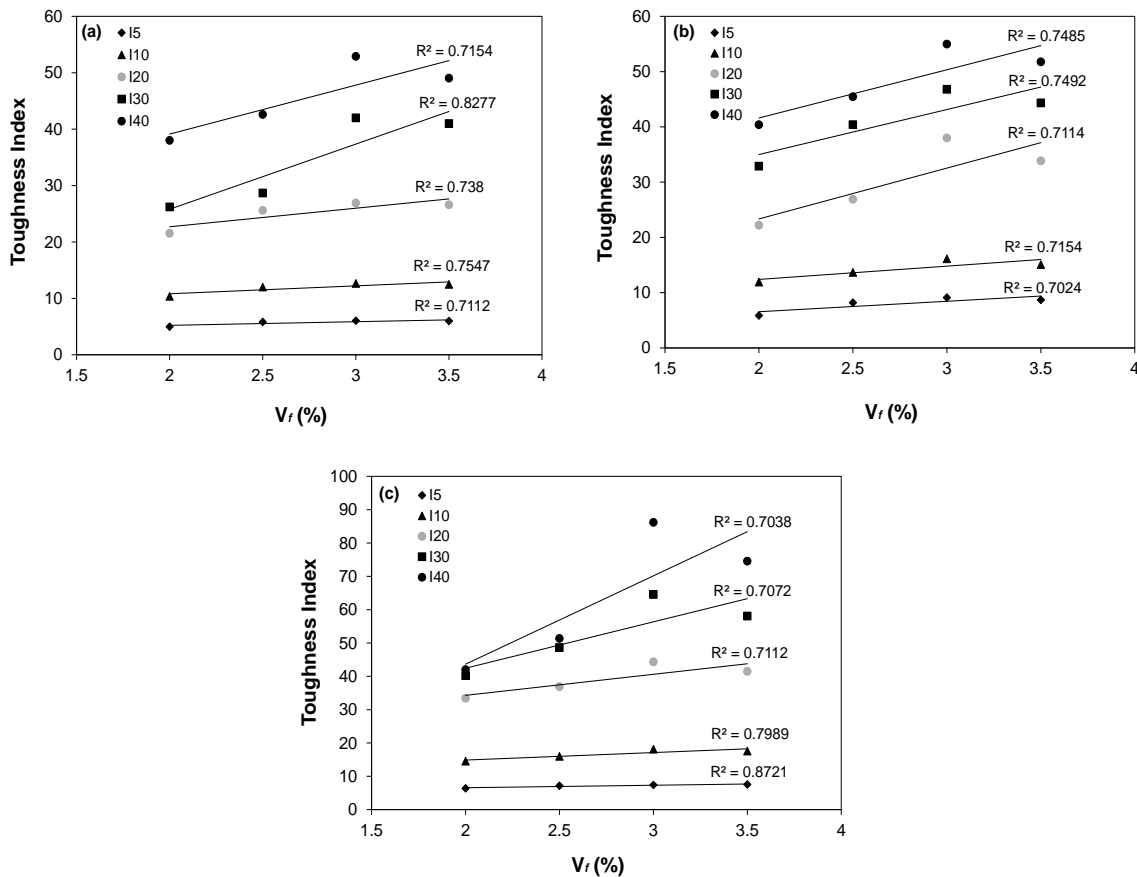


Figure 3-12: Effect of fibre volume fraction on toughness index of ECC specimens at different ages: a) 3 days, b) 28 days, and c) 90 days.

On the other hand, the slope of these lines increased with increasing toughness indices. For instance, the slope values of the fit lines corresponding to I_5 , I_{10} , I_{20} , I_{30} and I_{40} were 0.65, 1.41, 3.30, 11.54 and 8.69 at 3 days, 1.89, 2.40, 9.21, 8.15 and 8.72 at 28 days, and 0.75, 2.24, 6.32, 13.91 and 26.50 at the age of 90 days, respectively. At lower toughness indices, I_5 and I_{10} , the slope values were low, nearly parallel to the x-axis. However, at higher toughness indices, I_{20} and I_{40} , the fit lines had higher sloping trend. This is attributed to the fact that at the post-cracking stage (typically at lower toughness indices), the crack propagation and crack-arresting behaviour of fibres had not been fully activated yet. Conversely, at higher loading levels associated with higher deflections, the multiple cracks started to show up and the effect of fibre-bridging capability, which functions as a crack arrestor, started to activate. This performance reflects the higher flexural toughness, ductility and energy dissipation ability acquired at higher toughness indices (typically I_{20} and higher) as observed by Said *et al.* (2015). It can also be observed that using 2% PVA and

1% SMA fibres in ECC specimens (total V_f of 3%) achieved highest toughness indices at all testing ages, thus yielding superior ductility and energy dissipation capability, in agreement with tensile and flexural test results.

Since the toughness indices obtained using the ASTM C1018 method depend mainly on the location of the first crack, which is not easy to accurately determine, the post-cracking strength (PCS) method was utilized in this study to check the toughness characteristics of ECC specimens at all testing ages. The PCS method was first presented by Banthia and Trottier (1995) to evaluate the flexural toughness of beams. It can be used to check toughness properties during the loading process using the peak load point instead of the first crack point, which is easier to be accurately estimated. PCS was determined in this study for different ECC specimens, for a minimum deflection value at failure of 2.66 mm (typically span/120), as shown in **Table 3-4**.

Figure 3-13 displays the correlation between PCS_{120} and total V_f of fibres for different ECC specimens at all testing ages. It can be observed that PCS values increased with increasing SMA fibre addition at all testing ages. However, the ECC specimen with 2% PVA and 1% SMA fibres (ECC2-1) achieved the highest PCS at all testing ages. The general increase in PCS values and superior results of ECC2-1 reflect higher ductility and energy dissipation capability of the composite, confirming the results acquired using the ASTM C1018 method.

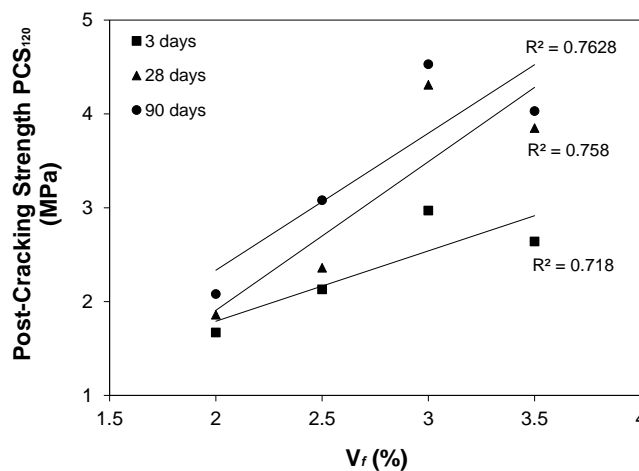


Figure 3-13: Effect of fibre volume fraction on post-cracking strength of ECC specimens.

To further investigate the effect of SMA fibre addition on ECC flexural toughness characteristics, the results were compared with the findings of previous study. Said *et al.* (2015) explored the

effects of the PVA fibre dosage on the toughness properties of ECC. The comparison focused on results acquired herein on ECC2-1 (2% PVA and 1% SMA fibres) and that of Said *et al.* (2015) for ECC incorporating 3% PVA fibres. **Figure 3-14** illustrates the relative enhancement in toughness indices acquired in both studies compared to that of control specimens incorporating 2% PVA fibre alone. It can be observed that all toughness indices were enhanced due to 1% SMA fibre addition, which is 5 times higher than that achieved by a similar volume of PVA fibre, reflecting better energy absorption capacity and superior ductility and confirming the beneficial effects of SMA fibres in ECC in view of SMA's superior engineering properties.

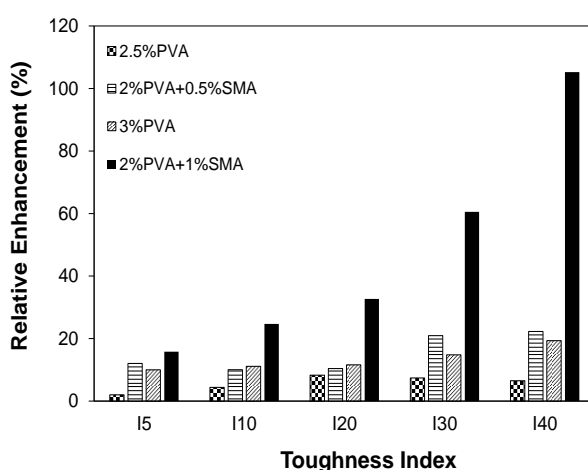


Figure 3-14: Relative enhancement in toughness index of ECC2-1.

Moreover, **Table 3-5** illustrates the toughness ranges achieved in the present study compared to that stated by ASTM C1018 and that acquired by Said *et al.* (2015). The toughness indices estimated in this study increased due to using SMA fibres.

Table 3-5: Toughness ranges for different concrete materials

Index designation	Deflection criterion	Toughness indices range			
		Plain concrete	Elastic-perfectly plastic material	Mono-fibre-reinforced ECC Said <i>et al.</i> (2015)	Hybrid-fibre-reinforced ECC (HECC-SMAF)
I_5	3δ	1.0	5.0	1 to 6	1 to 9
I_{10}	5.5δ	1.0	10.0	1 to 12	1 to 18
I_{20}	10.5δ	1.0	20.0	1 to 25	1 to 44
I_{30}	15.5δ	1.0	30.0	1 to 38	1 to 64
I_{40}	20.5δ	1.0	40.0	1 to 50	1 to 86

Since the ASTM C1018 defines the range of toughness indices I_5 , I_{10} and I_{20} only, the present study points to the possibility of defining new ranges for such indices for hybrid-fibre-reinforced cementitious composites. Additional indices such as I_{30} and I_{40} could indeed be defined and calculated as per ASTM C1018 for superior ductility composites.

3.3.5.3 Deflection

The mid-span deflection under four-point bending tests of specimens from the various ECC mixtures was measured as displayed in **Fig. 3-15**. The fibreless ECC matrix specimens exhibited brittle failure under flexural loading, suddenly shattering into three segments. Conversely, the mono- and hybrid- fibre reinforced ECC specimens incorporating SMA and/or PVA fibres deflected under flexural loading by 4 to 13 mm (depending on the fibre dosage and curing age) without fracturing. The fibre reinforcement transformed the mode of failure from brittle to ductile. Furthermore, it was observed that the mid-span deflection decreased as the curing time increased. This is attributed to the increase of volume of hydration products with curing time. Consequently, increasing the fibre-matrix interfacial bond, which in turn causes a decrease in the flexural deflection capacity. Similar conclusion was drawn by others (Altwair *et al.*, 2012; Li and Li, 2011).

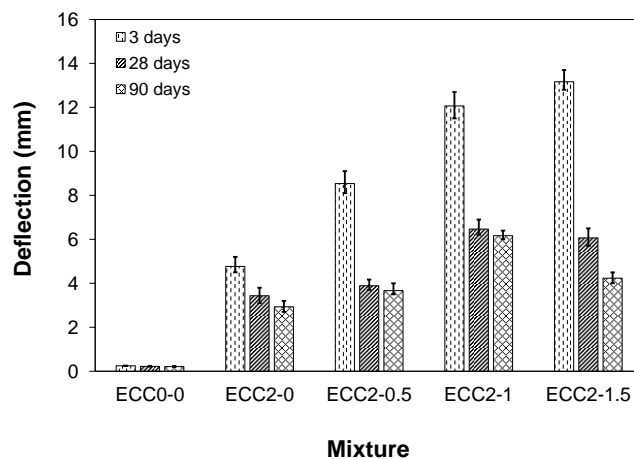


Figure 3-15: Flexural deflection of ECC prisms at different ages.

Generally, the hybrid-fibre reinforced ECC specimens displayed higher ductility than that of PVA-ECC specimens owing to SMA fibre addition. For instance, specimens ECC2-0.5, ECC2-1 and ECC2-1.5 deflected under flexural loading at 3-days by about 79%, 153.2% and 176.2% higher

than that of ECC2-0, respectively. Similar behaviour was observed at later ages. The mid-span deflection at failure of ECC2-0.5, ECC2-1 and ECC2-1.5 specimens increased by about 13.3%, 88.4% and 76.7% at 28 days, and by 25%, 110.2% and 44.3% at 90 days, respectively, compared to that of the control ECC2-0 at the same testing ages.

3.3.5.4 Crack pattern

The number of cracks which formed on the tensile side of flexure loaded ECC specimens was monitored to determine the effect of the fibre type and content on crack propagation. The crack pattern changed from two main cracks in the case of the fibreless specimens to multiple fine cracks with an average width of less than 100 μm on the tension face of the mono-ECC specimen reinforced by 2% PVA fibre. There were typically several main cracks running through the tension side of the specimen without crushing at the compression side. A similar trend was displayed by the hybrid fibre-reinforced ECC specimens utilizing hybrid PVA and SMA fibres. **Figure 3-16** displays the average number of cracks which propagated under four-point flexural bending for all ECC specimens at 3, 28 and 90 days.

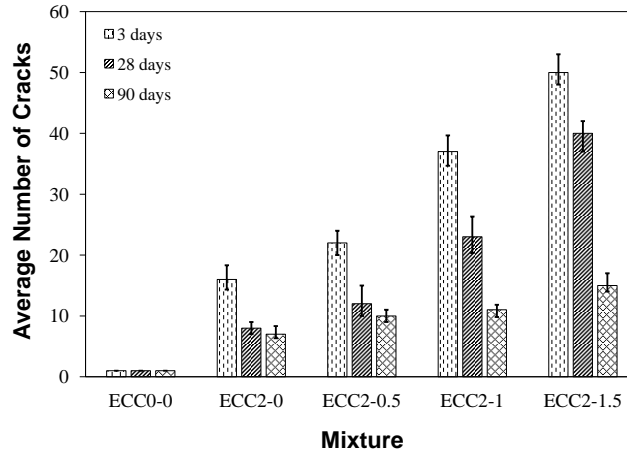


Figure 3-16: Average number of cracks of ECC prisms at different ages.

It can be observed that the number of cracks induced by flexural loading increased with the increase of the SMA fibre content at all testing ages. For instance, the number of cracks generated in the ECC2-0.5, ECC2-1 and ECC2-1.5 specimens increased by about 50%, 187.5% and 400% at 28 days, and by 42.9%, 57.1% and 114.3% at 90 days, respectively, compared to that of the

ECC2-0 specimens at the same testing age, owing to the SMA fibre crack bridging ability (**Fig. 3-17**).

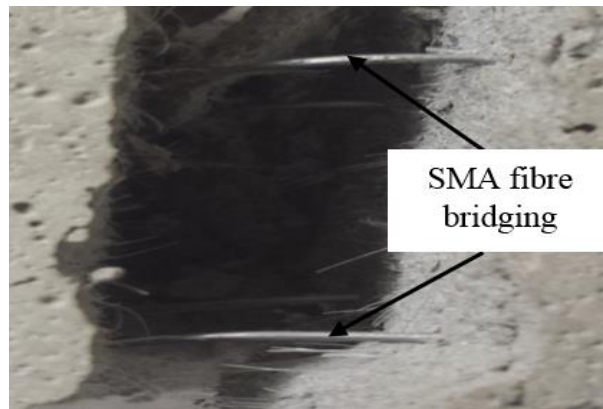


Figure 3-17: Fibre bridging capability of SMA.

3.3.5.5 Strain recovery

Strain recovery of ECC specimens was explored through applying heat treatment, immediately after removing the ECC cracked specimens from the flexural bending test. The strain recovery is defined as the percent difference in the average flexural crack width at the tensile face of prismatic specimens before and subsequent to heat treatment, as illustrated in **Eq. 3-6**:

$$\text{Strain Recovery (\%)} = \frac{W_A - W_B}{W_B} * 100 \quad (\text{Eq. 3-6})$$

Where W_A and W_B are the average flexural crack width after and before the heat treatment, respectively. **Figures 3-18 and 3-19** portrays the effect of heat treatment on the ECC specimens. Specimens showed multiple fine cracks, typically less than 10 μm wide, particularly at the front surface exposed directly to the heating (**Fig. 3-18**).

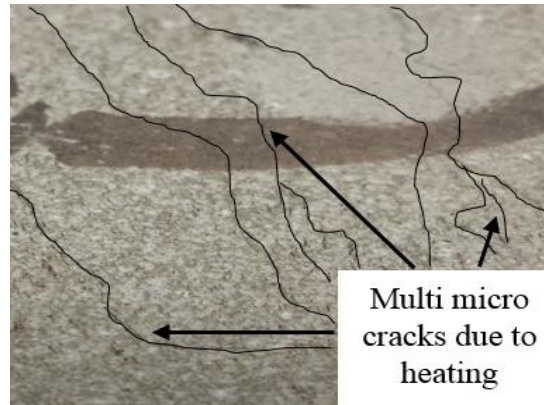


Figure 3-18: Surface cracking of ECC specimens due to heat treatment.

Moreover, PVA fibres were heat damaged, especially at the front surface facing the heat gun, thus jeopardizing the PVA mechanical properties (**Fig. 3-19**).

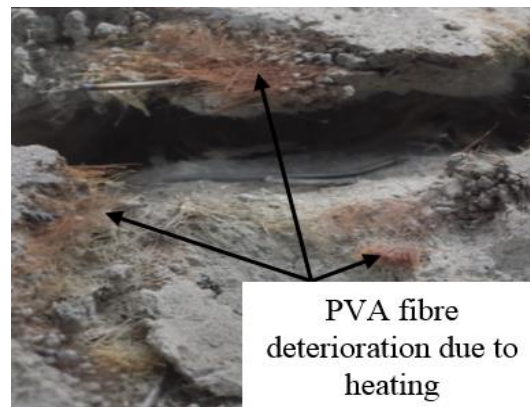


Figure 3-19: PVA fibre deterioration due to heat treatment effect.

Despite the appearance of multiple fine cracks and the deterioration of PVA fibres, the addition of SMA fibres contributed to superior performance of the heat-treated specimens subsequent to flexural loading. It was observed that the cracks were self-healed by up to 36% owing to the shape memory effect of SMA fibres. **Figure 3-20** illustrates the strain recovered by ECC specimens after heat treatment. The ECC matrix and PVA-ECC specimens did not achieve any recovered strain, but exhibited deterioration due to the heating process.

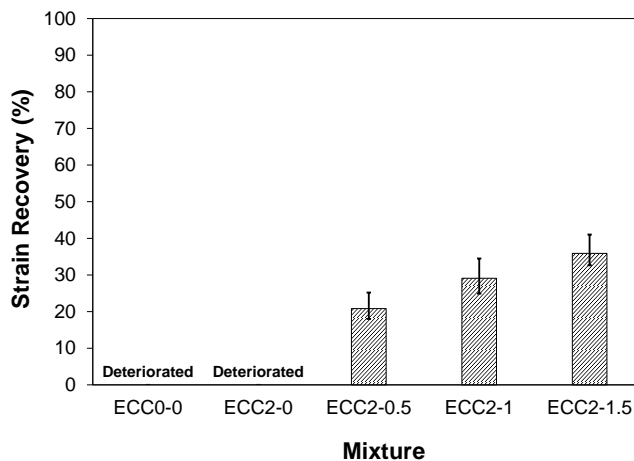


Figure 3-20: Percent enhancement in recovery strain of cracked ECC specimens.

Conversely, for the HECC-SMAF, the average crack width at the tension face of specimens ECC2-0.5, ECC2-1 and ECC2-1.5 decreased by about 20.8%, 29.1% and 35.9% upon the heating process compared to that of non-heated control specimens at 3, 28 and 90, respectively. This can be attributed to SMA fibres, which led to strain recovery, reflecting the unique possible benefits of SMA fibres in ECC composites.

3.3.6 Microstructural analysis

Both backscattered (BSE) and scanning electron microscopy (SEM) imaging of ECC specimens with and without SMA fibre were carried out. BSE images (**Figs. 3-21 and 3-22**) display the pore structure of the fibreless ECC matrix and that of the HECC-SMAF, respectively. Dark features represent pores, while the large white spots denote SMA fibres.

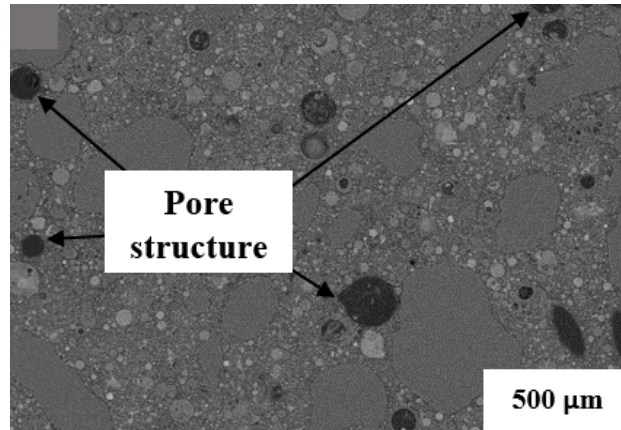


Figure 3-21: BSE images of ECC0-0 specimen.

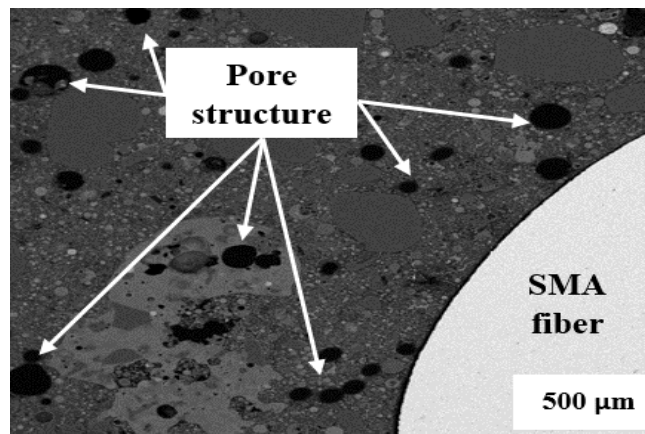


Figure 3-22: BSE images of ECC2-1.5 specimen.

Generally, the microstructure around SMA fibres was dense, with no presence of cracks (**Fig. 3-22**). The improved mechanical performance of the HECC-SMAF composite can be attributed to the dense fibre-matrix interfacial bond, mobilizing fibres to restrain the growth of micro-cracks, in agreement with previous studies (Choi *et al.*, 2015; Lee *et al.*, 2010) on steel fibre-reinforced concrete.

While the ECC matrix indicated smaller and more refined porosity (**Fig. 3-21**), once fibres have been added, larger size pores appeared (**Fig. 3-22**), likely due to the negative effect of fibres on workability and consolidation of the composite. The downward trend in mechanical properties of ECC specimens incorporating more than 2% PVA and 1% SMA fibres is likely due to such increased porosity along with fibre clustering induced by high fibre dosage. Fracture surfaces of

HECC-SMAF specimens subsequent to flexural tests were explored under SEM. **Figure 3-23** displays the fracture of a PVA fibre under flexural loading, while separation between SMA fibre and the matrix due to de-bonding at the fibre matrix interface is shown in **Fig. 3-24**.

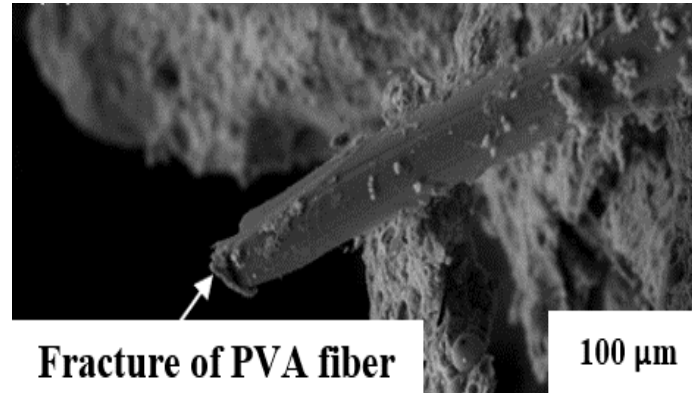


Figure 3-23: SEM for fracture of PVA fibres.

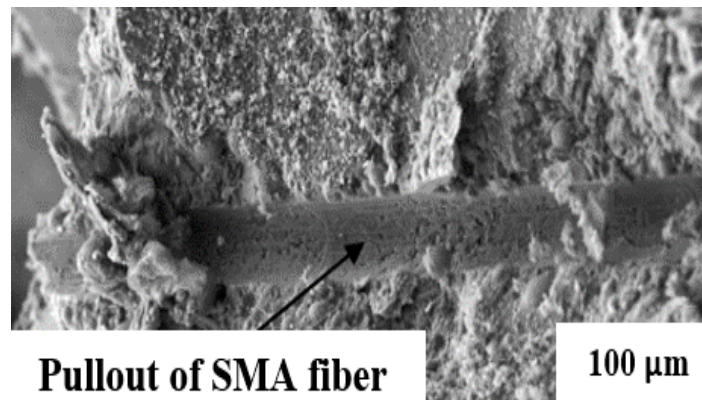


Figure 3-24: SEM for pullout of SMA fibres.

It has been reported (Soliman and Nehdi, 2012; Rathod and Patodi, 2010) that rupture of micro fibres, rather than pull-out, reflects strong adhesion between the micro fibres and the matrix. For instance, the effect of PVA fibre depends on the ability to transfer shear stresses between the matrix and fibres, which is a function of the interfacial fibre-matrix bond strength (Hameed *et al.*, 2009).

Thus, the general improvement in splitting tensile and flexural strengths of PVA-ECC specimens can be attributed to the frictional bond between PVA fibres and the cementitious matrix. Also, the enhanced mechanical behaviour of the SMA-ECC specimens is likely due to the ability of SMA fibres to effectively restrain cracks under tensile stresses.

It is intriguing to note that while the PVA fibre has a tensile strength of 1620 MPa and the SMA fibre has a tensile strength of 869 MPa, **Fig. 3-23** shows that PVA fibres tended to fracture while SMA fibres experienced pullout, as shown in **Fig. 3-24**. The fracture behaviour of micro-fibres implemented in composite materials depends mainly on the concept of critical fibre length and load carrying performance of composites. The critical fiber length is that length beyond which fibres rupture rather than pull-out. According to Bentur and Mindess (2007), the critical fiber length is determined as follows (**Eq. 3-7**):

$$L_c = \frac{\sigma_f * d}{2 * \tau} \quad (\text{Eq. 3-7})$$

Where L_c is the critical fibre length, σ_f is the ultimate tensile strength of fibre, d is the fibre diameter, and τ is the elastic shear stress at the interface (fibre-matrix bond strength). It can be observed that the fracture behaviour of fibres depends on its aspect ratio as well as the fibre-matrix interfacial bond strength. In order to better investigate the performance of PVA and SMA fibres in the ECC material, the critical fibre length for both fibres was estimated. The determined critical fibre length of PVA fibres in the composite is 3.8 mm, which is lower than the utilized PVA fibre length (8 mm). This reflects the tendency of PVA fibres to rupture within the ECC composite. Conversely, the critical fibre length of SMA fibres in the composite is 94.5 mm (higher than 16 mm), which reflects pull-out of SMA fibres rather than fracture.

On the other hand, as the cementitious matrix cracks, the load carried by the matrix starts to transfer to the PVA and SMA fibres bridging the crack. PVA fibres having slightly higher modulus and being larger in number carry a significant part of the load. The PVA fibres start fracturing as the crack opens due to their much lower elongation (6%) compared to that of SMA fibres (38%). The SMA fibres accommodate crack opening via their much higher ductility and end up pulling out of the matrix. The type of bond between the matrix and PVA fibres and matrix and SMA fibres could also play a key role. The much larger SMA fibre (diameter of 0.635 and length of 16 mm) offers much greater bond area than that of the PVA fibre (Diameter of 0.039 mm and length of 8 mm). Thus, the SMA fibre will first elongate till the PVA fibres fracture due to the excessive strain, then de-bond and pull out of the matrix.

Concrete repair strategies often depend on the width of cracks propagating in structural elements since the crack width controls permeability and the ingress of hostile media that can compromise durability (Huang *et al.*, 2013). **Figure 3-25** displays the crack pattern on the surface of an ECC specimen after unloading from the flexural test. Previous studies have shown the existence of a correlation between water permeability of ECC and the third power of its crack width (Wang *et al.*, 1997), while chloride ions penetrability increased exponentially with the crack width (Tsukamoto, 1990). Thus, cracked HECC-SMAF, which is endowed with strain recovery capability, will have lower permeability than that of both traditional concrete and conventional ECC, and should consequently achieve superior durability.

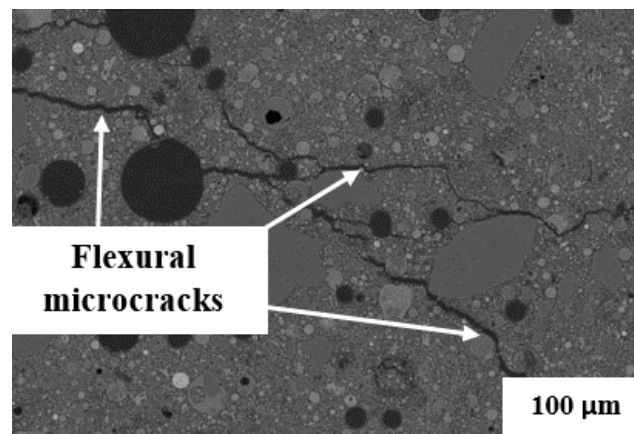


Figure 3-25: SEM for flexural crack pattern of ECC specimens.

Furthermore, thin sections from non-heated and heated ECC specimens were explored under SEM to investigate the effects of heat treatment on the microstructure. It was observed that heat treatment initiated a grid of multiple fine cracks (typically 10 μm in width or lower) in the ECC matrix (**Fig. 3-27**) without affecting the SMA fibre-matrix interfacial zone (**Fig. 3-26**). Yang *et al.* (2009) found that crack width smaller than 10 μm could be self-healed in cracked ECC sections, which can reduce its permeability and improve service life performance.

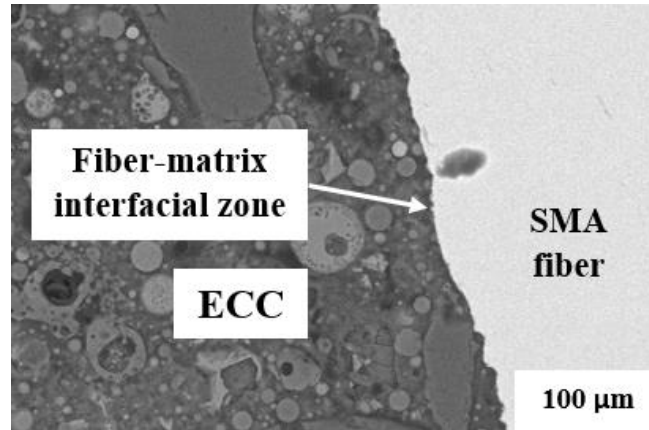


Figure 3-26: SEM for crack pattern of ECC specimens without heat treatment.

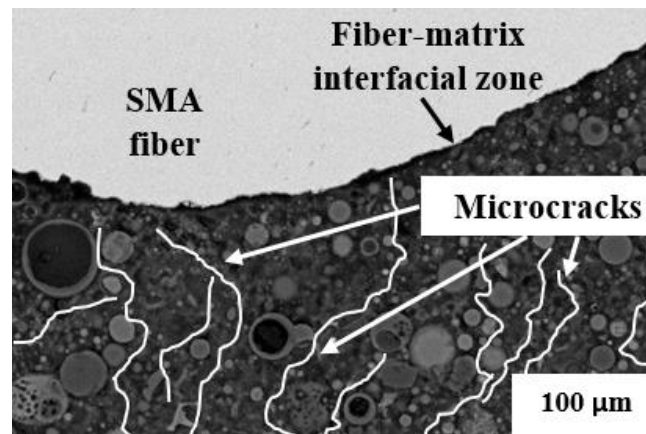


Figure 3-27: SEM for crack pattern of ECC specimens after heat treatment.

3.4 ANALYSIS OF VARIANCE OF TEST RESULTS

The analysis of variance (ANOVA) has been widely utilized for the analysis of experimental test results on cement-based materials (e.g. Ahmad and Alghamdi, 2014; Soliman and Nehdi, 2013; Nieves-Mendoza *et al.*, 2012). To explore whether an experimental variable such as SMA fibre addition is statistically significant using ANOVA, an F_o value is evaluated and compared to a standard F (critical) value of an F-distribution density function estimated from statistical tables correlated to a significance level (α) and degrees of freedom of error evaluated from an experiment using the number of variables and observations. The tested variable, namely SMA fibre addition, significantly affects the mean of the results if its F_o value exceeds the critical value of an F-

distribution density function, and vice versa (Montgomery, 2012). The F_o value can be determined after obtaining the sum of squares of test results as follows (Eqs. 3-8, 3-9 and 3-10):

$$SS_T = [\sum_{i=1}^a \sum_{j=1}^n y_{ij}^2] - [\frac{y_n^2}{N}] \quad (\text{Eq. 3-8})$$

$$SS_{Treatments} = [\frac{1}{n} \sum_{i=1}^a y_i^2] - [\frac{y_n^2}{N}] \quad (\text{Eq. 3-9})$$

$$SS_E = SS_T - SS_{Treatments} \quad (\text{Eq. 3-10})$$

Where SS_T is the total corrected sum of squares, $SS_{Treatments}$ is the sum of squares due to using different SMA fibre reinforcement ratios, SS_E is the sum of squares due to error (using replicates rather than testing only one specimen), a is the number of treatments (variables), n is the number of observations (specimens), y_{ij} is the j^{th} are observations under factor level of treatment i , and N is the total number of observations. The mean square of test data can be calculated as follows:

$$MS_{Treatments} = \frac{SS_{Treatments}}{a-1} \quad (\text{Eq. 3-11})$$

$$MS_E = \frac{SS_E}{N-a} \quad (\text{Eq. 3-12})$$

Where $MS_{Treatment}$ and MS_E are the mean square due to treatments and error, respectively. The F_o value can be determined as the ratio of the mean square due to treatments to that of obtained due to error as follows (Eq. 3-13):

$$F_o = \frac{MS_{Treatments}}{MS_E} \quad (\text{Eq. 3-13})$$

ANOVA at a significance level $\alpha_I = 0.05$ indicated that variation in the dosage of SMA fibre had an insignificant effect on the mean value of the compressive strength of the ECC composite. The obtained F_o value for the compressive strength results was 3.299, which is lower than the corresponding critical F value of 4.07 ($F_{0.05,3,8}$). Conversely, variation in the addition level of SMA fibre indicated a significant effect on the splitting tensile and flexural strengths of the ECC composite, as well as its recovery strain characteristic. The determined F_o values for the splitting tensile strength, flexural capacity and recovery strain were 17.635, 76.485 and 34.895, respectively. On the other hand, incorporating SMA fibres in ECC yielded insignificant effect on the lower toughness indices (I_5 and I_{10}) of the composite with corresponding F_o values of 2.06 and

3.43, respectively, which is lower than the corresponding critical $F_{0.05,3,8}$ value. Conversely, SMA fibre addition had a significant effect on the higher toughness indices of the ECC composite. The corresponding F_o values for the toughness indices I_{20} , I_{30} and I_{40} were 18.29, 48.7 and 68.41, respectively, which are significantly larger than the corresponding critical $F_{0.05,3,8}$ value.

3.5 SUMMARY AND CONCLUSIONS

An experimental investigation was conducted to explore the mechanical properties of a novel composite endowed with strain recovery and crack-healing capability. The engineered cementitious composite was made with 2% PVA along with 0%, 0.5%, 1% and 1.5% SMA short fibres by volume fraction and tested at the ages of 3, 28 and 90 days. Based on the experimental results, the conclusions below can be drawn:

- As expected, flow table values of ECC decreased due to PVA and/or SMA fibre addition. This can lead to less effective consolidation, thus affecting the mechanical properties. Hence, fibre-reinforced cementitious systems need to be carefully optimized to eliminate the effects of workability on mechanical performance.
- The compressive strength of ECC generally decreased due to PVA fibre addition at all testing ages. The SMA fibre addition did not have a significant effect on the compressive strength of the composite.
- Generally, the tensile capacity and flexural strength of the ECC composite were enhanced due to fibre addition. While, the control fibreless ECC matrix exhibited brittle failure, the mono- and hybrid-fibre-reinforced ECC specimens achieved ductile behaviour. ANOVA confirmed that the SMA fibre had significant positive effects on the tensile and flexural capacity and toughness of the ECC composite.
- ECC specimens incorporating 2% PVA and 1% SMA fibres acquired highest tensile and flexural capacity. Higher fibre dosage (e.g. ECC2-1.5 specimens) did not achieve superior tensile and flexural capacity due to fibre clustering and higher porosity compared to that of ECC2-1 specimens.
- Flexural strength and strain recovery by up to 35.4% and 36%, respectively, were achieved upon heat treatment of ECC specimens incorporating SMA fibres, owing to the crack-healing imparted by the shape memory effect. Conversely, an overall deterioration was

observed in the other specimens made with PVA fibres alone due to the heat treatment process, which caused multiple fine cracks at the front surface of specimens directly exposed to heating.

3.6 REFERENCES

- Ahmad, S. and Alghamdi, S.A., "A statistical approach to optimizing concrete mixture design." *The Scientific World Journal*, 2014, 561539, 7p.
- Akkaya, Y., Shah, S.P., and Ankenman, B., "Effect of fiber dispersion on multiple cracking of cement composites." *Journal of Engineering Mechanics*, 127(4), 2001, pp. 311-316.
- Akkaya, Y., Peled, A., and Shah, S.P., "Parameters related to fiber length and processing in cementitious composites." *Materials and Structures*, 33(8), 2000, pp. 515-524.
- Almusallam, T.H., Abadel, A.A., Al-Salloum, Y.A., Siddiqui, N.A., and Abbas, H., "Effectiveness of hybrid-fibers in improving the impact resistance of RC Slabs." *Int. Jr Imp. Eng.*, 81, 2015, pp. 61-73.
- Altwair, N.M., Johari, M.A.M., and Hashim, S.F.S., "Flexural performance of green engineered cementitious composites containing high volume of palm oil fuel ash." *Construction and Building Materials*, 37, 2012, pp. 518-525.
- ASTM C1018, "Standard Test Method for Flexural Toughness and First-Crack Strength of Fiber-Reinforced Concrete (Using Beam with Third-Point Loading)." *American Society for Testing and Materials*, ASTM International, West Conshohocken, USA, 1997, 8p.
- ASTM C150/C150M, "Standard specification for portland cement." *American Society for Testing and Materials*, ASTM International, West Conshohocken, USA, 2015, 9p.
- ASTM C1609/1609M, "Standard Test Method for Flexural Performance of Fiber-Reinforced Concrete (Using Beam with Third-Point Loading)." *American Society for Testing and Materials*, ASTM International, West Conshohocken, USA, 2012, 9p.

ASTM C1723, “Standard Guide for Examination of Hardened Concrete Using Scanning Electron Microscopy.” *American Society for Testing and Materials*, ASTM International, West Conshohocken, USA, 2010, 9p.

ASTM C230/C230M, “Standard Specification for Flow Table for Use in Tests of Hydraulic Cement.” *American Society for Testing and Materials*, ASTM International, West Conshohocken, USA, 2014, 6p.

ASTM C39/C39M, “Standard Test Method for Compressive Strength of Cylindrical Concrete Specimens.” *American Society for Testing and Materials*, ASTM International, West Conshohocken, USA, 2015a, 7p.

ASTM C469/C469M, “Standard Test Method for Static Modulus of Elasticity and Poisson’s Ratio of Concrete in Compression.” *American Society for Testing and Materials*, ASTM International, West Conshohocken, USA, 2014, 5p.

ASTM C494/C494M, “Standard specification for chemical admixtures for concrete.” *American Society for Testing and Materials*, ASTM International, West Conshohocken, USA, 2015a, 10p.

ASTM C496/C496M, “Standard Test Method for Splitting Tensile Strength of Cylindrical Concrete Specimens.” *American Society for Testing and Materials*, ASTM International, West Conshohocken, USA, 2011, 5p.

ASTM C618, “Standard specification for coal fly ash and raw or calcined natural pozzolan for use in concrete.” *American Society for Testing and Materials*, ASTM International, West Conshohocken, USA, 2015, 5p.

ASTM F2063, “Standard specification for wrought nickel-titanium shape memory alloys for medical devices and surgical implants.” *American Society for Testing and Materials*, ASTM International, West Conshohocken, USA, 2012, 6p.

Baddeley, A.J. and Silverman, B.W., “A cautionary example on the use of second-order methods for analyzing point patterns.” *Biometrics*, 40(4), 1984, pp. 1089-1093.

- Banthia, N. and Trottier, J-F., "Test methods for flexural toughness characterization of fiber reinforced concrete: some concerns and a proportion." *ACI Materials Journal*, 92(1), 1995, pp. 48-56.
- Bentur, A. and Mindess, S., "Fibre reinforced cementitious composites." *Taylor and Francis*, 2nd edition, New York, USA, 2007.
- Hameed, R., Turatsinze, A., Duprat, F. and Sellier, A., "Metallic fiber reinforced concrete: effect of fiber aspect ratio on the flexural properties." *ARPJ Jr. of Eng. and Applied Sciences*, 4(5), 2009, pp. 67-72.
- Hannant, D.J., "Fibre reinforcement in the cement and concrete industry." *Materials Science and Technology*, 11(9), 1995, pp. 853-861.
- Hirata, T., Kawanishi, T., Okano, M., Watanabe, S., "Study on material properties and structural performance of high-performance cement composites using polypropylene fiber." *Proceedings of Japan Concrete Institute*, 31(1), 2009, pp. 289-94.
- Huang, X., Ranade, R., Ni, W., and Li, V., "On the use of recycled tire rubber to develop low E-modulus ECC for durable concrete repairs." *Construction and Building Materials*, 46, 2013, pp. 134-141.
- Kim, M.K., Kim, D.J., Chung, Y-S., and Choi, E., "Direct tensile behavior of shape-memory-alloy fiber-reinforced cement composites." *Construction and Building Materials*, 102, 2016, pp. 462-470.
- Lee, Y., Kang, S-T., and Kim, J-K., "Pullout behavior of inclined steel fiber in an ultra-high strength cementitious matrix." *Construction and Building Materials*, 24(10), 2010, pp. 2030-2041.
- Li, M. and Li, V.C., "High-early-strength engineered cementitious composites for fast, durable concrete repair-material properties." *ACI Materials Journal*, 108(1), 2011, pp. 3-12.
- Li, W and Xu, J., "Mechanical properties of basalt fiber reinforced geopolymeric concrete under impact loading." *Materials Science and Engineering A*, 505, 2009, pp. 178-186.

- Liu, J., Li, C., Liu, J., Du, Z., and Cui, G., "Characterization of fiber distribution in steel fiber reinforced cementitious composites with low water-binder ratio." *Indian Journal of Engineering and Materials Sciences*, 18(6), 2011, pp. 449-457.
- MacVicar, R., Matuana, L.M., and Balatinez, J.J., "Aging mechanism in cellulose fiber reinforcement cement composite." *Cement and Concrete Composites*, 21, 1999, pp. 189-196.
- Montgomery D.C., "Design and Analysis of Experiments." *8th Edition*, John Wiley & Sons, 2012, 724p.
- Nehdi, M., Alam, M.S., and Youssef, M.A., "Development of corrosion-free concrete beam-column joint with adequate seismic energy dissipation." *Engineering Structures*, 32(9), 2010, pp. 2518-2528.
- Nehdi, M. and Ladanchuk, J.D., "Fiber synergy in fiber-reinforced self-consolidating concrete." *ACI Materials Journal*, 101(6), 2004, pp. 508-517.
- Nieves-Mendoza, D., Gaona-Tiburcio, C., Hervert-Zamora, H.L., Tobias J.R., Castro-Borges, P., Colas O.R., Zambrano Robledo, P., Martínez-Villafañe A., and Almeraya-Calderón, F., "Statistical analysis of factors influencing corrosion in concrete structures." *International Journal of Electrochemical Science*, 7, 2012, pp. 5495-5509.
- Pan, Z., Wu, C., Liu, J., Wang, W., and Liu, J., "Study on mechanical properties of cost-effective polyvinyl alcohol engineered cementitious composites (PVA-ECC)." *Constr. Build. Mat.*, 78(1), 2015, pp. 397-404.
- Rahmani, T., Kiani, B., Shekarchi, M., and Safari, A., "Statistical & experimental analysis on the behavior of fiber reinforced concretes subjected to drop weight test." *Const. Build. Mat.*, 37, 2012, pp. 360-369.
- Rathod, J.D. and Patodi, S.C., "Interface tailoring of polyester-type fiber in engineered cementitious composite matrix against pullout." *ACI Materials Journal*, 107(2), 2010, pp. 114-122.

- Romualdi, J.P. and Mandel, J.A., "Tensile strength of concrete affected by uniformly distributed closely spaced short lengths of wire reinforcement." *ACI Journal*, 61(6), 1964, pp. 657-671.
- Said, S.H., Razak, H.A., and Othman, I., "Flexural behavior of engineered cementitious composites (ECC) slabs with polyvinyl alcohol fiber." *Construction and Building Materials*, 75, 2015, 176-188.
- Soe, K.T., Zhang, Y.X., and Zhang, L.C., "Impact resistance of hybrid-fiber engineered cementitious composite panels." *Composite Structures*, 104, 2013, pp. 320-330.
- Soe, K.T., Zhang, Y.X., and Zhang, L.C., "Material properties of a new hybrid-fibre reinforced engineered cementitious composite." *Construction and Building Materials*, 43, 2013, pp. 399-407.
- Soliman, A.M. and Nehdi, M.L., "Effect of natural wollastonite microfibers on early age behavior of UHPC." *Journal of Materials in Civil Engineering*, 24(7), 2012, pp. 816-824.
- Soliman, A.M. and Nehdi, M.L., "Effect of partially hydrated cementitious materials and superabsorbent polymer on early-age shrinkage of UHPC." *Construction and Building Materials*, 41, 2013, pp. 270-275.
- Song, P.S., Hwang, S., and Sheu, B.C., "Strength properties of nylon- and polypropylene-fiber-reinforced concretes." *Cement and Concrete Research*, 35(8), 2005, pp. 1546-1550.
- Stoyan, D., Kendall, W.S., and Mecke, J., "Stochastic geometry and its applications." *John Wiley & Sons, Chichester*, 2nd edition, 1995, 257p.
- Tsukamoto, M., "Tightness of fiber concrete." *Darmstadt Concrete, Annual Journal on Concrete and Concrete Structures*, 5, 1990, pp. 215-225.
- Wang, K., Jansen, D.C., Shah, S.P., and Karr, A.F., "Permeability study of cracked concrete." *Cement and Concrete Research*, 27(3), 1997, pp. 381-393.

Yang, Y., Lepech, M.D., Yang, E-H., and Li, V.C., "Autogenous healing of engineered cementitious composites under wet-dry cycles." *Cement and Concrete Research*, 39(5), 2009, pp. 382-390.

Yuan, F., Pan, J., Dong, L., and Leung, C.K.Y., "Mechanical behavior of steel reinforced ECC or ECC/concrete composite beams under reversed cycling loading." *Mat. in Civil Eng.*, 26(8), 2014, 8p.

Chapter 4

4 TENSILE AND FLEXURAL BEHAVIOUR OF HYBRID FIBRE REINFORCED ENGINEERED CEMENTITIOUS COMPOSITE WITH STRAIN RECOVERY³

4.1 INTRODUCTION

The tensile properties of ECCs have often been characterized via uniaxial tensile testing (UTT). However, the test is laborious, costly and requires sophisticated test procedures (Kanakubo, 2006; Ostergaard et al., 2005). Thus, there is interest in developing simpler alternatives. Stang and Li (2004) proposed the four-point bending test (FPBT) as an efficient alternative to UTT in determining the tensile behaviour of fibre-reinforced cementitious materials (FRCC). The proposed test was extended with inverse analysis to transform the bending behaviour into tensile characteristics. Recently, there has been growing interest in utilizing the inverse analysis of FPBT in the quality control of cementitious materials (e.g. Qian and Zhang, 2012; Qian and Li, 2008; Qian and Li, 2007).

³ A version of this chapter was submitted for publication to the *Composite Part B Journal*. Part of this chapter was also published in the *5th International conference of the CSCE*, London, Canada, (2016).

In the present chapter, experimental uniaxial tensile test results obtained on different hybrid self-centering ECC mixtures will be critically analyzed. Subsequently, the inverse analysis approach will be discussed to establish an effective approach for acquiring the tensile properties of ECC from the much simpler and cost-effective four-point bending test data obtained in Chapter 3.

4.2 EXPERIMENTAL PROCEDURES

A series of uniaxial tensile tests were performed on 160 mm x 50 mm x 20 mm ECC coupon specimens (**Fig. 4-1**) to investigate the tensile characteristics of the different ECC mixtures. Three coupon specimens from each ECC mixture were prepared for the evaluation of the tensile behaviour at the ages of 90 days using an Instron testing machine with a capacity of 250 kN.

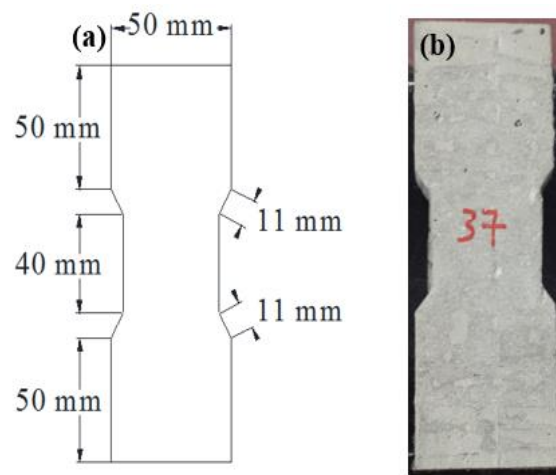


Figure 4-1: Illustration of ECC coupon specimens: a) schematic, and b) photograph.

The tests were carried out under displacement control with a loading rate of 0.5 mm/min as per the guidelines of the Japan Society of Civil Engineers (JSCE, 2008) for direct tension testing of high-performance fibre-reinforced concrete (HPFRC). During setup, the wedge pressure was adjusted to provide uniform friction and pressure, assuring that the failure occurs within the failure zone (mid-zone) of specimens, as shown in **Fig. 4-2**.

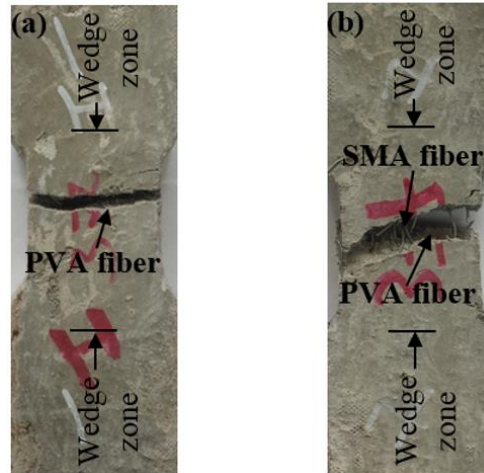


Figure 4-2: Failure patterns of ECC coupon specimens: a) PVA-ECC, and b) HECC-SMAF.

MIP testing was also conducted to determine variations in the pore structure of specimens retrieved from the tested ECC mixtures. Three samples from each ECC mixture were tested using a Micromeritics AutoPore IV 9500. The ECC specimen was dried till reaching a constant mass, then placed in a glass tube (penetrometer), which was then filled with mercury under low-pressure (less than 50 $\mu\text{m}/\text{Hg}$). Thereafter, the penetrometer including the sample and mercury was placed in a high-pressure (14.7 psi to 60,000 psi) vertical port to further infiltrate mercury into the pores of the specimen. The volume of the intruded mercury was recorded at each pressure level.

4.3 INVERSE ANALYSIS FOR DETERMINING TENSILE PROPERTIES

Considering the complications associated with direct tensile testing of concrete, there is growing interest in using much simpler four-point bending as an alternative. Different methods have been proposed to inversely determine the tensile properties of cement-based materials from bending test results. This includes the iterative method (Roelfstra and Wittmann, 1986), multi-layer procedures (Hordijk, 1991), cracked hinge model (Stang and Olesen, 1998), and poly-linear approximation (Kitsutaka, 1995). Qian and Li (2007) developed an inverse analysis that consists of a set of simplified equations used in evaluating the tensile strain capacity and effective tensile strength of cementitious materials from FPBT results. The tensile strain capacity and its deviation can be calculated as follows:

$$\varepsilon_{tu} = (0.5 * \delta_u) - 0.22 \quad (\text{Eq. 4-1})$$

$$PD = (0.5 * SD) + 0.18 \quad (\text{Eq. 4-2})$$

Where ε_{tu} is the predicted average tensile strain capacity in percent, δ_u is the average deflection capacity of FPBT in mm, PD is the predicted deviation for tensile strain capacity in percent, and SD is the standard deviation of the deflection capacity in mm. The tensile strength of cementitious materials can be evaluated within a lower limit (Naaman and Reinhardt, 1996) and upper limit (Billington, 2004) using **Eqs. 4-3 and 4-4**, respectively, as follows:

$$\sigma_{tl} = \frac{MOR}{(0.09 * Ln(\varepsilon_{tu}) + 2.69)} \quad (\text{Eq. 4-3})$$

$$\sigma_{tu} = \frac{MOR}{(0.14 * Ln(\varepsilon_{tu}) + 2.42)} \quad (\text{Eq. 4-4})$$

Where σ_{tl} and σ_{tu} are the lower and upper limits of the predicted effective tensile strength in MPa, respectively, MOR is the modulus of rupture obtained from FPBT in MPa, and Ln is the natural logarithm.

4.4 RESULTS AND DISCUSSION

4.4.1 Tensile Performance

Figure 4-3 illustrates typical UTT stress-strain curves of different ECC specimens at 90 days. ECC specimens exhibited strain capacity of up to 8% with appearance of multiple cracking till failure. After first crack, the stress continued to raise with inelastic strain and started to decline after reaching the peak strength. SMA fibre addition generally improved the tensile properties of the composite. For instance, the ultimate tensile strength of the ECC2-0.5, ECC2-1 and ECC2-1.5 specimens increased by about 29.8%, 74% and 39.8%, respectively compared to that of the ECC specimens incorporating 2% PVA fibre by volume fraction alone. The achieved tensile strength of the hybrid ECC reinforced with SMA fibres (coined herein HECC-SMAF) ranged between 6 MPa and 8 MPa, depending on the SMA fibre content. Likewise, the strain capacity corresponding to the peak strength was substantially enhanced by SMA fibre addition. The strain capacity of the

HECC-SMAF specimens reached nearly two orders of magnitude higher than that of the mono-PVA-ECC specimens. For example, the strain capacity at peak strength of the ECC2-0.5, ECC2-1 and ECC2-1.5 specimens was improved by about 90%, 146% and 111%, respectively, compared to that of ECC2-0. The superior tensile performance of HECC-SMAF specimens can be ascribed to the higher fibre content which enhanced the load carrying capacity of the composite. On the other hand, the decreased tensile capacity of ECC2-1.5 specimens can be attributed to higher porosity and non-uniformity of fibre distribution compared to that of ECC2-1 specimens. However, ECC2-1.5 specimens still achieved superior tensile capacity to that of the mono-PVA-ECC specimens. The consolidation of the ECC matrix was affected by the high fibre content, yielding additional porosity due to the development of fibre clustering and appearance of more fibre free-area. Evidence for the aforementioned issues is provided in subsequent sections.

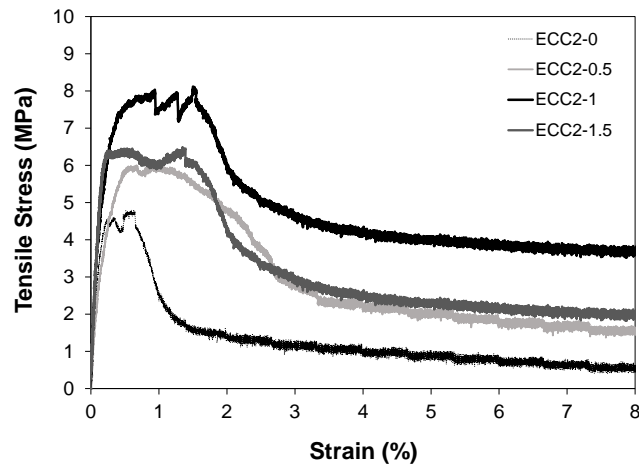


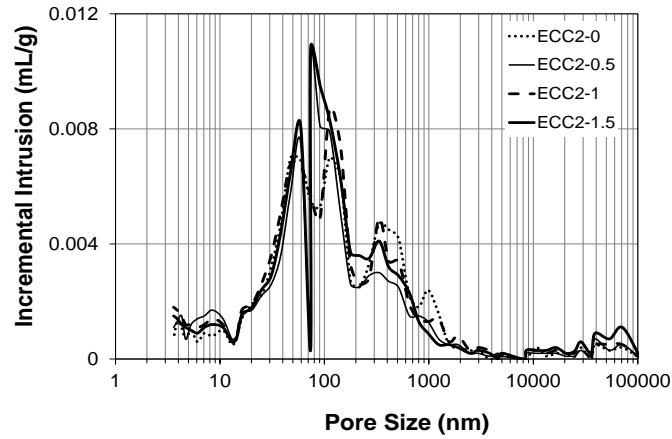
Figure 4-3: Typical tensile stress-strain curve of different ECC specimens.

4.4.2 Effect of Porosity

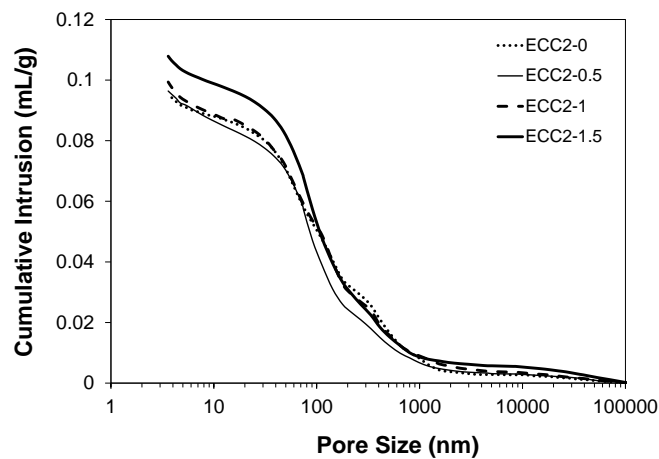
Table 4-1 reports the average mercury intrusion volumes propagated in the different ECC specimens. **Figure 4-4** displays the variation of mercury intrusion volume along with the pore size diameter in specimens from the different ECC mixtures. It can be observed that most existing pores in the ECC matrix had diameters ranging between 45 and 90 nm. However, the pore structure of the composite shifted to a wider range due to incorporating SMA fibres. For instance, the pore diameter in the mono- and hybrid- fibre reinforced specimens ranged from 25 to 500 nm.

Table 4-1: Cumulative mercury intrusion volume of ECC specimens (mL/g)

Mixture ID	Specimen 1	Specimen 2	Specimen 3	Average
ECC2-0	0.09391	0.09135	0.09112	0.09213
ECC2-0.5	0.09539	0.09088	0.10028	0.09552
ECC2-1	0.09306	0.09635	0.10467	0.09803
ECC2-1.5	0.11066	0.10914	0.10447	0.10809

**Figure 4-4: Incremental mercury intrusion volume and pore size distribution for ECC specimens.**

The cumulative mercury intruded volume in the ECC specimens is portrayed in **Fig. 4-5**. It can be observed that the pore volume in the hybrid- fibre-reinforced ECC specimens was higher than that of the control ECC matrix.

**Figure 4-5: Cumulative mercury intrusion volume and pore size distribution for ECC specimens.**

Incorporating SMA fibres in hybrid PVA-SMA ECC specimens slightly increased the porosity of the composite compared to that of mono PVA-ECC specimens. For instance, the porosity of the ECC2-0.5 and ECC2-1 specimens was 3.6% and 6.4% higher than that of the control ECC2-0 specimens, respectively. However, incorporating more than 1% SMA fibres in the composite exacerbated this effect. For instance, the ECC specimen with 2% PVA and 1.5% SMA fibres had about 17.3% higher porosity than that of the mono-PVA-ECC specimens.

4.5 UTT AND FPBT data correlation

Table 4-2 summarizes the tensile and flexural test data of mono- and hybrid-fibre ECC specimens at 90 days. **Figure 4-6** displays a comparison between the predicted strain capacity from FPBT deflection and the tensile strain capacity obtained from UTT for the different ECC specimens. The tensile strain capacity obtained from UTT on different ECC specimens was compared to corresponding data predicted by the inverse method (**Eq. 4-1**) using FPBT results.

Table 4-2: Tensile and flexural behaviour of ECC specimens at 90 days

Specimen ID	Tensile behaviour			Flexural behaviour		
	First crack strength (MPa)	Ultimate tensile strength (MPa)	Tensile strain capacity (%)	First crack strength (MPa)	MOR (MPa)	Deflection at failure (mm)
ECC2-0	1.62	4.71	8.00	3.66	7.13	2.93
ECC2-0.5	2.05	6.00	8.00	3.53	8.11	3.66
ECC2-1	2.76	8.04	8.00	4.25	12.52	6.17
ECC2-1.5	2.21	6.63	8.00	4.92	10.54	4.24

Reasonable agreement was observed within an average variation of 15%. According to Qian and Zhang (2012), a difference within 20% reflects adequate agreement and reasonable accuracy of the proposed method. Furthermore, a comparison of the predicted tensile strength and MOR for the different ECC specimens with respect to tensile strain capacity is portrayed in **Fig. 4-7**. Tensile strength is defined as the average of first cracking strength and ultimate tensile strength. It can be observed that the effective tensile strength predicted from FPBT results is located within the upper and lower limit strengths proposed using **Eqs. 4-3 and 4-4** with an average variation of 8.2% from the upper limit strength.

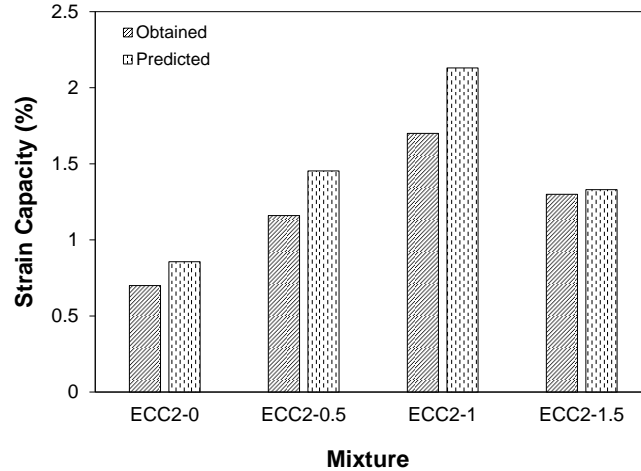


Figure 4-6: Comparison between tensile strain capacity of UTT and FPBT.

According to Rahmani *et al.* (2012), a coefficient of determination (R^2) of 0.7 or higher is sufficient for a reasonable reliability model. Since the R^2 value shown in **Fig. 4-7** for the MOR/effective tensile strength ratio of ECC specimens is about 0.75, **Eqs. 4-3 and 4-4** could reasonably be used to represent the correlation between the ultimate effective tensile strength and MOR of ECC with respect to tensile strain capacity.

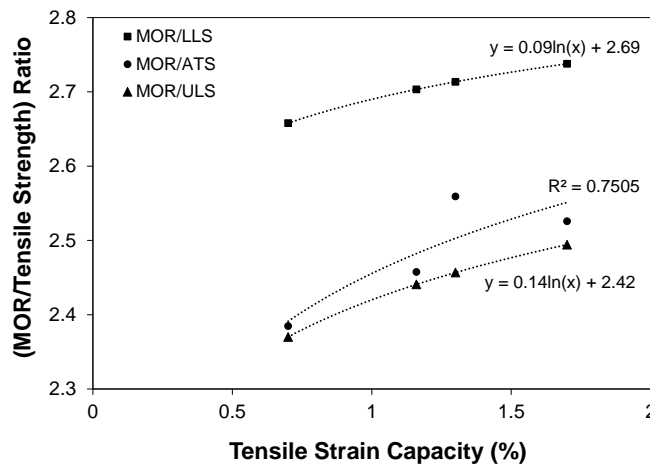


Figure 4-7: Predicted tensile strength and MOR relationship with respect to tensile strain capacity of ECC.

4.6 STATISTICAL ANALYSIS

4.6.1 Analysis of Variance of Test Results

At a significance level $\alpha_I = 0.05$, ANOVA of test results indicated that variation in the addition level of SMA fibre had a significant effect on the mean value of the tensile strength of the ECC composite. The determined F_o values for the tensile strength of test results was 25.21. This value is higher than the corresponding critical F value of 4.07 ($F_{0.05,3,8}$), which reflects the significant effect of utilizing SMA fibres in the production of hybrid ECC composites. This is inconsistent with aforementioned observations in the analysis of experimental results.

4.6.2 Analysis of fibre dispersion

The mechanical properties of fibre-reinforced composites are significantly affected by fibre distribution and fibre free areas (Akkaya *et al.*, 2001). Better fibre distribution with decreased fibre-free area can improve the first crack stress, multiple cracking response and fracture toughness of the composite (Akkaya *et al.*, 2000). Similarly, by achieving enhanced fibre spatial distribution with minimal fibre clumping, the fibre crack bridging ability and transferring of load to other parts of the composite could be improved. Fibre-reinforced concrete elements with higher fibre clumping percentages would crack at lower load than that of similar mixtures with better fibre dispersion (Akkaya *et al.*, 2001). In the present study, image processing analysis was conducted for cracked surfaces of ECC prismatic specimens, as displayed in **Fig. 4-8**. The cracked surface was finely snipped with diamond cut and then polished and exposed to strong white light. Subsequently, a Canon EOS Rebel T5 digital camera with a resolution of 18 million (5184 x 3456) pixels was used to take images of the prepared section. The best contrast between fibres and the surrounding matrix was obtained using the light reflecting properties of SMA fibres. Cross-sections of ECC specimens of 80 mm x 40 mm [32 in x 16 in] were divided into eight areas, 17.5 mm x 15 mm [7 in x 6 in] each, to better analyze the fibre dispersion through the composite and a photo of each was taken. This represents a resolution of about 0.0035 mm/pixel, which was sufficient for identifying the 0.625 mm diameter SMA fibres through the section. The edge area was excluded due to irregularity of fibre dispersion in this zone (Akkaya *et al.*, 2001). The determination of SMA fibre dispersion through the composite was performed on a fibre spacing basis as proposed by Romualdi (1964) and utilized by Liu *et al.* (2011). It was observed that ECC2-

1 specimens showed better dispersion of SMA fibre with smaller fibre-free areas compared to that of the ECC2-0.5 specimens. Conversely, ECC2-1.5 specimens displayed less uniform dispersion of SMA fibre with existence of fibre clustering and appearance of fibre-free areas.

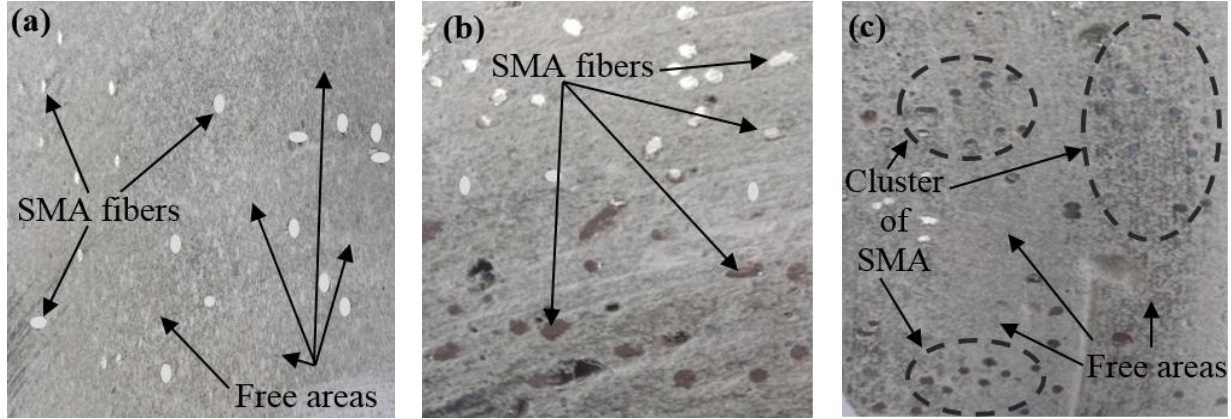


Figure 4-8: Dispersion of SMA fibres: a) ECC2-0.5, b) ECC2-1, and c) ECC2-1.5.

Furthermore, the method of statistical point approaches was utilized for the statistical analysis of fibre distribution. To statically analyze the SMA fibre dispersion in ECC specimens, two statistical functions known as *K*-function and *F*-function were utilized. The *K*-function measures the tendency of fibres to clump, while the *F*-function evaluates the fibre-free area (Stoyan *et al.*, 1995). After applying the flexural test, the cracked cross-section orthogonal to the loading direction was divided into central (defined as all points laying at least 1/8 of the specimen smallest dimension from edges), edge, and corner zones. The central area was investigated while the other regions were not investigated due to limitation of the analysis process for these zones (Akkaya *et al.*, 2001). The *K*-function can be estimated as follows (Eq. 4-5):

$$K(r) = \left[\sum_{fibers \in A_R} \frac{\text{number of fibers within } r \text{ for a given fiber}}{(\text{total number of fibers in } A_R)^2} \right] * (A_R) \quad (\text{Eq. 4-5})$$

Where r is the distance from fibre, ranging between zero and R ($R = 15$ mm; half the smallest dimension of central area), A_R is the central area. Thereafter, the calculated *K*-function was compared to the complete spatial randomness *K*-function. The random *K*-function can be evaluated as follows (Eq. 4-6):

$$K(r) = \pi * r^2 \quad (\text{Eq. 4-6})$$

A better distribution of fibres can be observed in specimens with K -function of less than the random distribution pattern (fibres avoid each other), while specimens with a K -function higher than the random distribution pattern indicates tendency for fibre clumping. **Equation 4-7** can be used to evaluate the percentage of fibres clumping in a specimen with respect to the random dispersion as follows:

$$\% \text{ clumping} = \left(\frac{C}{\pi} - 1 \right) * 100 \quad (\text{Eq. 4-7})$$

Where C is a constant. According to Baddeley and Silverman (1984), the fibre clumping performance cannot be captured using the K -function alone. The F -function together with the K -function can be used in representing unusual behaviour (Akkaya *et al.*, 2000). The F -function can be evaluated through planning a regular grid of points on A_R and then finding the nearest fibre to each grid point. The F -function is calculated as follows (**Eq. 4-8**):

$$F(r) = \frac{\text{number of grid points in } A_R \text{ whose nearest fiber is lesser than } r \text{ away}}{\text{total number of grid points in } A_R} \quad (\text{Eq. 4-8})$$

Likewise, the F -function is compared to the F -function under the complete spatial randomness condition and can be estimated as follows (**Eq. 4-9**):

$$F(r) = 1 - e^{-\pi * \lambda * r^2} \quad (\text{Eq. 4-9})$$

Where λ is the fibre density, which can be calculated by dividing the cross-sectional area of all fibres by the area of the cracked section. The term $1-F(r)$ is utilized in evaluating the fibre-free area. Higher values of $1-F(r)$ denote the existence of fibre-free area and vice-versa. Fibre-reinforced specimens with F -function higher than the complete spatial randomness F -function denote a uniform distribution behaviour. Conversely, specimens with lower F -function than that of the random F -function refer to a clumping trend.

Figure 4-9 displays the calculated K -function values of different ECC specimens compared to that estimated under the random K -function. It can be observed that incorporating 1.5% SMA fibres in ECC2-1.5 specimens produced a fibre clumping behaviour with a trend higher than that of the K -function under the spatial randomness condition. The percentage of fibre clumping of ECC2-1.5 is about 22.28% with respect to the random K -function. Conversely, the ECC2-0.5 and ECC2-1

specimens showed better dispersion of SMA fibres with K -values lower than that of the random K -function. This is consistent with visual observation mentioned earlier. Although, ECC2-0.5 and ECC2-1 specimens displayed regular distribution of SMA fibres, ECC2-1 specimens displayed superior dispersion of SMA fibres than that of ECC2-0.5 specimens, especially at higher r distances. This can be observed via the lower K -function values at $r > 8$ mm of ECC2-1 specimens.

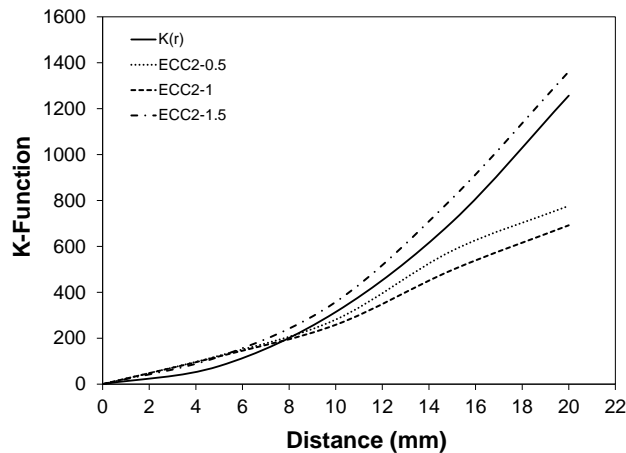


Figure 4-9: Typical statistical K-function of ECC specimens and random dispersion.

Likewise, **Fig. 4-10** portrays the estimated F -function values of different ECC specimens compared to that of the F -function under the spatial randomness condition. The highest F -function trend was acquired by ECC2-1 compared to that of ECC2-0.5, ECC2-1.5 specimens, and random F -function, which reflects regularity of SMA fibre dispersion. This is consistent with results achieved previously by K -function analysis. The F -function of ECC2-0.5 and ECC2-1.5 specimens had similar trend to that of the random F -function, which indicates their random fibre dispersion behaviour. However, at higher r distances, this trend was not effective for the ECC2-1.5 specimens. The F -function was much lower than the random F -function (typically at $r > 12$ mm), which reflects a probability of fibre clumping.

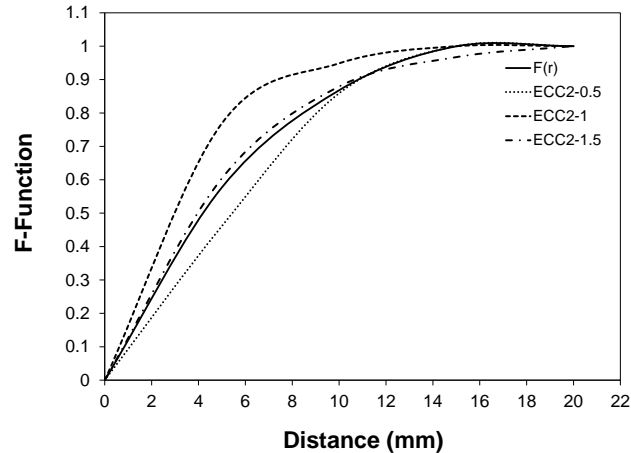


Figure 4-10: Typical statistical F-function of ECC specimens and random dispersion.

Furthermore, **Fig. 4-11** illustrates the percentage of fibre-free area for different ECC specimens with respect to r distances. It can be observed that all ECC specimens displayed availability of fibre-free areas at lower and medium r distances (typically lower than 10 mm). The lowest fibre-free area was achieved in ECC2-1 specimens, which indicates uniformity of SMA fibre dispersion with relatively small spaces between fibres. Conversely, ECC2-0.5 specimens yielded the highest percentage of fibre-free area, followed by ECC2-1.5 specimens.

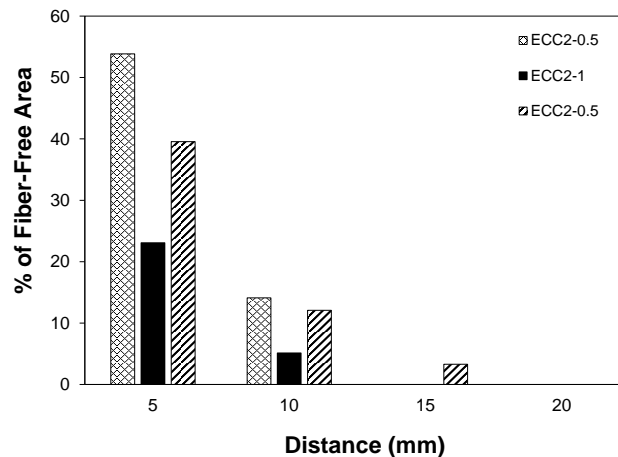


Figure 4-11: Fibre-free areas percentage of ECC specimens with respect to r distance.

Furthermore, in ECC2-0.5 and ECC2-1 specimens, it is revealed that the fibre-free area no longer existed at higher r distances (more than 10 mm), reflecting more uniformity of fibre dispersion. However, in the ECC2-1.5 specimens, the free areas between SMA fibres at higher r distances still

existed, which reflects the tendency of SMA fibres to cluster at high fibre dosage. The analysis of fibre distribution above clarifies the effect of fibre dosage on mechanical performance of the hybrid- fibre-reinforced ECC composite.

4.7 CONCLUSIONS

In this chapter, uniaxial tensile testing (UTT) was carried out on a novel hybrid-ECC composite incorporating hybrid PVA and SMA short fibres (HECC-SMAF) at 90 days. An inverse analysis was used to predict the tensile characteristics of the composite using FPBT data achieved in chapter 3. The following conclusions can be drawn:

- Generally, the tensile characteristics of the ECC composite were enhanced owing to SMA fibre addition. The ECC specimens incorporating 2% PVA and 1% SMA fibres achieved the highest tensile strength.
- Fibre dosages beyond 2% PVA and 1% SMA by volume fraction led to fibre clustering and caused higher porosity in the hybrid ECC composite, which resulted in reduced performance under tensile loading.
- Statistical ANOVA treatment demonstrated that SMA fibre addition had significant effects on the tensile capacity of the ECC composite.
- Analysis of fibre dispersion revealed that the ECC2-1 specimens displayed superior fibre dispersion compared to that of the ECC2-0.5 and ECC2-1.5 specimens, which is consistent with observed better mechanical performance.
- An inverse method was successfully validated for estimating the tensile properties of different ECC mixtures based on results of the simple four point bending test. This method could save time and cost required for conducting complicated uniaxial tensile testing, while achieving adequate accuracy.

4.8 REFERENCES

- Akkaya, Y., Peled, A., and Shah, S.P., "Parameters related to fiber length and processing in cementitious composites." *Materials and Structures*, 33(8), 2000, pp. 515-524.
- Akkaya, Y., Shah, S.P., and Ankenman, B., "Effect of fiber dispersion on multiple cracking of cement composites." *Journal of Engineering Mechanics*, 127(4), 2001, pp. 311-316.

- Aveston, J. and Kelly, A., "Theory of multiple fracture of fibrous composites." *Journal of Materials Science*, 8(3), 1973, pp. 352-362.
- Billington, S.L., "Damage-tolerant cement-based materials for performance based earthquake engineering design: research needs." In *LI VC ed. Proceedings of Int. Conf. on Fracture Mechanics of Concrete and Concrete Structures (Framcos-5)*, Ia-FraMCos, 2004, pp. 53-60.
- Bolander, J.E., Choi, S., and Duddukuri, S.R., "Fracture of fiber-reinforced cement composites: effects of fiber dispersion." *Int. Journal of Fracture*, 154(1), (2008), pp. 73-86.
- Bordelon, A.C. and Roesler, J.R., "Spatial distribution of synthetic fibers in concrete with X-ray computed tomography." *Cement and Concrete Composites*, 53, 2014, pp. 35-43.
- Dupont, D. and Vandewalle, L., "Distribution of steel fibres in rectangular sections." *Cement and Concrete Composites*, 27(3), 2005, pp. 391-398.
- Hordijk, D.A., "Local approach to fatigue of concrete." *Ph.D. Thesis, Department of Concrete Structures, Faculty of Civil Engineering, Delft University of Technology*, 1991.
- JSCE, "Recommendations for Design and Construction of High Performance Fiber Reinforced Cement Composites with Multiple Fine Cracks. *Japan Soc. Civil Eng.*, 2008, 14p.
- Kanakubo, T., "Tensile characteristics evaluation method for DFRCC." *Journal of Advanced Concrete Technology*, 4(1), 2006, pp. 3-17.
- Kitsutaka, Y., "Fracture parameters for concrete based on poly-linear approximation analysis of tension softening diagram." *Fracture mechanics of concrete structures*, Proceedings of FramCos-2, 1995, pp. 199-208.
- Lee, B.Y., Kang, S-T., Yun, H-B., and Kim, Y.Y., "Improved sectional image analysis technique for evaluating fiber orientations in fiber-reinforced cement-based materials." *Materials*, 9(1), 2016, pp. 1-13.

- Liu, J., Li, C., Liu, J., Du, Z., and Cui, G., "Characterization of fiber distribution in steel fiber reinforced cementitious composites with low water-binder ratio." *Indian Journal of Engineering and Materials Sciences*, 18(6), 2011, pp. 449-457.
- Naaman, A. E. and Reinhardt, H. W., "Characterization of high performance fiber reinforced cement composites (HPFRCC)." *In High Performance Fiber Reinforced Cementitious Composites, RILEM Proceedings*, 31, 1996, pp. 1-23.
- Ostergaard, L., Walter, R., and Olesen, J.F., "Method for determination of tensile properties of engineered cementitious composites (ECC)." *ConMat '05*, Vancouver, Canada, 2005, 10p.
- Ozyurt, N., Woo, L.Y., Mason, T.O., and Shah, S.P., "Monitoring fiber dispersion in fiber-reinforced cementitious materials: Comparison of ac-impedance spectroscopy and image analysis." *ACI Materials Journal*, 103(5), 2006, pp. 340-347.
- Qian, S. and Zhang, Z., "Comparison of tensile properties of strain hardening cementitious composite cured in normal and accelerated conditions." *Jour. Test. & .* 40(5), 2012, pp. 1-6.
- Qian, S.Z. and Li, V.C., "Simplified inverse method for determining the tensile strain capacity of strain hardening cementitious composites." *Journal of Advanced Concrete Technology*, 5(2), 2007, pp. 235-246.
- Qian, S.Z. and Li, V.C., "Simplified inverse method for determining the tensile properties of strain hardening cementitious composites (SHCC)." *Journal of Advanced Concrete Technology*, 6(2), 2008, pp. 353-363.
- Rahmani, T., Kiani, B., Shekarchi, M., and Safari, A., "Statistical and experimental analysis on the behavior of fiber reinforced concretes subjected to drop weight test." *Construction and Building Materials*, 37, 2012, pp. 360-369.
- Roelfstra, P.E. and Wittmann, F.H., "Numerical method to link strain softening with failure of concrete." *In: Wittmann, F.H., 18th ed., Fracture Toughness and fracture energy*, Elsevier, London, 1986, pp. 163-175.

Romualdi, J.P. and Mandel, J.A., "Tensile strength of concrete affected by uniformly distributed closely spaced short lengths of wire reinforcement." *ACI Journal*, 61(6), 1964, pp. 657-671.

Stang, H. and Li, V. C., "Classification of fiber reinforced cementitious materials for structural applications." *Proceedings of BEFIB, 6th RILEM Symposium on Fiber-Reinforced Concretes (FRC)*, Varenna, Lake Como, Italy, 2004, pp. 197-218.

Stang, H. and Olesen J.F., "On the interpretation of bending tests on FRC-materials." *Fracture mechanics of concrete structures*, Proceedings of FramCos-3, 1, 1998, pp. 511-520.

Chapter 5

5 EXPLORING BEHAVIOUR OF NOVEL HYBRID-FIBRE REINFORCED ENGINEERED CEMENTITIOUS COMPOSITE UNDER IMPACT LOADING⁴

5.1 INTRODUCTION

Concrete reinforced with steel rebar (RC) has been utilized for many decades in the construction of protective structures to resist impact and dynamic loads (Soe *et al.*, 2013). Subsequent to the attack on the world trade center twin towers, research on the resistance of structures to impact loading, explosive waves and penetration of fragments has become a very active research topic, especially for military and defense facilities. Under impact loading, the failure of RC elements has often led to partial or total collapse of buildings, causing substantial economic and human life losses (Alemdar and Sezen, 2010).

⁴ A version of this chapter was published in the *Materials and Design Journal* (2017). Parts of this chapter were also published in the *6th International conference of the CSCE*, Vancouver, Canada, (2017) and in the *11th International conference on Civil and Architecture Engineering*, Cairo, Egypt, (2016).

Reinforced concrete has been the construction material of choice for critical civilian infrastructure and defensive structures. Due to its low tensile strength, concrete exhibits brittle failure under dynamic loading, which can compromise structural integrity and safety within and near protective facilities. When a structural concrete element is subjected to dynamic loading, such as impacts or explosions, it experiences unique states of stresses. For instance, near the impacted location, severe hydrostatic compression can propagate and the state of stress irreversibly compresses the concrete. Simultaneously, away from the impacted area, confinement stresses are decreased, and the concrete undergoes compression with a moderate state of stress. Moreover, the reflected rear face compressive wave of the target produces tensile waves, which interacts with compressive waves possibly leading to spalling of the concrete (Li and Zhang, 2012).

Most pertinent recent research work focused on the impact behaviour of cement-based materials reinforced by mono-fibres (Song *et al.*, 2005; Li and Xu, 2009; Yoo *et al.*, 2015) and/or hybrid-fibres with two different types of fibres or more (Soe *et al.*, 2013; Nehdi and Duquette, 2004; Nia *et al.*, 2012). For instance, Almusallam *et al.* (2015) investigated the effect of utilizing more than two different types and sizes of fibres on the impact resistance of hybrid-FRC slabs. They tested a set of slabs reinforced with steel (SE), polypropylene (PP) and Kevlar fibres under the effect of high-velocity projectiles of up to 657 m/s. Results showed that the geometrical properties of fibres were more influential than their material properties in improving the impact resistance of the hybrid-fibre reinforced slabs. The notion behind the growing interest in using hybrid fibres with two or more fibre types and sizes is that they could create synergistic effects through their different elastic properties and/or various sizes since micro-fibres can control the growth of micro-cracks, while large fibres restrain the growth of larger cracks.

With the advent of engineered cementitious composites (ECC) and emergence of smart materials such as shape memory alloys (SMA), new opportunities in tailoring high-impact resistance cement-based materials have opened up. Maalej *et al.* (2005) explored the behaviour of hybrid-fibre ECC panels reinforced with 1.5% polyethylene (PE) and 0.5% steel fibres subjected to a high velocity projectile. Results demonstrated the potential of ECC to perform as a protective material in various applications, such as improving shatter resistance with reduced scabbing and spalling associated with distributed micro-cracking. Moreover, a series of drop weight impact tests were conducted by Yang and Li (2012) on hybrid-fibre-reinforced ECC panels and beams incorporating

PVA and PE fibres. It was concluded that the material ductility of ECC specimens led to enhanced impact resistance through improving the load carrying capacity and energy dissipation ability of the tested structural elements. Furthermore, Soe *et al.* (2013) showed that a hybrid-fibre ECC incorporating a combination of 1.75% PVA and 0.58% steel fibres achieved superior performance, absorbing more energy than that of the control normal concrete when subjected to high velocity projectiles.

On the other hand, fire is believed to be one of the main factors in bringing down the world trade center tower during the catastrophic event in September 2001, New York, USA (Ali *et al.*, 2004). Hence, researchers became more proactive towards developing advanced fire-resistive materials for structural applications. Fire resistance is a major requirement for buildings since it could be the last line of defense when all other sources of restraining a fire fail (Kodur, 1999). Concrete behaviour under fire stimuli depends mainly on its constituents (e.g. moisture content, aggregates and cement type), size of concrete element and its geometry, load intensity, and fire duration and temperature profile (Husem, 2006).

The principal effects of fire on concrete are compressive strength degradation and spalling. Spalling is described as the explosive ejection of concrete chunks from its surface due to breakdown in surface tensile strength (Khoury, 2000). As concrete gets exposed to fire, the water within its internal voids transfers to the gaseous state, thus resulting in an increase in internal pressure in the concrete pore structure. If concrete prevents water vapor from escaping, high pressure will be induced in the internal concrete structure, leading to brittle failure, which could be explosive, leading to catastrophic consequences (Husem, 2006). To avoid such events, several investigations have been conducted worldwide for the development of concrete with improved fire resistance.

Although, many research works have been conducted to establish the mechanical properties of ECC material. However, its performance under fire has not yet been duly studied. Zhang *et al.* (2014) developed a spray-applied fire resistive material using ECC technology (SFR-ECC). It was observed that the essential high ductility of ECC enhanced the overall durability and fire protection compared to that of conventional concrete and brittle spray-applied fire-resistive materials (SFRM). Similarly, Zhang and Li (2015) found that the SFR-ECC material showed superior tensile

characteristics, ductility and better adhesion to steel compared to the brittle performance and poor tensile properties of conventional SFRM. Consequently, the superior characteristics of SFR-ECC could improve the fire protection performance. Furthermore, Byung-Chan *et al.* (2007) studied the applicability of utilizing ECC as a fire-resistive material in tunnel lining applications. They found that the ECC achieved better fire resistance in such applications compared to that of conventional concrete. Although, the CSA Standard A23.3-14 (Design of Concrete Structures) and National Building Code of Canada 2015 (NBC) provide detailed guidelines for the design of structural concrete elements, there is lack of information regarding the evaluation of fire performance of ECC members in such standards.

Although there is significant research on the impact resistance of ECC as a material, there is dearth of information on the performance of ECC structural members under the effects of impact loads especially subsequent to fire. Therefore, in the present chapter, the impact resistance of innovative hybrid fibre-reinforced ECC mixtures incorporating a combination of randomly dispersed polyvinyl alcohol (PVA) and nickel titanium shape memory alloy (NiTi-SMA) short fibres was investigated. The study aims to ultimately coin a composite with superior resistance to impact loading under normal conditions and after exposure to fire, possibly with self-healing capability to create novel alternatives in designing ductile structural elements capable of mitigating damage inflicted by impact, explosive and dynamic loading.

5.2 TESTING METHOD

5.2.1 Drop-Weight Impact Test

Considering that large-scale missile impact tests are costly and their results are often not made available in the public domain, smaller laboratory-scale tests are more common (Martin, 2010). The drop-weight impact test is one of the most widely used techniques for evaluating the impact resistance of fibre-reinforced cementitious materials (Murnal and Chatorikar, 2015; Xiang-yu *et al.*, 2011; Patel *et al.*, 2012). In the present chapter, the drop weight impact test was carried out in compliance with the procedure outlined by the American Concrete Institute (ACI) Committee 544, on four different ECC mixtures at the age of 90 days. The ECC mixtures were cast in cylindrical moulds having dimensions of 100 mm x 200 mm [4 in x 8 in]. Each cylindrical specimen was cut into three 100 mm x 50 mm [4 in x 2 in] discs using a diamond saw. The discs were then tested

under a drop weight impactor using an Instron impact loading machine (**Fig. 5-1**) with a maximum impact force of 44000 N in order to evaluate the behaviour of the composite under impact loading. Further details about the test method can be found elsewhere (Nehdi and Soliman, 2013).

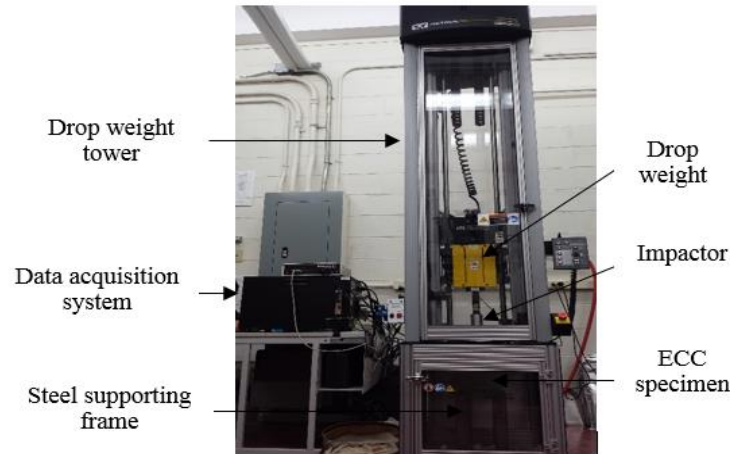


Figure 5-1: Instron impact loading testing machine setup.

Moreover, another series of specimens were subjected to impact loading induced by a 4.5-kg weight dropped from 457 mm height above the specimen, which was able to produce an impact energy of 20.167 J per hit in order to determine the first crack and fracture energy of ECC specimens, as shown in **Fig. 5-2**. The numbers of impacts to induce the first visible crack (N_1), and failure (N_2), respectively were recorded.

Furthermore, a series of drop weight tests were conducted on similar ECC specimens after applying heat treatment. The heat treatment procedure was similar to that suggested by Kim *et al.* (2016). A heating gun was fixed at 35 mm from the specimen's front surface for twenty-five minutes to mobilize the pre-stressing effect of NiTi-SMA fibres owing to its shape memory effect. The heat gun raised the specimen's temperature by about 150°C, leading to the appearance of multiple micro-cracks at the front face of the tested specimens. The temperature of the specimens' core and surface were measured every minute during the heating process using embedded thermal sensors and an infra-red (IR) thermometer. The specimens were left to cool down to room temperature, and then the drop weight test was carried out.

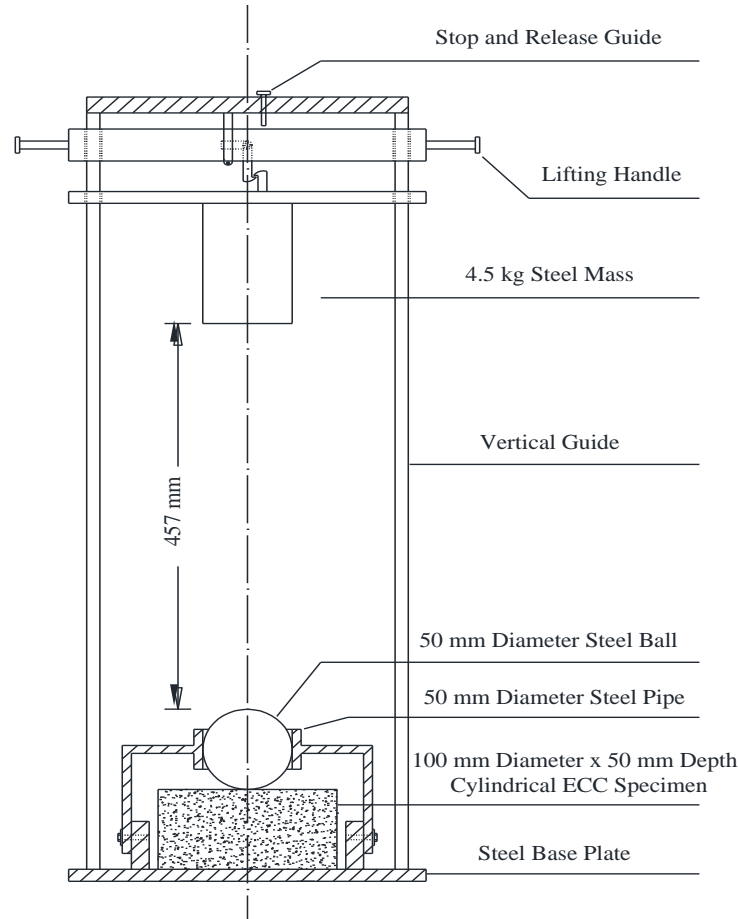


Figure 5-2: Schematic diagram of of the drop weight impact testing system.

The impact energy for each ECC specimen was calculated according to ASTM standard D5628 using the following equation (Eq. 5-1):

$$IE = N_i \cdot h \cdot w \cdot f \quad (\text{Eq. 5-1})$$

Where IE is the impact energy in Joule, N_i is the number of blows, h is the falling height of the steel mass in mm, w is the mass of the steel hammer in kg, and f is a constant with a value of 9.806×10^{-3} .

According to Canisius *et al.* (2003), concrete spalling could be observed at early stages of a fire. Likewise, Both *et al.* (1999) found that this phenomenon could occur at temperatures as low as 200°C. In addition, Chen and Liu (2004) recognized that spalling could happen for high strength concrete at a temperature of about 400°C. Therefore, in order to evaluate the effect of fire on the

impact resistance of ECC mixtures, specimens were first cracked under impact loading, then subjected to fire stimuli inside a heating chamber, which was able to heat the specimens up to 400°C temperature for an hour as shown in **Fig. 5-3**. Thereafter, the specimens were left to cool down to room temperature, and then reloaded using the drop weight test up to failure.



Figure 5-3: Heating chamber setup.

5.3 RESULTS AND DISCUSSION

5.3.1 Impact Behaviour

5.3.1.1 Energy-Penetration

Figures 5-4a, b, c and d display the energy-penetration curves for different ECC specimens at different drop levels obtained via the Instron impact loading testing machine. Each specimen was subjected to multiple impacts at different drop levels such that the first, second and third impacts were at 50 mm, 100 mm and 150 mm, respectively, measured from the upper end of the spherical steel ball up to the lower end of the impactor. It was observed that all tested ECC specimens did not fail or crack under the effect of multiple impacts up to the maximum capacity of the testing machine. The computerized system, which was used in the data acquisition during impact, was programmed to calculate the energy dissipation capacity of the different ECC specimens through estimating the difference between the applied impact energy and that remaining in the system upon impact.

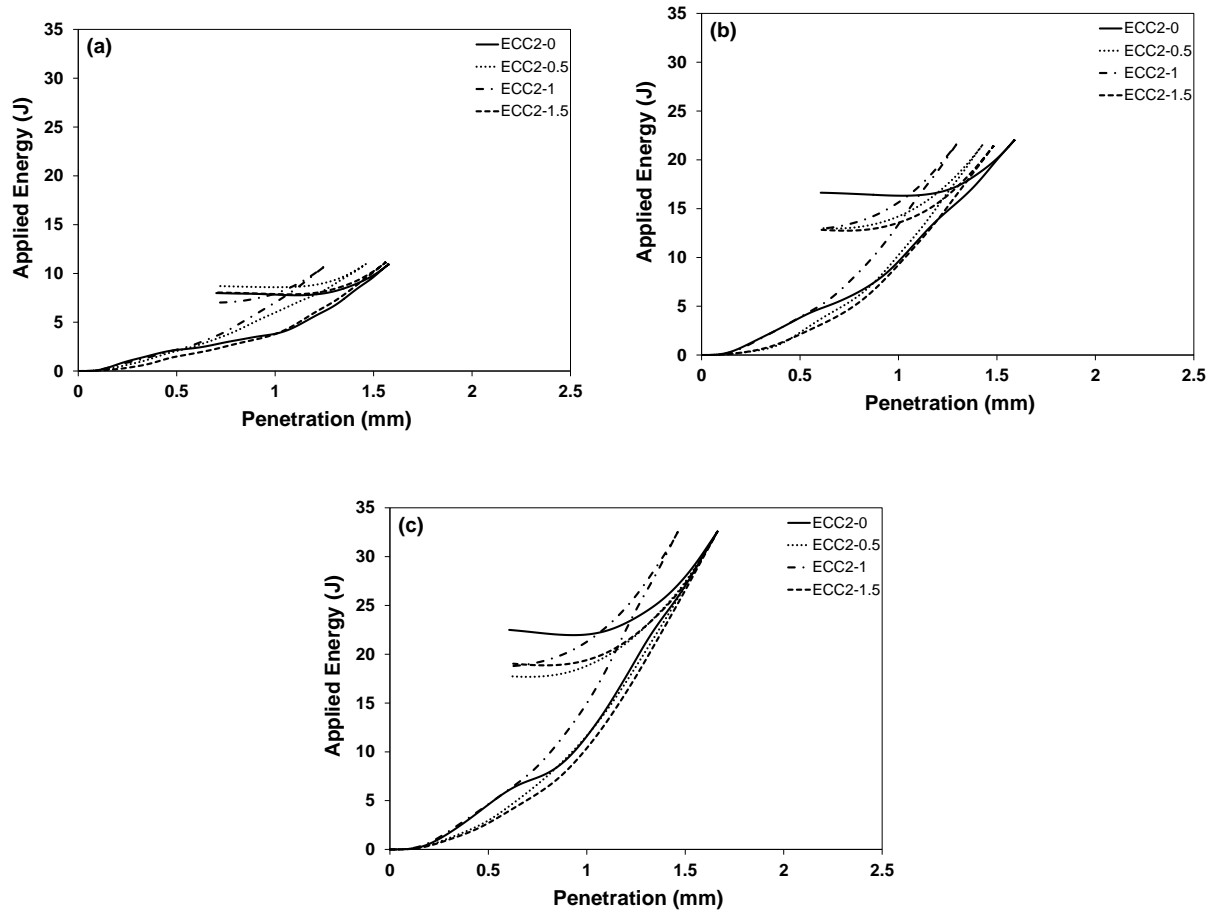


Figure 5-4: Typical Energy-penetration curves for different ECC mixtures at different drop levels: a) 1st hit, b) 2nd hit, and c) 3rd hit.

The cumulative enhancement in energy dissipation capability of the ECC specimens is illustrated in **Fig. 5-5**. It can be observed that the energy dissipation capability was generally improved by SMA fibre addition. For instance, the ECC2-0.5, ECC2-1 and ECC2-1.5 specimens achieved dissipated energy of 23.39%, 30.43% and 11.53% higher than that of the control ECC specimens made with PVA fibres alone, respectively. This underscores the significant enhancement in impact resistance of the composite owing to SMA fibre addition.

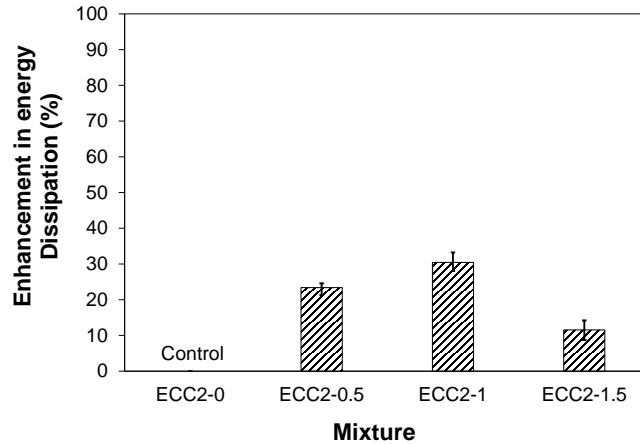


Figure 5-5: Percent enhancement in energy dissipation capability of ECC specimens.

The accumulated impactor penetration depth in the different ECC specimens is illustrated in **Fig. 5-6**. Only small penetration occurred upon impact loading. A general reduction in penetration depth was observed owing to SMA fibre addition. For example, the ECC2-0.5, ECC2-1 and ECC2-1.5 specimens had 6.3%, 10.1% and 2.6% lower penetration depth compared to that of the control ECC2-0 specimens, respectively. This is ascribed to the resistance of the composite's fibre-matrix interfacial frictional bond. The ECC specimen incorporating 2% PVA and 1% SMA fibres achieved highest energy dissipation capacity and lowest penetration depth among all tested specimens. Higher fibre dosage led to impact strength degradation due to increased porosity via fibre clustering, which evidence was provided in chapter 4.

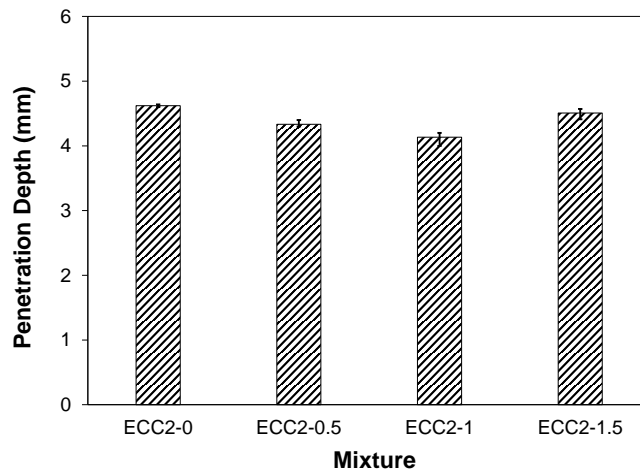


Figure 5-6: Accumulated penetration depth in ECC specimens.

5.3.1.2 Impact Load-Time History

The impact load was measured during each impact as derived from the accelerometer measurements (Instron testing machine) and impact load-time history curves are displayed in **Figs. 5-7a, b, c and d**. It was observed that all ECC specimens did not fail or even crack under the effect of multi-impacts up to the maximum capacity of the testing machine (44000 N). The peak impact force for hybrid mixtures incorporating 0.5%, 1% and 1.5% SMA fibre addition slightly increased by about 2.38%, 7.19% and 3.03%, respectively, compared to that of the control mono PVA-ECC mixture.

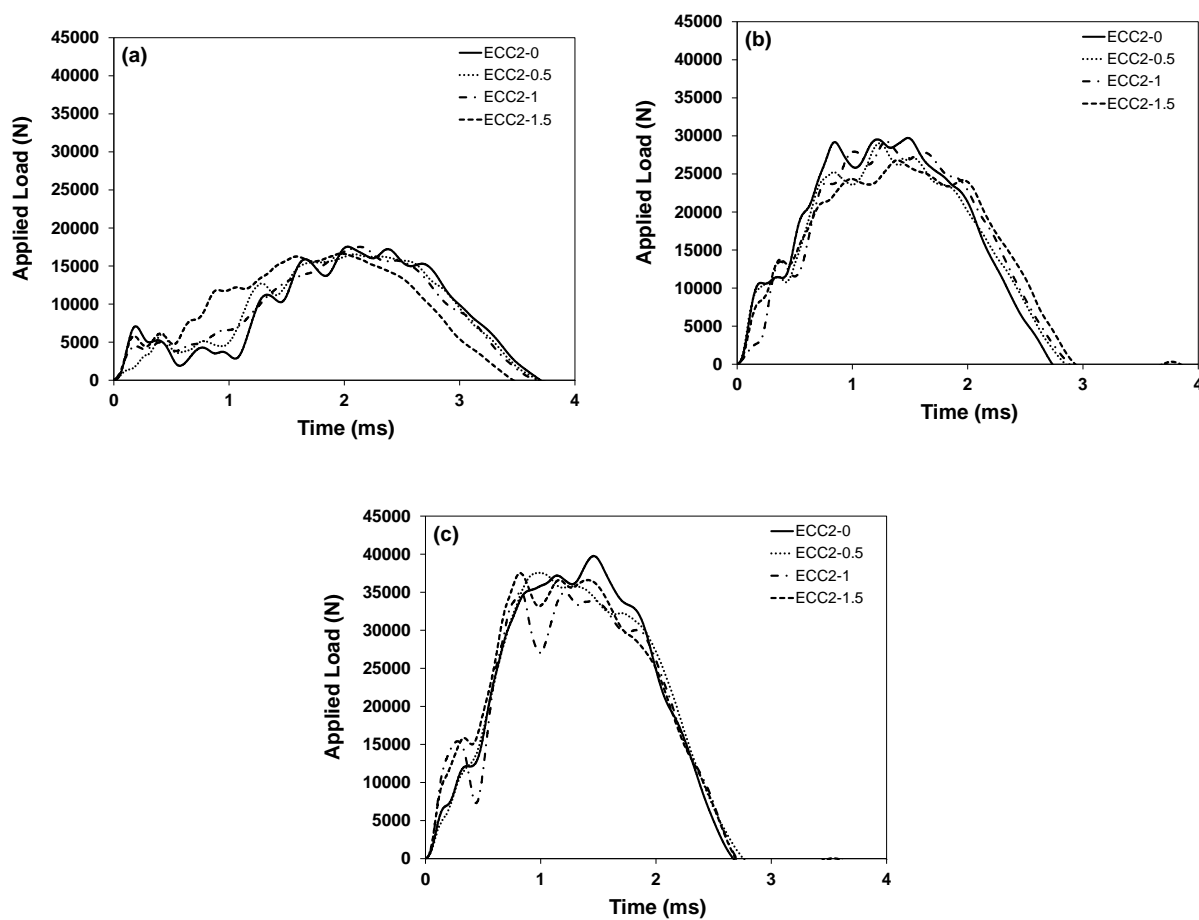


Figure 5-7: Impact load-time history curves for different ECC specimens at different drop levels: a) 1st hit, b) 2nd hit, and c) 3rd hit.

The ability of ECC specimens to resist impact load mainly depended on the fibre type and content. The material's response under impact load depends on its interactive behaviour under compressive

and shear stresses (Li *et al.*, 2000). Since all ECC mixtures had a slight difference in compressive strength, it appears that the SMA fibres-matrix bond allowed to better resist shear stresses induced by the impact load, thus leading to higher impact resistance.

5.3.2 Fracture Performance

5.3.2.1 At Normal Temperature

Table 5-1 summarizes the experimental impact test results, following the drop weight impact test (ACI 544 guidelines), for specimens from all tested ECC mixtures. All specimens were tested up to failure and the average values for impact failure energy were calculated. Moreover, the statistical analysis of test results obtained from the experimental drop weight impact test is reported in **Table 5-1**. Where N_1 and N_2 are the number of impacts up to first crack initiation and failure, respectively.

Table 5-1: Statistical analysis of test results (N_1/N_2)

Specimen ID	ECC0-0	ECC2-0	ECC2-0.5	ECC2-1	ECC2-1.5
Mean	1/1	13/39	50/594	75/697	63/674
Standard deviation	0/0	1/2	2/4	2/7	4/6

The impact energy sustained by the ECC specimens up to first crack and up to failure is reported in **Fig. 5-8**. Specimens from the control mixture (ECC0-0) without fibre addition failed after only one hit by the drop weight and split into multiple fragments, which reflects its brittle behaviour under impact loading. Conversely, adding 2% of PVA fibre by volume enhanced the composite's behaviour under impact loading. For instance, specimens from the mixture ECC2-0 sustained impact loading up to first crack and failure of about 13 and 39 times that of the control ECC0-0 specimens, respectively. This reflects the beneficial effect of incorporating PVA fibres in ECC specimens, which led to altering the mode of failure of ECC under impact loads from prematurely brittle to more ductile failure, in agreement with previous study (Soe *et al.*, 2013).

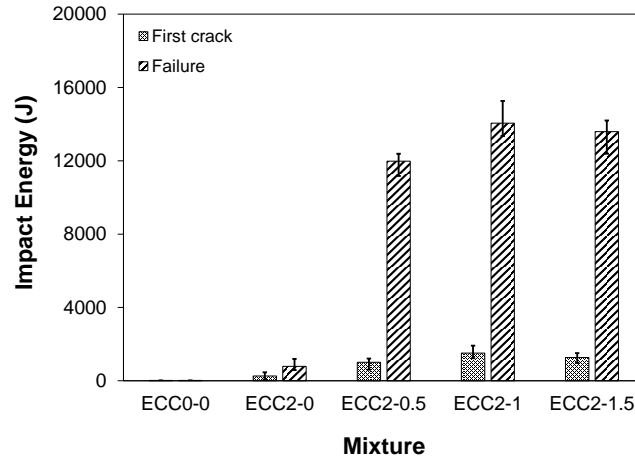


Figure 5-8: Impact energy sustained by ECC specimens up to failure.

Generally, SMA fibre addition also improved the impact resistance of ECC specimens in a similar trend to that achieved by PVA fibre addition. For instance, 0.5% SMA fibre addition by volume fraction increased the impact resistance to reach first crack and failure by about 284% and 1423% compared to that of the ECC specimens incorporating 2% PVA fibre alone, respectively. Furthermore, increasing the SMA fibre addition level increased the number of impacts to reach first crack and failure of the specimens. For instance, the impact resistance to first crack and failure of specimens from mixtures ECC2-1 and ECC2-1.5 increased by about 477% and 1687%, and 384% and 1628%, compared to that of the ECC specimens incorporating 2% PVA fibre alone, respectively. This demonstrates the superior ability of SMA fibres to restrain crack propagation in ECC specimens under impact loading.

However, the hybrid-ECC specimen comprising a combination of 2% PVA and 1% SMA fibres exhibited the highest impact resistance compared to all other tested specimens. Using higher dosage of SMA fibres in the ECC mixture (e.g. ECC2-1.5) decreased the impact resistance compared to that of ECC2-1. This can be attributed to less effective spatial distribution of fibres due to agglomeration and possibly the increased porosity induced in the mixtures incorporating higher than 2% PVA and 1% SMA fibres by volume fraction.

5.3.2.2 After Heat Treatment

Figure 5-9 displays the results of ECC specimens with and without heat treatment tested up to failure under the effect of repeated impact loading as per the ACI 544 guidelines. The impact

failure energy sustained by the heated ECC2-0 specimens was only 11% lower than that of identical non-heated specimens, which indicates some degradation due to heat treatment. This can be ascribed to the fact that PVA fibres (which have a glass transition temperature of 85°C) lost mechanical strength due to the heating process which reached 150°C, particularly at the front surface of specimens where the heating was more intensive. Hence, it is expected that at higher temperature, the degradation will be more significant, in agreement with previous study (Kim *et al.*, 2016).

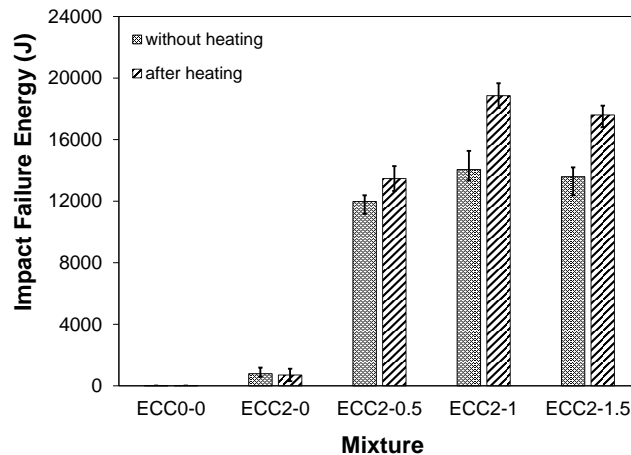


Figure 5-9: Impact failure energy of ECC specimens with and without heat treatment.

On the other hand, the impact resistance of the hybrid PVA-SMA fibre-reinforced ECC specimens was enhanced subsequent to the heat treatment, despite that the contribution of the PVA fibres was simultaneously degraded as discussed above. For instance, the impact failure energy for specimens containing 0.5% SMA and 2% PVA fibres was increased by about 12.46% compared to that of the non-heated specimens. Also, the impact failure energy for the heated specimens increased as the SMA fibre addition increased. For example, the impact failure energy of the heat treated ECC 2-1 and ECC2-1.5 specimens increased by about 34.15% and 29.53% compared to that of identical non-heated specimens, respectively. This can be attributed to the beneficial pre-stressing effect in ECC specimens owing to the shape memory alloy fibres, which restrained crack growth, a behaviour also reported by Kim *et al.* (2016). The local pre-stressing effect of SMA fibres as evidenced by the enhanced impact resistance subsequent to heat treatment opens interesting research directions for its application in protective systems in critical facilities for national security.

5.3.3 Behaviour Subsequent to Fire Exposure

Figure 5-10 displays the impact test results of ECC specimens with and without fire exposure using the drop weight impact test (following the ACI 544 guidelines). It was observed that the impact resistance of the ECC composite was generally degraded due to fire exposure. For instance, the impact energy at failure of ECC specimens incorporating 2% PVA fibre decreased by about 48.7% due to fire compared to that of its counterpart at normal temperature. Similarly, the impact failure energy of ECC2-0.5, ECC2-1 and ECC2-1.5 decreased by about 41.1%, 16.8% and 34.7%, respectively, compared to their counterparts which were tested at normal conditions. The general impact resistance degradation of the ECC composite can be attributed to the melting of PVA fibres due to fire, leading to higher porosity in the composite. This is consistent with findings of a previous study (Sahmaran *et al.*, 2010). Moreover, it was observed that SMA fibres restrained the strength degradation three times more than that occurring in PVA-ECC specimens owing to the shape memory effect. Among all tested specimens, the ECC specimens incorporating 2% PVA and 1% SMA fibres still achieved the highest impact resistance, even after fire exposure. Furthermore, no explosive spalling during or after fire tests was observed in any of these specimens. This can be attributed to the formation of a network of pathways in the ECC specimens, which served as channels for water vapor escaping outside the specimens, leading to reduced tensile stresses propagated due to thermal expansions.

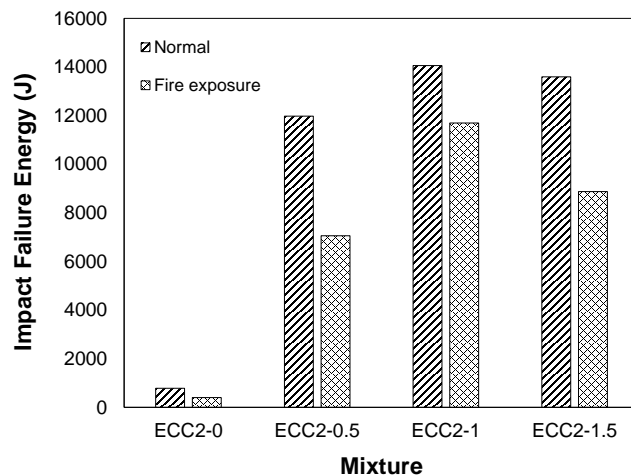


Figure 5-10: Impact failure energy of ECC specimens with and without fire exposure.

Generally, all hybrid ECC specimens incorporating SMA and PVA fibres exhibited a degradation in impact resistance subsequent to fire exposure. Nonetheless, they achieved impact higher than that acquired by mono-PVA-ECC specimens even at normal temperature. This is attributed to the superior capability of SMA fibres to restrain crack propagation under impact loading in ECC specimens, thus leading to enhanced post-cracking behaviour of ECC specimens, even after exposure to high temperatures due to fire. Similar observations were reported by others (e.g. Sahmaran *et al.*, 2010; Chen and Liu, 2004; Kodur *et al.*, 2003) who used steel-fibre-reinforced concrete (SFRC).

5.3.4 Mode of Failure

The mode of failure of tested specimens under impact loading depends essentially on the matrix strength and fibre-matrix interfacial bond strength. **Figure 5-11** illustrates the different failure modes under impact loading. The failure mode of the control specimens consisting of the fibreless ECC matrix was brittle (**Fig. 5-11a**). The specimens were broken suddenly under the effect of the first hit and shattered into multiple fragments. Conversely, the mono-fibre ECC specimens (incorporating 2% PVA fibre) exhibited a different mode of failure (**Fig. 5-11b**). The PVA fibre reinforcement transformed the mode of failure from brittle to ductile through sustaining multiple impacts before failure. Moreover, the crack pattern changed from one main crack in the case of the control specimens, to multiple fine cracks in the PVA fibre-reinforced ECC2-0 specimens. The area under the impactor was shriveled, displaying a small indent diameter and depth in the PVA-ECC specimens. This is consistent with findings of previous investigations (Soe *et al.*, 2013; Maalej *et al.*, 2005; Zhang *et al.*, 2007).

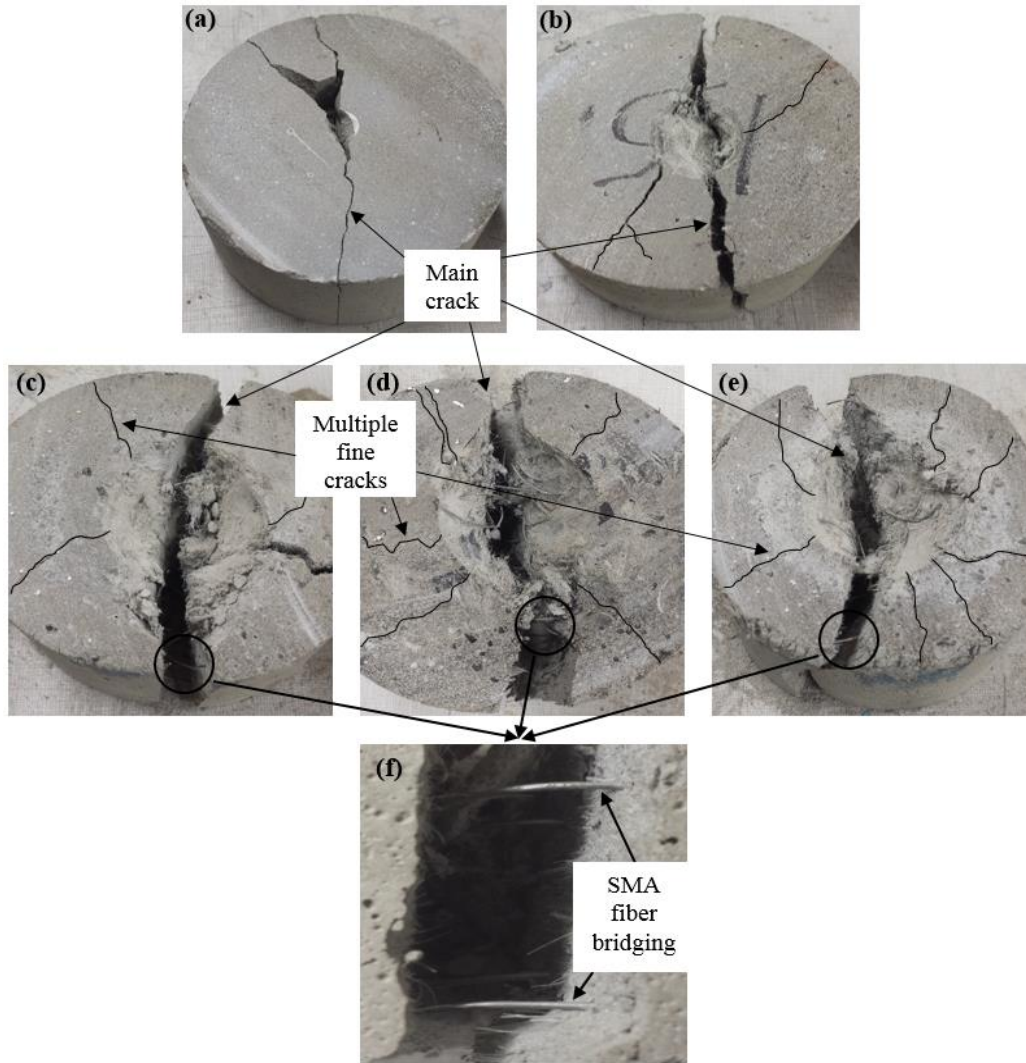


Figure 5-11: Failure patterns of ECC disc specimens: a) ECC0-0, b) ECC2-0, c) ECC2-0.5, d) ECC2-1, e) ECC2-1.5, and f) SMA fibre bridging.

A similar trend was displayed by the hybrid fibre-reinforced ECC specimens incorporating a combination of PVA and SMA fibres, as shown in **Figs. 5-11c, d and e**. The number of cracks induced by impact loading increased with the increase of the SMA fibre content. For instance, as displayed in **Figs. 5-11c, d and e**, the number of cracks was increased by about 66%, 133% and 167% in the ECC2-0.5, ECC2-1 and ECC2-1.5 specimens compared to that of ECC2-0. Also, the shriveling area, indent diameter and its depth increased with increasing SMA fibre content likely owing to the SMA fibre crack bridging capability, which held the specimen together across growing cracks and performed as a crack growth restraint (**Fig. 5-11f**).

5.3.5 Statistical Analysis of Test Results

5.3.5.1 Weibull Distribution

Different probabilistic models have been used over the last few decades to statistically analyze the fatigue and impact test data of concrete. In particular, the two-parameter Weibull distribution was widely used in many research works for describing the fatigue life and impact performance of concrete (Li *et al.*, 2007; Raif and Irfan, 2008; Raman and Rakesh, 2009). The Weibull distribution function is characterized by a probability density function as follows (**Eq. 5-2**):

$$f(n) = \frac{\alpha}{u} \left(\frac{n}{u}\right)^{\alpha-1} e^{-\left(\frac{n}{u}\right)^\alpha} \quad (\text{Eq. 5-2})$$

Where α represents the shape parameter (i.e. Weibull slope), u is the scale parameter, and n is the specific value of the random variable N (i.e. N_1 and N_2 in the present study). Integrating **Eq. (5-2)** gives the following (**Eq. 5-3**):

$$F_N(n) = 1 - e^{-\left(\frac{n}{u}\right)^\alpha} \quad (\text{Eq. 5-3})$$

Where $F_N(n)$ is the cumulative distribution function. According to Saghafi *et al.* (2009), the probability of survivorship function is represented by (**Eq. 5-4**):

$$L_N = 1 - F_N(n) = e^{-\left(\frac{n}{u}\right)^\alpha} \quad (\text{Eq. 5-4})$$

Taking the natural logarithm twice on both sides of **Eq. 5-5**, it can be rewritten as follows (**Eq. 5-5**):

$$\ln \left[\ln \left(\frac{1}{L_N} \right) \right] = \alpha \ln(n) - \alpha \ln(u) \quad (\text{Eq. 5-5})$$

Equation 5-5 represents a linear relationship between $\ln [\ln (1/L_N)]$ and $\ln (n)$. In order to illustrate **Eq. 5-5** graphically, the empirical survivorship function L_N for impact test data is obtained from the following relation (Raman and Rakesh, 2009) (**Eq. 5-6**):

$$L_N = 1 - \frac{i-0.3}{k+0.4} \quad (\text{Eq. 5-6})$$

Where i represents the failure order number and k denotes the number of data points. A linear regression analysis was applied to the $\ln [\ln (1/L_N)]$ and $\ln (\text{impact energy})$ values as shown in **Figs. 5-12 and 5-13**.

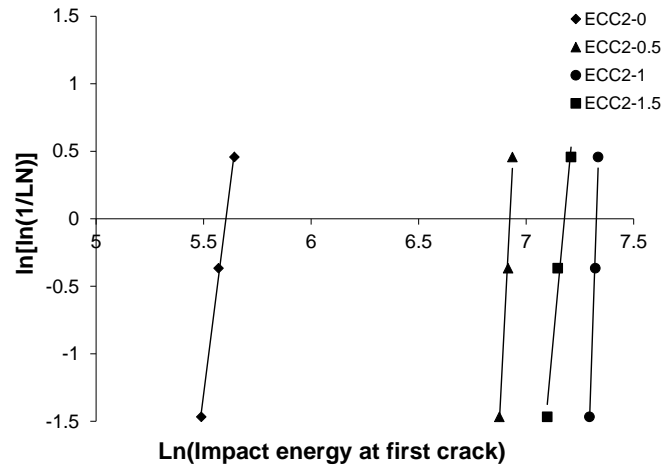


Figure 5-12: Weibull distribution of first crack impact energy of ECC specimens.

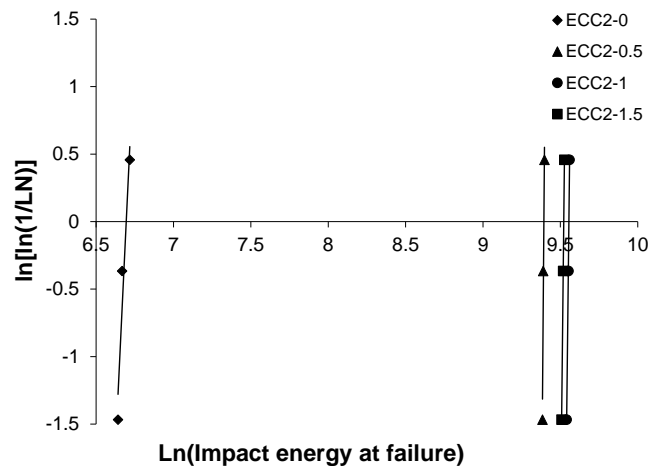


Figure 5-13: Weibull distribution of impact energy at failure of ECC specimens.

The linear trend is established by drawing the best fit line between data points using the method of least squares. The slope of the line provides an estimate of the shape parameter (α) and the scale parameter (u), which can be obtained by calculating the value at which the line intersects the $\ln [\ln (1/L_N)]$ axis. The shape parameter (α), scale parameter (u) and the coefficient of determination (R^2) for the ECC specimens are shown in **Table 5-2**.

Table 5-2: Shape, scale parameters and coefficient of determination of ECC specimens

Specimen ID	α		u		R^2	
	N_2	N_I	N_2	N_I	N_2	N_I
ECC2-0	24.146	12.505	-161.7	-70.08	0.9322	0.9963
ECC2-0.5	138.44	31.038	-1300	-214.9	0.9505	0.9869
ECC2-1	102.41	46.759	-978.6	-342.6	0.9973	0.9874
ECC2-1.5	107.96	17.272	-1028	-123.98	0.9998	0.9778

Tables 5-3 and 5-4 display the impact energy values for ECC specimens at the first visible crack and failure stage, respectively based on reliability analysis. The first crack impact energy of ECC2-0, ECC2-0.5, ECC2-1, and ECC2-1.5 specimens was approximately equal to or higher than 187.927, 876.453, 1377.93, and 1004.0088 with R^2 of 0.9963, 0.9869, 0.9874, and 0.9778, respectively.

Table 5-3: Weibull distribution for first crack impact energy of ECC specimens

Reliability Level	ECC2-0	ECC2-0.5	ECC2-1	ECC2-1.5
0.99	187.927	876.453	1377.93	1004.0088
0.90	226.776	945.382	1448.94	1150.3270
0.80	240.801	968.518	1472.39	1201.4080
0.70	250.004	983.264	1487.23	1234.4780
0.60	257.289	994.710	1498.70	1260.4200
0.50	263.646	1004.540	1508.51	1282.8900
0.40	269.597	1013.610	1517.54	1303.7890
0.30	275.548	1022.570	1526.43	1324.5640
0.20	282.019	1032.180	1535.94	1347.0120
0.10	290.213	1044.160	1547.75	1375.2350
0.01	306.753	1067.740	1570.86	1431.5470

Likewise, the impact energy at failure of ECC2-0, ECC2-0.5, ECC2-1, and ECC2-1.5 was approximately equal to or higher than 667.926, 11614.5, 13502.0, and 13087.796 with R^2 of 0.9322, 0.9505, 0.9973, and 0.9998, respectively. Since all impact test data had R^2 were equal to or higher than 0.93, a two-parameter Weibull distribution can be used to establish the statistical distribution of impact test data for ECC incorporating SMA fibres. These developed reliability curves can be considered as a useful tool to quickly estimate the impact resistance of ECC at cracking and failure, without conducting costly and time-consuming additional impact testing. Similar conclusions were drawn by others (Murali *et al.*, 2014; Xiang-yu *et al.*, 2011) for steel fibre-reinforced concrete.

In this study, the analysis was conducted on a limited number of tests (3 data points per mixture) due to limitations of the costly and time-consuming impact test. Since, additional tests could

confirm or disprove the observed trend, further testing is required to generalize this concept for ECC composites with different characterizations.

Table 5-4: Weibull distribution for impact energy at failure of ECC specimens

Reliability Level	ECC2-0	ECC2-0.5	ECC2-1	ECC2-1.5
0.99	667.926	11614.5	13502.0	13087.796
0.90	736.193	11813.3	13815.4	13375.778
0.80	759.432	11877.5	13917.0	13469.077
0.70	774.328	11917.8	13980.9	13527.718
0.60	785.933	11948.8	14030.0	13572.802
0.50	795.930	11975.2	14071.9	13611.228
0.40	805.183	11999.3	14110.3	13646.460
0.30	814.340	12023.0	14147.9	13681.018
0.20	824.189	12048.3	14188.1	13717.850
0.10	836.504	12079.5	14237.8	13763.433
0.01	860.866	12140.1	14334.5	13852.084

Furthermore, **Fig. 5-14** portrays a linear trend between data points in order to determine the coefficient of determination (R^2) for impact test results of ECC specimens after fire exposure.

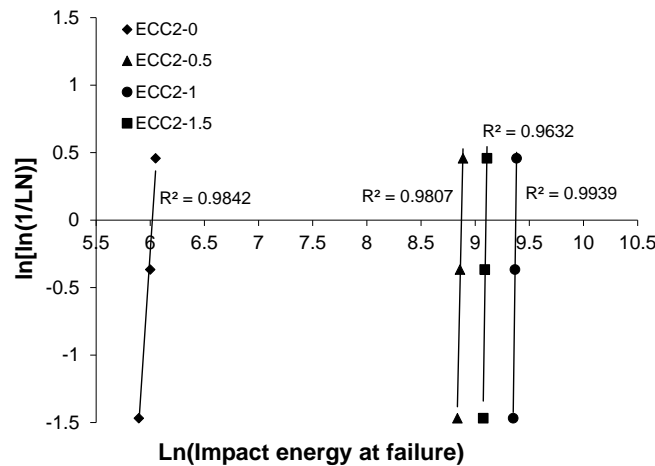


Figure 5-14: Weibull distribution for impact energy of ECC specimens at failure after fire exposure.

Table 5-5 illustrates the impact energy corresponding to failure of ECC specimens after fire exposure established using reliability analysis. The impact energy at failure of ECC2-0, ECC2-0.5, ECC2-1, and ECC2-1.5 was approximately equal to or higher than 242.94, 5885.55, 10978.30, and 6800.09 J, respectively. As shown in **Fig. 5-14**, since all impact test results had R^2 values equal to or higher than 0.9632, a two-parameter Weibull distribution can be utilized to predict the impact

energy at failure of ECC specimens after fire exposure in order to save the time and cost required for additional testing. Murali *et al.* (2014) and Chen *et al.* (2011) among others, have drawn similar conclusions for SFRC.

Table 5-5: Weibull distribution for impact energy of ECC specimens at failure

Reliability Level	ECC2-0	ECC2-0.5	ECC2-1	ECC2-1.5
0.99	242.94	5885.55	10978.30	6800.09
0.90	293.23	6266.94	11402.20	7088.71
0.80	311.39	6393.87	11541.00	7183.44
0.70	323.31	6474.50	11628.60	7243.29
0.60	332.74	6536.95	11696.10	7289.46
0.50	340.98	6590.48	11753.80	7328.92
0.40	348.68	6639.81	11806.80	7365.19
0.30	356.39	6688.43	11858.90	7400.86
0.20	364.77	6740.51	11914.50	7438.96
0.10	375.38	6805.32	11983.50	7486.24
0.01	396.80	6932.54	12118.20	7578.59

5.3.5.2 Regression analysis of drop weight test results

Figure 5-15 illustrates the correlation between the number of blows which caused the first visible crack of the fibre-reinforced ECC specimens and the number of blows which caused its failure. This correlation was used to develop prediction equations for the number of blows which can cause failure of ECC specimens under impact loading as shown in **Table 5-6**.

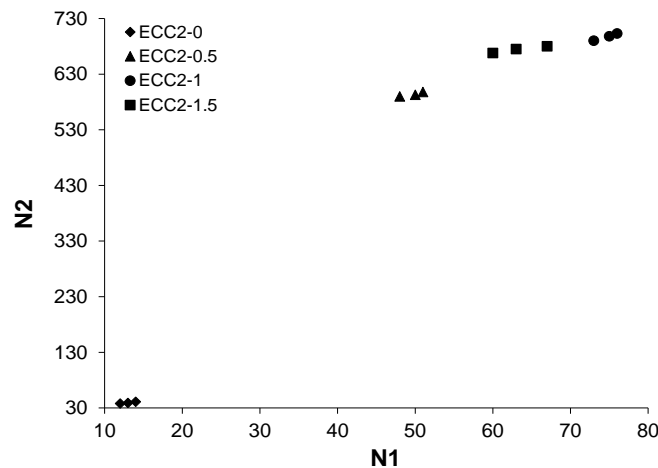


Figure 5-15: Relationship between N2 and N1 of ECC specimens.

Since the R^2 values displayed in **Table 5-6** for ECC specimens are equal to or higher than 0.89, which exceeds the limit (0.7) suggested by Rahmani *et al.* (2012), these equations can be used with reasonable accuracy to represent the correlation between the number of blows causing the first visible crack and the ultimate failure of the ECC specimens produced with and without SMA fibres.

Table 5-6: Relationship between N2 and N1 of ECC specimens

Reliability Level	Equation	R ²
ECC2-0	$N_2 = 1.5 N_1 + 19.833$	0.9643
ECC2-0.5	$N_2 = 2.5 N_1 + 469.5$	0.8929
ECC2-1	$N_2 = 4.2857 N_1 + 377$	0.9967
ECC2-1.5	$N_2 = 1.6892 N_1 + 567.35$	0.9686

5.3.5.3 Analysis of variance of test results

ANOVA at a significance level $\alpha_I = 0.05$, displayed that variation in the addition level of SMA fibre had a significant effect on the mean value of the impact resistance of the ECC composite. The determined F_o value for impact test results was 77.51, which is higher than the corresponding critical F value of 4.07 ($F_{0.05,3,8}$). This reflects the significant effect of incorporating SMA fibres in the production of ECC composites which is consistent with results obtained earlier. Due to the overlap observed in impact test results due strength degradation of ECC2-1.5 compared to that of ECC2-1 (**Fig. 5-8**) owing to fibre clustering and that of ECC2-0 due to heat treatment (**Fig. 5-9**), further ANOVA had been applied especially for these results. The determined F_o value estimated for impact resistance of HECC-SMAF composite reinforced by more than 2% PVA and 1% SMA fibres was 7.286 which is higher than the corresponding critical F value of 5.79 ($F_{0.05,2,5}$). This reflects the significant effect of using higher dosage of SMA fibres in the ECC mixture (ECC2-1.5) leading to decreased impact resistance compared to that of ECC2-1. This is consistence with aforementioned observations. Conversely, heat treatment indicated an insignificant effect on the impact resistance of the PVA-ECC composite (ECC2-0). The estimated F_o value for the impact resistance results of the heated and non-heated ECC2-0 specimen was 3.675 which is lower than the corresponding critical F value ($F_{0.05,2,5}$).

5.4 CONCLUSIONS

The performance of engineered cementitious composite specimens incorporating hybrid PVA-SMA fibre reinforcement under impact loading with and without exposing to fire was evaluated by conducting drop weight impact tests. Based on the experimental results the following conclusions are drawn:

- The impact resistance of mono- and hybrid-fibre ECC specimens was found to be 30 to 700 times higher than that of the plain fibreless ECC control specimens.
- The addition of PVA and SMA fibres into the ECC matrix changed the failure mode of ECC specimens under the effect of impact loading from brittle to ductile.
- The performance of ECC specimens subjected to impact loading was improved due to SMA fibre addition. However, the ECC mixture incorporating 2% PVA and 1% SMA fibres by volume fraction achieved the highest impact resistance compared to that of all other specimens. Fibre dosages beyond this level seemed to compromise fibre dispersion and create fibre clustering, while disrupting the matrix and causing higher porosity, which resulted in reduced performance under impact loading.
- Heat treatment damaged the PVA fibres and generally compromised the impact resistance of ECC specimens incorporating PVA fibres alone, leading to the appearance of multiple fine cracks at the front surface of specimens directly subjected to the heating.
- Conversely, the heat treatment process activated the SMA fibres to exert a local pre-stressing effect in the ECC composite, consequently improving its impact resistance. This is despite the damage caused by the heating to the coexisting PVA fibres.
- PVA fibres melt upon exposure to fire, which resulted in reduced performance under impact loading. However, the presence of SMA fibres seemed to restrain strength degradation and crack propagation owing to the shape memory effect.
- Melting of PVA fibres due to fire created pathways for water vapor removal through the composite and led to spalling free specimens during and after fire exposure.
- Although the hybrid ECC specimens exposed to fire showed strength degradation under impact loading compared to their counterparts tested without fire exposure, they still acquired impact resistance better than that of the control mono-PVA-ECC specimens tested under normal conditions.

- The Weibull distribution function proved capable of adequately representing the impact test data with a linear correlation between the number of impact which causes the first visible crack and that which initiated the ultimate failure for all ECC specimens.

5.5 REFERENCES

- ACI Standard, "Measurement of properties of fiber reinforced concrete." ACI Standard 544.2R-89, Farmington Hills, MI 48331-3439 USA, Reapproved 2009.
- Ali, F., Nadjai, A., Silcock, G., and Abu-Tair, A., "Outcomes of a major research on fire resistance of concrete columns." *Fire Safety Journal*, 39, 2004, pp. 433-445.
- Alemdar, F. and Sezen, H., "Shear behaviour of exterior reinforced concrete beam-column joints." *Structural Engineering and Mechanics*, 35(1), 2010, pp. 123-126.
- Almusallam, T.H., Abadel, A.A., Al-Salloum, Y.A., Siddiqui, N.A., and Abbas, H., "Effectiveness of hybrid-fibers in improving the impact resistance of RC Slabs." *International Journal of Impact Engineering*, 81, 2015, pp. 61-73.
- ASTM Standard, "Standard test method for impact resistance of flat, rigid plastic specimens by means of a falling dart (tup or falling mass)." ASTM Standard D5628, ASTM International, West Conshohocken, USA, 2015.
- Both, C., van de Haar, P., Tan, G., and Wolsink, G., "Evaluation of passive fire protection measures for concrete tunnel linings." *Proceedings of International Conference on Tunnel Fires and Escape from Tunnels*, Lyon, France, 1999, pp. 95-104.
- Byung-Chan, H., Young-Jin, K., and Jae-Hwan, K., "Behavior of fire resistance engineered cementitious composites (FR-ECC) under fire temperature." *Journal of the Korea Concrete Institute*, 19(2), 2007, pp. 189-197.
- Canisius, T.D.G., Waleed, N., and Matthews, S.L., "Evaluation of effects of the fire test on Cardington concrete building." *Proceedings of International Conference on Tall Buildings*, Kuala Lumpur, Malaysia, 2003, pp. 353-360.

- Chen, B. and Liu, J., "Residual strength of hybrid-fiber-reinforced high-strength concrete after exposure to high temperatures." *Cement and Concrete Research*, 34, 2004, pp. 1065-1069.
- Chen, X-Y., Ding, Y-N., and Azevedo, C., "Combined effect of steel fibres and steel rebars on impact resistance of high performance concrete." *Journal of Central South University of Technology*, 18, 2011, pp. 1677-1784.
- Husem, M., "The effects of high temperature on compressive and flexural strengths of ordinary and high-performance concrete." *Fire Safety Journal*, 41, 2006, pp. 155-163.
- Khoury, G.A., "Effect of fire on concrete and concrete structures." *Progress in Structural Engineering and Materials*, 2(4), 2000, pp. 429-447.
- Kim, M.K., Kim, D.J., Chung, Y-S., and Choi, E., "Direct tensile behavior of shape-memory-alloy fiber-reinforced cement composites." *Construction and Building Materials*, 102, 2016, pp. 462-470.
- Kodur, V.K.R., "Fire resistance requirements for FRP structural members." *Proceedings of Annual Conference for Canadian Society of Civil Engineering*, Regina, Canada, 1999, pp. 83-94.
- Kodur, V.K.R., Cheng, F-P., Wang, T-C., and Sultan, M.A., "Effect of strength and fiber reinforcement on fire resistance of high-strength concrete columns." *Journal of Structural Engineering*, 129(2), 2003, pp. 253-259.
- Li, H., Zhang, M., and Ou, J., "Flexural fatigue performance of concrete containing nanoparticles for pavement, *International Journal of Fatigue*." 29(7), 2007, pp. 1292-1301.
- Li, J. and Zhang, Y.X., "Evaluation of constitutive models of hybrid-fibre engineered cementitious composites under dynamic loadings." *Construction and Building Materials*, 30, 2012, pp. 149-160.
- Li, W. and Xu, J., "Mechanical properties of basalt fiber reinforced geopolymeric concrete under impact loading." *Materials Science and Engineering A*, 505, 2009, pp. 178-186.

- Maalej, M., Quek, S.T., and Zhang, J., "Behaviour of hybrid-fiber engineered cementitious composites subjected to dynamic tensile loading and projectile impact." *Journal of Materials in Civil Engineering*, 17(2), 2005, pp. 143-152.
- Martin, O., "Comparison of different constitutive models for concrete in ABAQUS/explicit for missile impact analyses." *JRC Scientific and Technical Reports*, 2010, DOI: 10.2790/19763, 44p.
- Murnal, P.B. and Chatorikar, R.N., "Impact resistance of steel fiber reinforced concrete." *IJRET: International Journal of Research in Engineering and Technology*, 4(13), 2015, pp. 241-246.
- Nehdi, M. and Duquette, J. "Fibre synergy in hybrid fibre-reinforced self-consolidating concrete." *ACI Materials Journal*, 101(6), 2004, pp. 508-517.
- Nia, A.A., Hedayatian, M., Nili, M., and Sabet, V.A., "An experimental and numerical study on how steel and polypropylene fibers affect the impact resistance in fiber-reinforced concrete." *International Journal of Impact Engineering*, 46, 2012, pp. 62-73.
- Patel, U.R., Rathod, J.D., and Chauhan, D.K., "Comparative study of engineered cementitious composites and self-compacting engineered cementitious composites on response under impact loading." *International Journal of Emerging Technology and Advanced Engineering*, 2(2), 2012, pp. 262-264.
- Rahmani, T., Kiani, B., Shekarchi, M., and Safari, A., "Statistical and experimental analysis on the behavior of fiber reinforced concretes subjected to drop weight test." *Construction and Building Materials*, 37, 2012, pp. 360-369.
- Raif, S. and Irfan, A., "Statistical analysis of bending fatigue life data using Weibull distribution in glass-fiber reinforced polyester composites." *Materials and Design*, 29(6), 2008, pp. 1170- 1181.
- Raman, B. and Rakesh, C., "Fatigue-life distributions and failure probability for glass-fiber reinforced polymeric composites." *Composites Science and Technology*, 69(9), 2009, pp. 1381-1387.

- Saghafi, A., Mirhabibi, A.R., and Yari, G.H., "Improved linear regression method for estimating Weibull parameters." *Theoretical and Applied Fracture Mechanics*, 52(3), 2009, pp. 180-182.
- Sahmaran, M., Lachemi, M., and Li, V.C., "Assessing mechanical properties and microstructure of fire-damaged engineered cementitious composites." *ACI Materials Journal*, 107(3), 2010, pp. 297-304.
- Soe, K.T., Zhang, Y.X., and Zhang, L.C., "Impact resistance of hybrid-fiber engineered cementitious composite panels." *Composite Structures*, 104, 2013, pp. 320-330.
- Song, P.S., Hwang, S., and Sheu, B.C., "Strength properties of nylon- and polypropylene-fiber-reinforced concretes." *Cement and Concrete Research*, 35(8), 2005, pp. 1546-1550.
- Xiang-yu, C., Yi-ning, D., and Azevedo, C., "Combined effect of steel fibres and steel rebars on impact resistance of high performance concrete." *Journal of Central South of University of Technology*, 18, 2011, pp. 1677-1684.
- Yang, E-H. and Li, V.C., "Tailoring engineered cementitious composites for impact resistance." *Cement and Concrete Research*, 42, 2012, pp. 1066-1071.
- Yoo, D-Y., Banthia, N., Kim, S-W., and Yoon, Y-S., "Response of ultra-high-performance fiber-reinforced concrete beams with continuous steel reinforcement subjected to low-velocity impact loading." *Composite Structures*, 126, 2015, pp. 233-245.
- Xiang-Yu, C., Yi-ning, D., and Azevedo, C., "Combined effect of steel fibres and steel rebars on impact resistance of high performance concrete." *Journal of Central South University of Technology*, 18, 2011, pp. 1677-1684.
- Zhang, J., Maalej, M., and Quek, S.T., "Performance of hybrid-fiber ECC blast/shelter panels subjected to drop weight impact, *Journal of Materials in Civil Engineering*.' 19(10), 2007, pp. 855-863.

Zhang, Q. and Li, V.C., "Development of durable spray-applied fire-resistive engineered cementitious composites (SFR-ECC)." *Cement and Concrete Composites*, 60, 2015, pp. 10-16.

Zhang, Q., Ranade, R., and Li, V.C., "Feasibility Study on Fire-Resistive Engineered Cementitious Composites." *Materials Journal*, 111(6), 2014, pp. 651-660.

Zollo, R.F., "Fiber-reinforced concrete: an overview after 30 years of development." *Cement and Concrete Composites*, 19(2), 1997, pp. 107-122.

Chapter 6

6 EXPERIMENTAL AND NUMERICAL INVESTIGATION ON NOVEL SMA-PVA HYBRID FIBRE REINFORCED ENGINEERED CEMENTITIOUS COMPOSITE UNDER IMPACT LOADING⁵

6.1 INTRODUCTION

Missiles, bombs, aircraft and truck crashes, accidental explosions, and rock falls have become major threats to civilian structures and military facilities (El-Tehewy and El-Sayed, 2015). There have been rapid advances in the technology of explosives and ammunitions over the last few decades, not only with regards to its destructive capacity, but also its sophisticated ability to penetrate the aimed target. A superior level of protection against explosive and impact loading will be required in the future.

⁵ A version of this chapter was submitted for publication to the *Cement and Concrete Composites Journal*.

The unique behaviour of ECC structural elements under impact loading triggered significant research aiming at the development of design guidelines for ECC in protective structures. Several experimentally and numerical investigations have been conducted on the impact resistance of ECC elements. Due to technical difficulties and high cost of conducting large-scale missile impact tests, often small-scale drop weight impact testing has rather been adopted, despite the limitations associated with such a testing approach. For instance, Ali *et al.* (2017) experimentally investigated the impact resistance of SMA-ECC composites under drop weight impacting. Up to six hundred blows were applied per specimen to cause fracture, which reflects the time and efforts required to conduct such tests. Therefore, numerical simulation is highly attractive alternative considering the costs and difficulties of experimental tests.

For accurate numerical prediction of the impact behaviour of ECC structures, adequate material models which can represent the dynamic behaviour of ECC are essential (Li and Zhang, 2012). Various commercial codes have emerged to model the dynamic behaviour of concrete materials such as ABAQUS, ANSYS, AUTODYN and LS-DYNA. Various material models representing different types of concrete have been proposed for impact analysis (Wu *et al.*, 2005; Tai and Tang, 2006; (Teng *et al.*, 2008). However, they often require many input parameters, some of which have no clear physical meaning and cannot be estimated by traditional material tests (Farnam *et al.*, 2010). So far, there is dearth of numerical studies on the behaviour of ECCs under dynamic loading.

For instance, Chin (2006) utilized the LS-DYNA code in modeling the behaviour of a hybrid-fibre ECC panels under drop-weight impact loading. It was observed that the Finite Element (FE) model gave reasonable prediction of the local and global responses of the ECC panels and closely predicted the impact load-time histories of the impactor. Likewise, Li and Zhang (2012) performed a numerical simulation of ECC panels under high velocity impact loading also using the LS-DYNA code. Their results demonstrated the effectiveness of the proposed model in simulating the dynamic behaviour of ECC materials. Recently, Anil *et al.* (2016) conducted a FE study on ECC beams under impact loading using the commercial ABAQUS software package to observe the stress distribution in beams and attain an accurate and verified model capable of simulating such loading conditions. Their analytical results were in good agreement with the experimentally measured data in terms of maximum displacement and load values. Also, they observed that the

stress distribution through the beams was in reasonable agreement with the experimental crack distribution. Hence, it appears that accurate simulation and prediction of the structural response under dynamic load can be a convenient way to decrease the cost and efforts related to testing new materials and applications. The availability of powerful FE modeling codes with flexibility to incorporate new material models developed by the user have stimulated such efforts.

In the present chapter, numerical simulations of the mono- and hybrid-fibre-reinforced engineered cementitious composite under impact loading were carried out. The modelling results obtained in this chapter were compared to that achieved experimentally in Chapter 5 and the findings are discussed below.

6.2 FINITE ELEMENT MODELLING OF ECC

Generally, there is significant difference between the constitutive behaviour of ECC and that of normal concrete, especially for tension stiffening. According to the aforementioned behaviour of HECC-SMAF, SMA fibres enhanced the post-cracking performance of ECC through maintaining some load-carrying capacity subsequent to crack formation. De-bonding, pulling-out, and rupture of fibres, are the main parameters that affect the fracture energy of cementitious materials (Bentur and Mindess, 2007). Therefore, presenting accurate constitutive modelling of ECC is essential in order to achieve a reliable technique that can estimate its structural behaviour.

In this study, a finite element analysis was carried out using the commercial finite element (FE) ABAQUS/Explicit software in order to conduct the parametric study. This tool incorporates various constitutive models for concrete, including the Drucker/Prager (DP) and Concrete Damage Plasticity (CDP) models. According to Tahmasebinia (2008), the DP model can better simulate the behaviour of ductile concrete, especially under low velocity impact loading compared to Brittle-Cracking models. While, Li and Zhang (2012) demonstrated the effectiveness of simulating the dynamic behaviour of cementitious materials under impact loading using the CDP Model. In the present study, both the DP and CDP models were utilized. Their effectiveness in modeling the behaviour of HECC-SMAF composite under impact loading was explored and compared with experimental results achieved in Chapter 5.

6.2.1 Plasticity Models

The DP model is a plasticity model that describes the behaviour of granular materials in which the yield behaviour is affected by the equivalent pressure stress. It also takes into consideration inelastic deformations that may be associated with frictional mechanisms, such as sliding of particles across each other. On the other hand, the CDP model assumes isotropic damage and is suitable for applications in which the concrete is subjected to arbitrary loading conditions, such as cyclic loading and/or dynamic loading under low confining pressure (ABAQUS Analysis User's Manual, 2012). It can also be used to model plain and reinforced concrete. It accounts for degradation of the elastic stiffness created by plastic straining that takes place in tension and compression, and for stiffness recovery effects under cyclic loading. The main two failure mechanisms that govern the plasticity model are tensile cracking and compressive crushing of concrete. The evolution of the failure surface is controlled by the compressive (ε_c^{pl}) and/or tensile plastic strain (ε_t^{pl}).

Figures 6-1 and 6-2 illustrates the assumed stress-strain behaviour of concrete under uniaxial tensile and compressive loading, respectively. The model follows a linear elastic relationship until the tensile failure stress (σ_{to}) or the compressive yielding stress (σ_{co}). The tensile failure stress (σ_{to}) corresponds to micro-cracking initiation in concrete, thereafter, progressive cracking is represented by a softening stress-strain behaviour, as shown in **Fig. 6.1**.

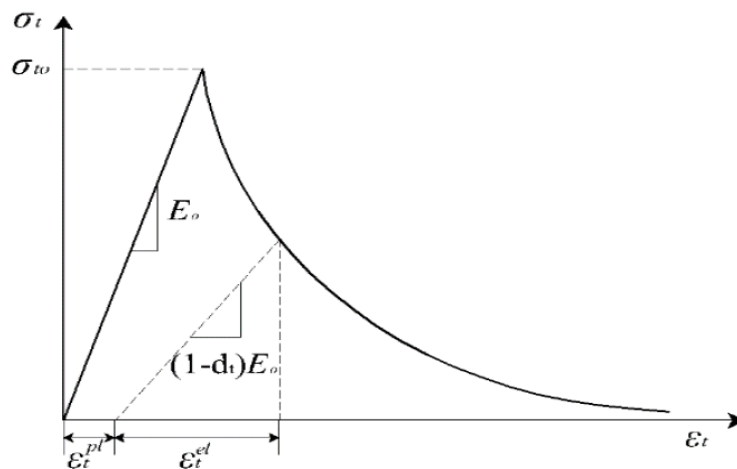


Figure 6-1: Concrete behaviour under uniaxial tensile loading (ABAQUS Analysis User's Manual, 2012).

On the other hand, in compression, the behaviour in the plastic zone is characterized by stress hardening, followed by strain softening subsequent to the ultimate stress (σ_{cu}), as portrayed in **Fig. 6.2**.

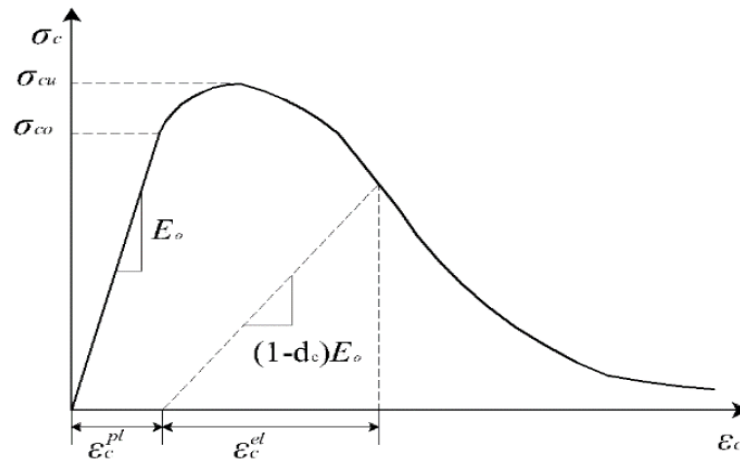


Figure 6-2: Concrete behaviour under compression loading (ABAQUS Analysis User's Manual, 2012).

6.2.2 Defining Tensile and Compressive Behaviour

Tension stiffening can be defined by means of a post-cracking stress-strain relation or by applying a fracture energy cracking criterion. In this study, the post-cracking stress-strain criterion was utilized. The post-cracking stress is given as a function of the cracking strain (ϵ_t^{ck}). The cracking strain is defined as the total strain (ϵ_t) minus the elastic strain corresponding to the undamaged material (ϵ_{to}^{el}), as shown in **Fig. 6.3** where: $\epsilon_{to}^{el} = \sigma_t/E_o$ and E_o is the modulus of elasticity (ABAQUS Analysis User's Manual, 2012). On the other hand, the compressive behaviour in the plastic regime is defined as a stress-inelastic strain (ϵ_c^{in}) relation. The compressive inelastic strain is defined as the total strain (ϵ_c) minus the elastic strain corresponding to the undamaged material (ϵ_{co}^{el}), as illustrated in **Fig. 6.4**, $\epsilon_{co}^{el} = \sigma_c/E_o$ (ABAQUS Analysis User's Manual, 2012).

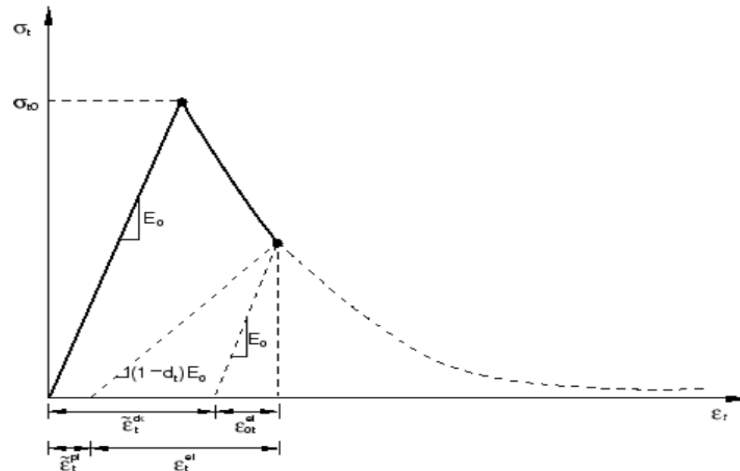


Figure 6-3: Tension stiffening variables (ABAQUS Analysis User's Manual, 2012).

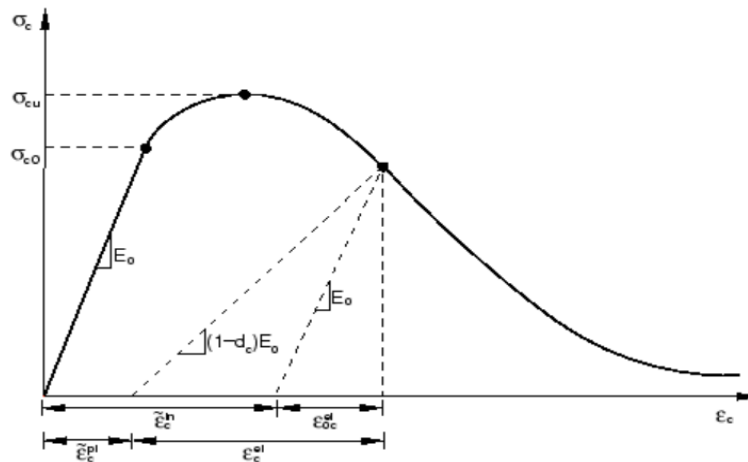


Figure 6-4: Compression hardening variables (ABAQUS Analysis User's Manual, 2012).

6.2.3 Defining Modeling Parameters

Table 6-1 shows the parameters used in this study to define the DP and CDP models of the ECC material. The friction angle (β), dilatation angle (ψ), and eccentricity (m) reflect the plastic straining response of the ECC material. Also, K represents the ratio of the flow stress in triaxial tension to the flow stress in triaxial compression. While, the ratio σ_{col}/σ_{bo} and K_c determine the shape and size of the bi-linear yield surface (Blazejowski, 2012). Since the response of the ECC material under impact will be mostly uniaxial, it is not anticipated that these parameters will vary. Also, assuming that there is no strain rate effect, then viscosity (μ) has been set to zero. Values of parameters in **Table 6-1** were set based on previous studies by (Nedal and Nehdi, 2016; Attrade,

2014; Tahmasebinia, 2008). Further definition of each of these parameters can be found in ABAQUS User's Manual (2012).

Table 6-1: Input parameters of plasticity models.

Parameter	DP	CDP
β	30	-
ψ	20	20
m	-	0.1
K	1	-
σ_{co}/σ_{bo}	-	1.16
Kc	-	0.667
μ	-	0

6.2.4 Simulation Technique

Three-dimensional finite element models of the tested ECC specimens were constructed in ABAQUS/Explicit solver. The cylindrical ECC specimen, spherical steel ball, hollow steel ring holder and steel drop weight were modeled using their actual dimensions in the experimental test setup. The drop weight was modeled as a prismatic bar with a cylindrical head as shown in **Fig. 6-5**. The different ECC specimens were modeled using 8-noded hexagonal solid elements (C3D8R), which is commonly used in the simulation of impact behaviour in the ABAQUS library. A sensitivity analysis was conducted to determine an optimum number of elements. The problem was solved with increasingly finer mesh size and the analysis was assumed to be optimum when the numerical response nearly matched the corresponding experimental data.

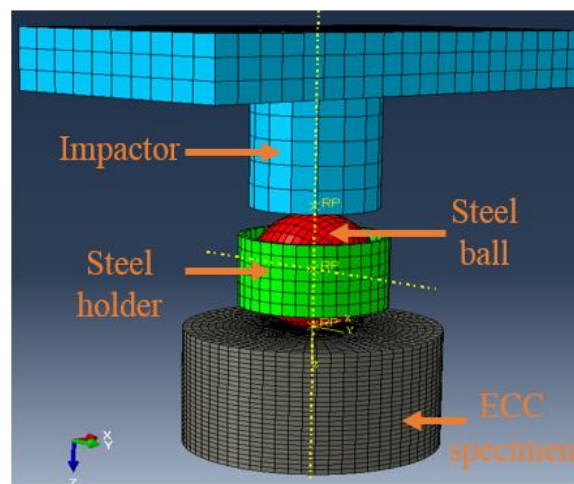


Figure 6-5: Finite element modelling of drop weight impact test.

6.2.5 Damage Criterion

Since there is no material model for ECC composites in ABAQUS, the CDP and DP material models were tested as concrete material models to capture the ductile behaviour of ECC. Also, the Damage Initiation Criterion and Element Deletion options were utilized in these models for defining the material's tensile failure criterion (Qian *et al.*, 2009). Pertinent ECC material parameters, including compressive strength, modulus of elasticity and Poisson's ratio, density and tensile behaviour, were implemented in the models using actual corresponding experimental values as shown in **Table 6-2**.

Table 6-2: Mechanical properties of different ECC specimens

	ECC2-0	ECC2-0.5	ECC2-1	ECC2-1.5
Tensile strength (MPa)	4.8	5.9	8.1	6.5
Compressive strength (MPa)	70.1	69.6	68.7	66
Elastic modulus (GPa)	19.86	19.08	18.96	18.92
Poisson's ratio	0.185	0.183	0.17	0.14
Density (kg/m ³)	18.08	17.36	17.58	17.9

6.2.6 Initial and Boundary Conditions

Two types of conditions were adopted in the modeling procedures, initial and boundary conditions. The initial condition was assigned to the impactor with a velocity of 1.38 m/s when it touches the spherical ball, as displayed in **Fig. 6-6a**.

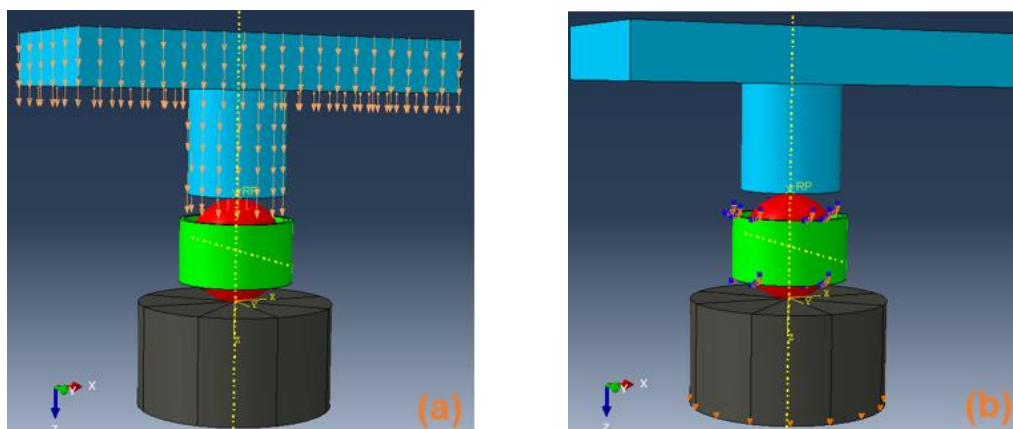


Figure 6-6: a) initial conditions and b) boundary conditions.

All the nodes of the impactor and spherical ball could move only in the Z-direction. All the nodes of the hollow steel ring were prevented from movement in all directions, while all the nodes of the lower base of the ECC specimen were prevented from moving in Z-direction, as shown in **Fig. 6-6b**.

6.3 ANALYSIS OF RESULTS AND DISCUSSION

Dynamic analysis in this numerical simulation was conducted for the first, second and third free drops of the impactor. Thereafter, the accumulated damage due to multiple impacts was presented. Numerical predictions were compared to corresponding experimental data achieved in chapter 5 as discussed below.

6.3.1 Effect of Mesh Density on Model Accuracy

To investigate the effectiveness of utilizing different mesh densities on model accuracy, the load-time history and applied energy-penetration curves resulting from the numerical analysis were compared with corresponding results obtained from the experimental investigation as portrayed in **Figs. 6-7a and b**. Five different meshing densities were examined ranging from very fine to coarse.

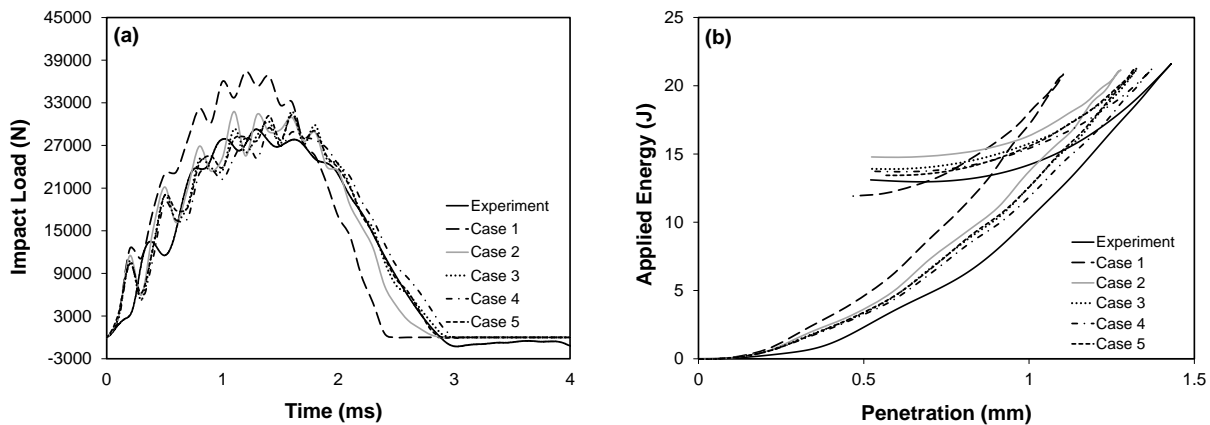


Figure 6-7: Effect of different mesh densities on numerical results: a) load-time history, and b) applied energy-penetration depth.

Table 6-3 displays the number of elements utilized in each case and the ratio between the results obtained from the finite element analysis (FEA) and the corresponding experimental results. It can be observed that as the number of elements increased, the shape of the predicted curves became

smoother and progressively converged toward the experimental behaviour. Cases 1 and 2 were far from the experimental curve. Conversely, cases 3 and 5 almost gave similar results to the experimental curves. Case 4 achieved closest prediction of the experimental results. Based on results in **Table 6-3**, the near optimum number of elements utilized in simulating the ECC specimens was 15180 elements. Since the spherical steel ball, holder steel ring and drop weight were considered rigid, their elements sizes had no significant effect on the solution.

Table 6-3: Sensitivity analysis on mesh density

Mixture		Case 1	Case 2	Case 3	Case 4	Case 5
Number of elements		111	1926	8609	15180	28014
FEA/Exp. ratio	Applied load	1.28	1.09	1.08	1.01	1.07
	Applied energy	0.97	0.98	0.98	0.99	0.98
	Penetration depth	0.77	0.89	0.93	0.96	0.92

6.3.2 Energy-Penetration Behaviour

Dynamic loading on structures is accompanied with large transfer of mechanical energy. In order to numerically explore the behaviour of structural elements under impact loading, consideration of the energy balance should be the first step (Martin, 2010). In the FEA, the impactor and the concrete element were presented as a single mechanical system. Before impact, the drop weight only had kinetic energy, while during impact, the drop weight slowed down significantly (lost a substantial part of its kinetic energy) due to the energy dissipation capability of the concrete element. **Figure 6-8** presents the experimental and numerical applied energy-penetration depth curves for the ECC specimens at different drop levels. It can be observed that the CDP and DP models could closely estimate the experimental behaviour of the ECC specimens under impact loading.

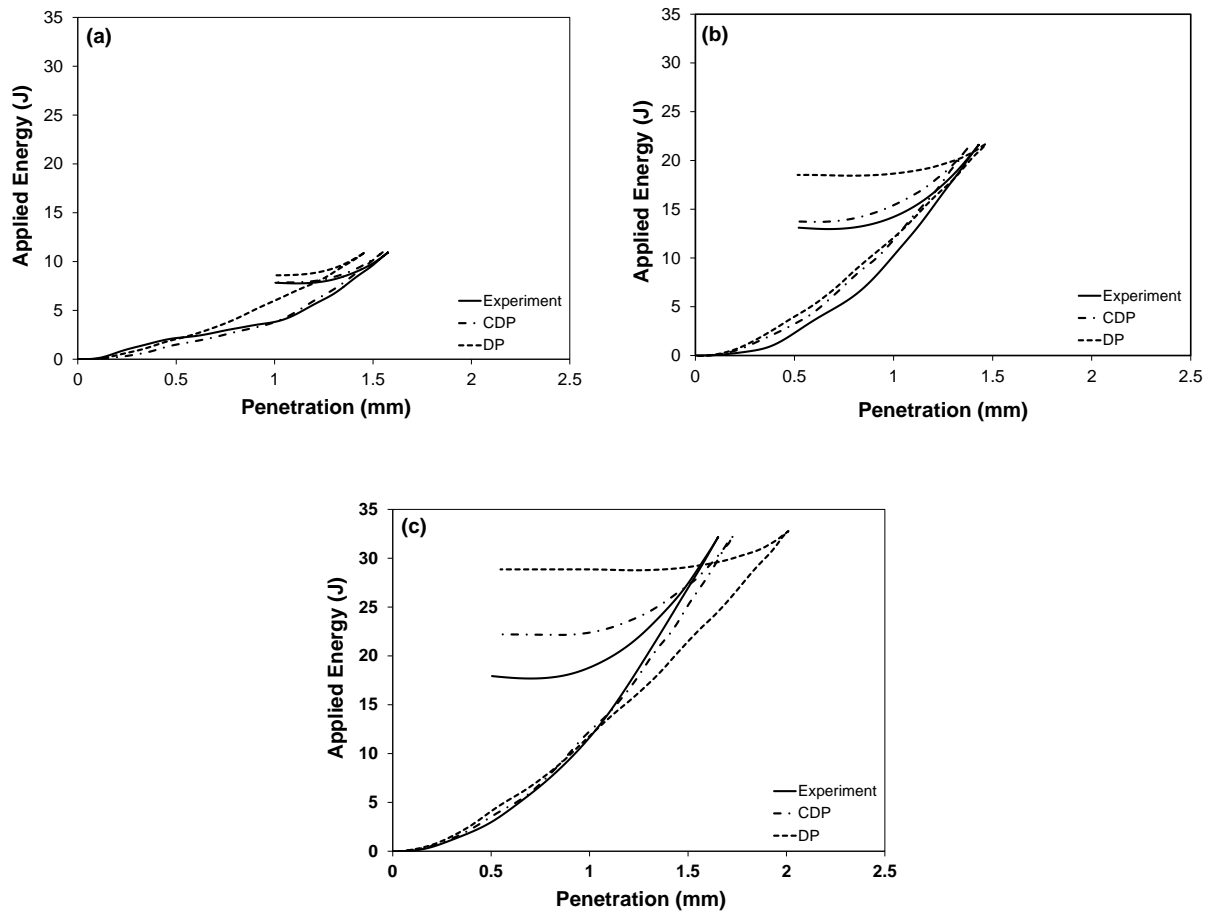


Figure 6-8: Applied energy-penetration depth curves for ECC specimens at different drop levels; a) 1st hit, b) 2nd hit, and c) 3rd hit.

Table 6-4 reports the experimental and numerical results for all tested specimens. Although the DP model exhibited good estimation of the applied energy at the first impact, the CDP model generally displayed better performance in simulating experimental results at higher impact levels.

Table 6-4: Experimental and numerical impact test results

	Hit no.	ECC2-0					ECC2-0.5					ECC2-1					ECC2-1.5				
		Exp.	CDP	DP	CDP /Exp	DP/ Exp.	Exp.	CDP	DP	CDP /Exp	DP/ Exp.	Exp.	CDP	DP	CDP/ Exp.	DP/ Exp.	Exp	CD P	DP	CDP /Exp	DP/ Exp.
Energy (J)	1	10.3	10.3	11.1	1.00	1.01	11.0	11.3	11.1	1.03	1.01	10.9	11.1	11.0	1.02	1.00	10.5	10.8	11.1	1.03	1.05
	2	21.8	20.3	21.9	0.98	1.06	21.2	21.3	21.7	1.00	1.02	21.6	21.3	21.7	0.99	1.01	21.3	20.8	22.0	0.98	1.03
	3	31.5	31.4	33.1	0.99	1.05	32.2	32.4	33.0	1.01	1.03	32.2	32.4	32.8	1.01	1.02	31.7	31.8	32.9	1.01	1.04
Load (kN)	1	17.1	16.1	14.1	0.94	0.83	16.5	15.6	13.5	0.94	0.82	17.6	16.6	14.4	0.95	0.82	16.8	15.8	13.8	0.94	0.82
	2	27.4	28.2	17.7	1.03	0.65	28.9	28.7	20.0	0.99	0.69	29.3	29.5	22.9	1.01	0.78	27.1	28.8	21.2	1.07	0.78
	3	35.7	31.9	20.5	0.89	0.57	36.9	35.2	22.7	0.95	0.62	36.4	36.0	24.6	0.99	0.68	36.5	34.0	23.8	0.93	0.65
Pen. (mm)	1	1.45	1.53	1.44	1.06	0.99	1.35	1.53	1.44	1.13	1.06	1.37	1.56	1.46	1.13	1.06	1.42	1.50	1.41	1.06	0.99
	2	1.52	1.38	1.85	0.91	1.22	1.43	1.37	1.62	0.96	1.13	1.33	1.37	1.46	1.03	1.10	1.48	1.40	1.56	0.95	1.05
	3	1.65	1.76	2.49	1.07	1.51	1.55	1.74	2.20	1.12	1.42	1.45	1.73	2.01	1.19	1.38	1.60	1.77	2.11	1.10	1.32

Note: Hit no. = number of impacts. Pen. = Penetration depth. Exp. = Experimental results.

Figure 6-9 displays the strain energy magnitude propagated through the ECC specimens due to impact loading at different time intervals along with that remaining in the specimen after impact. It can be observed that the propagated energy kept increasing through the specimen during the impact process, while it was partially reversed (dissipated) upon removal of the load. The amount of applied energy which remained or dissipated through the system depended mainly on the energy dissipation capability of the tested material.

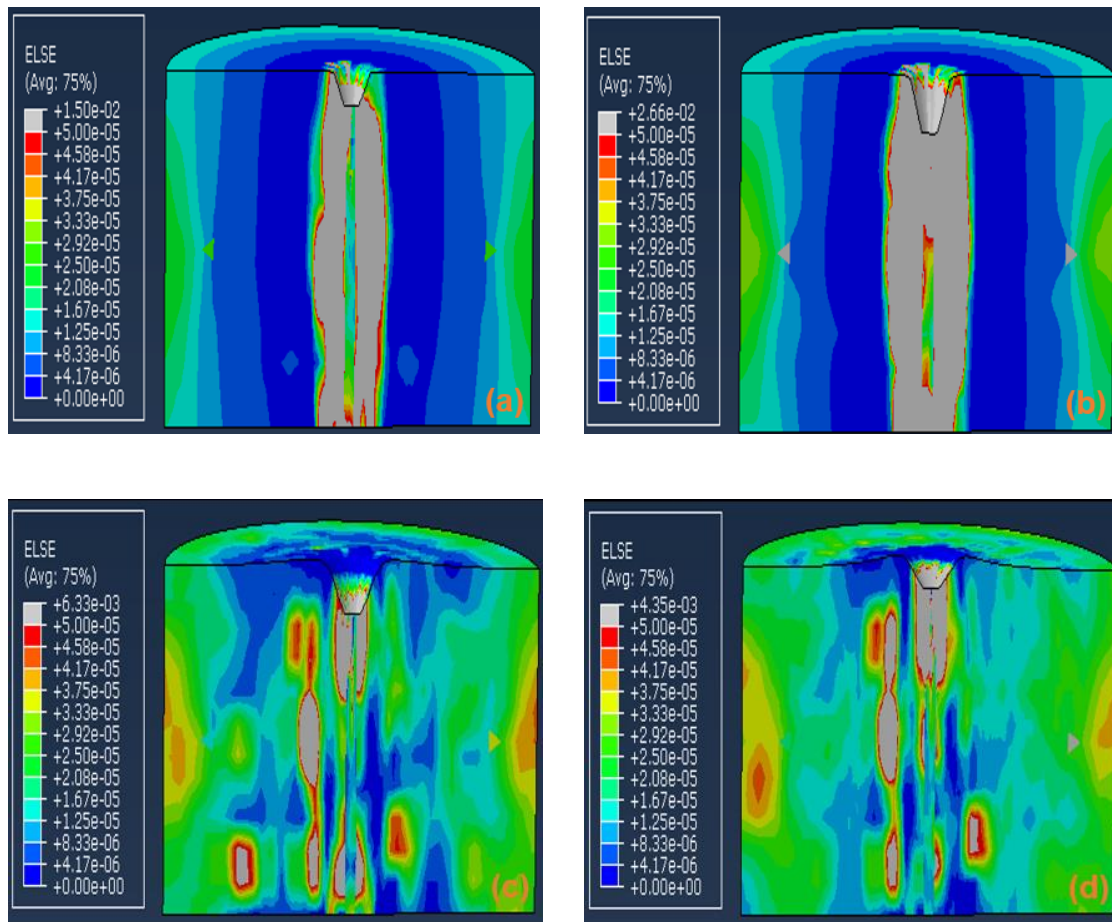


Figure 6-9: Strain energy magnitude in ECC specimens due to impact at: a) 2.5 ms, b) 5 ms, c) 7.5 ms, and d) 10 ms.

Figure 6-10 illustrates the total energy dissipated through all impact levels for the various ECC specimens. It can be observed that numerical and experimental values of dissipated energies are in good agreement. During experimental testing, cracks were usually captured when their width was sufficiently developed, while in numerical simulations, they could

be detected at earlier stages. This could result in estimating numerical dissipated energies that are lower than their corresponding experimental values. Also, it can be observed that the total energy dissipated through the ECC specimens using the CDP model was in better agreement with the experimental results compared to that of the DP model. For instance, the total energy dissipated through the ECC2-0, ECC2-0.5, ECC2-1, and ECC2-1.5 specimens using the CDP model was 24.4%, 17.3%, 18.8%, and 21.9% lower than that of the experimental results, respectively. However, using the DP model, the total energy dissipated was 58.0%, 61.5%, 61.1%, and 56.6% lower than the corresponding experimental results, respectively.

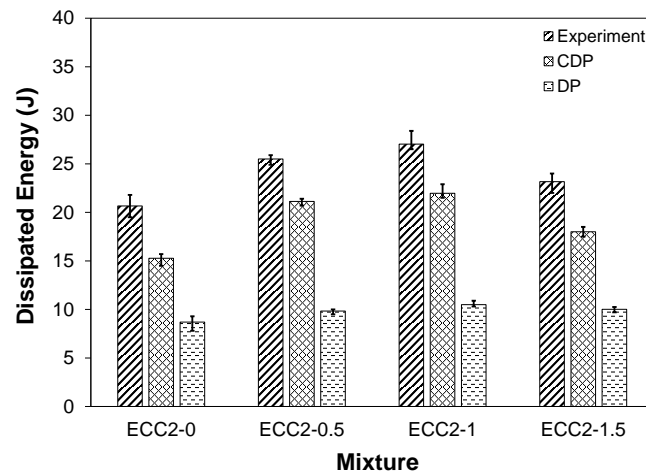


Figure 6-10: Accumulated dissipated energy of different ECC specimens due to multiple impacts: a) experimental, b) CDP, and c) DP.

Similarly, the numerically estimated penetration depth of the different ECC specimens under multiple impacts was in good agreement with corresponding experimental observation as shown in **Table 6-4**. **Figure 6-11** displays the accumulated penetration depth measured through the different ECC specimens due to multiple impacts. Furthermore, **Figs. 6-12 and 6-13** show the total numerically estimated penetration depth using the CDP and DP models, respectively.

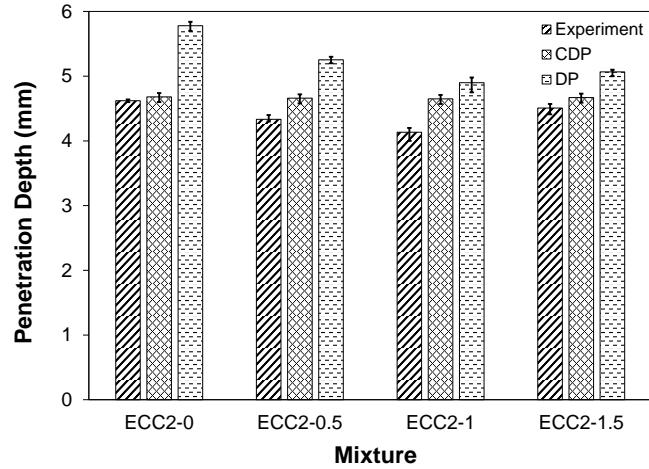


Figure 6-11: Accumulated penetration depth for various ECC specimens due to multiple impacts: a) experimental, b) CDP, and c) DP.

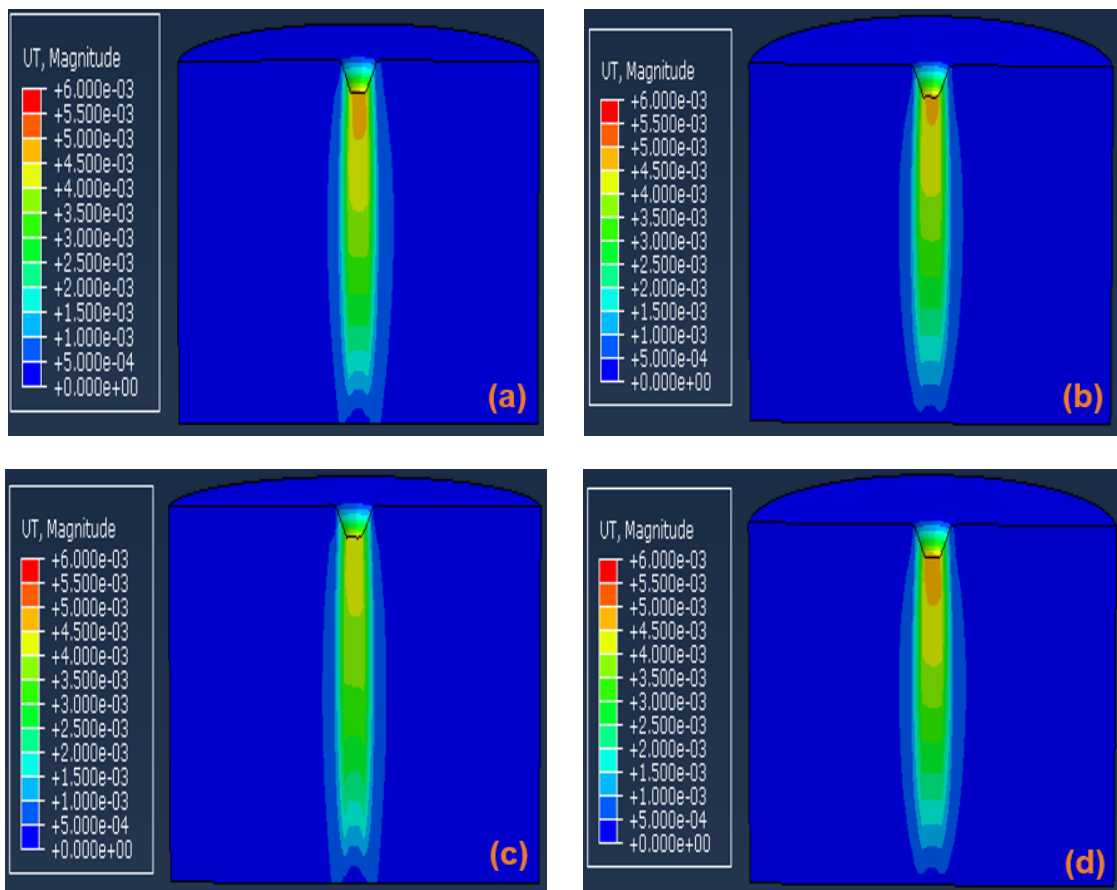


Figure 6-12: Penetration depth for ECC specimens due to multiple impacts using the CDP model: a) ECC2-0, b) ECC2-0.5, c) ECC2-1, and d) ECC2-1.5.

It can be observed that CDP model was more accurate than the DP model in predicting the penetration depth upon multiple impacts. For instance, the total penetration depth determined by the CDP model for the ECC2-0, ECC2-0.5, ECC2-1, and ECC2-1.5 specimens was 1.1%, 7.2%, 12.1%, and 3.7% higher than the experimental results, respectively. However, the total penetration depth estimated using the DP model was 25.1%, 21.2%, 18.7%, and 12.6% higher than the experimental results, respectively.

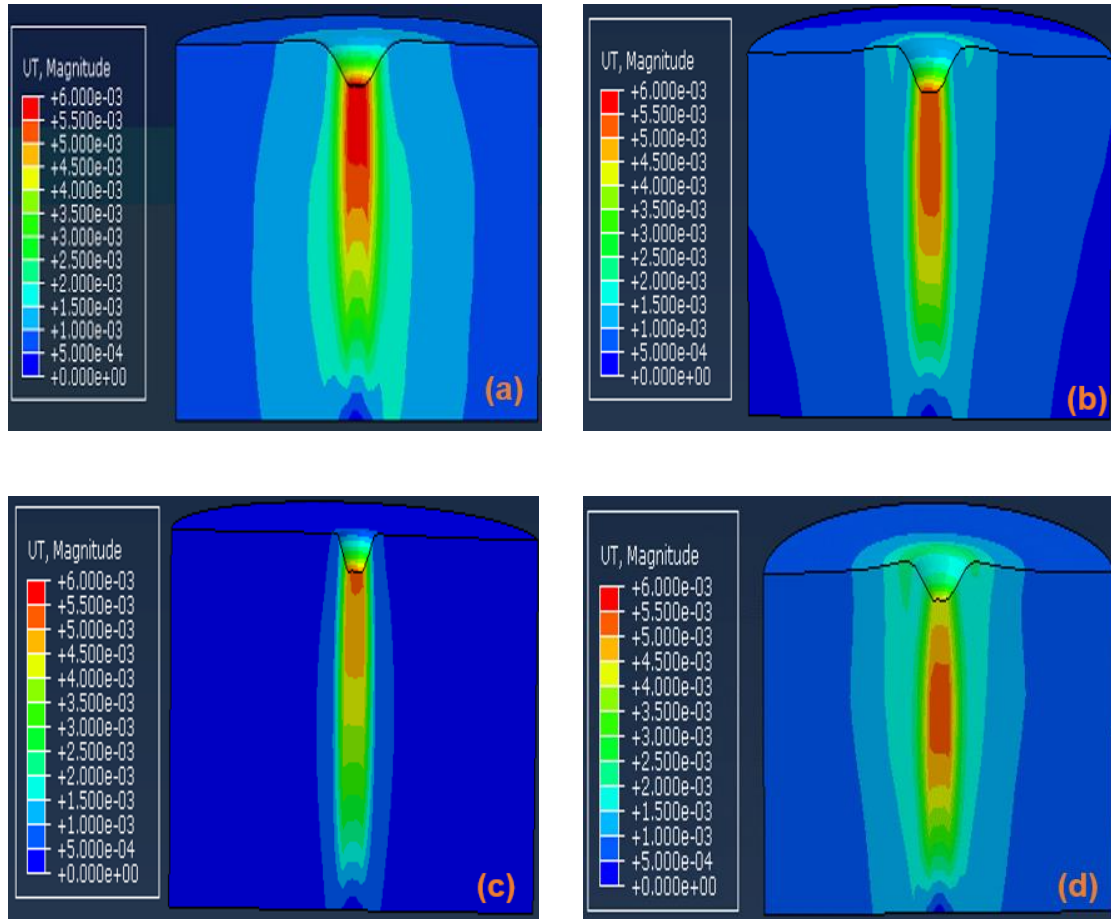


Figure 6-13: Penetration depth for ECC specimens due to multiple impacts using the DP model: a) ECC2-0, b) ECC2-0.5, c) ECC2-1, and d) ECC2-1.5.

6.3.3 Impact Load-Time History

The ductility features imparted into the CDP and DP models enable simulating the behaviour of ECC materials under dynamic loading close to experimental findings, as shown in **Fig. 6-14**, with the CDP model exhibiting superior performance.

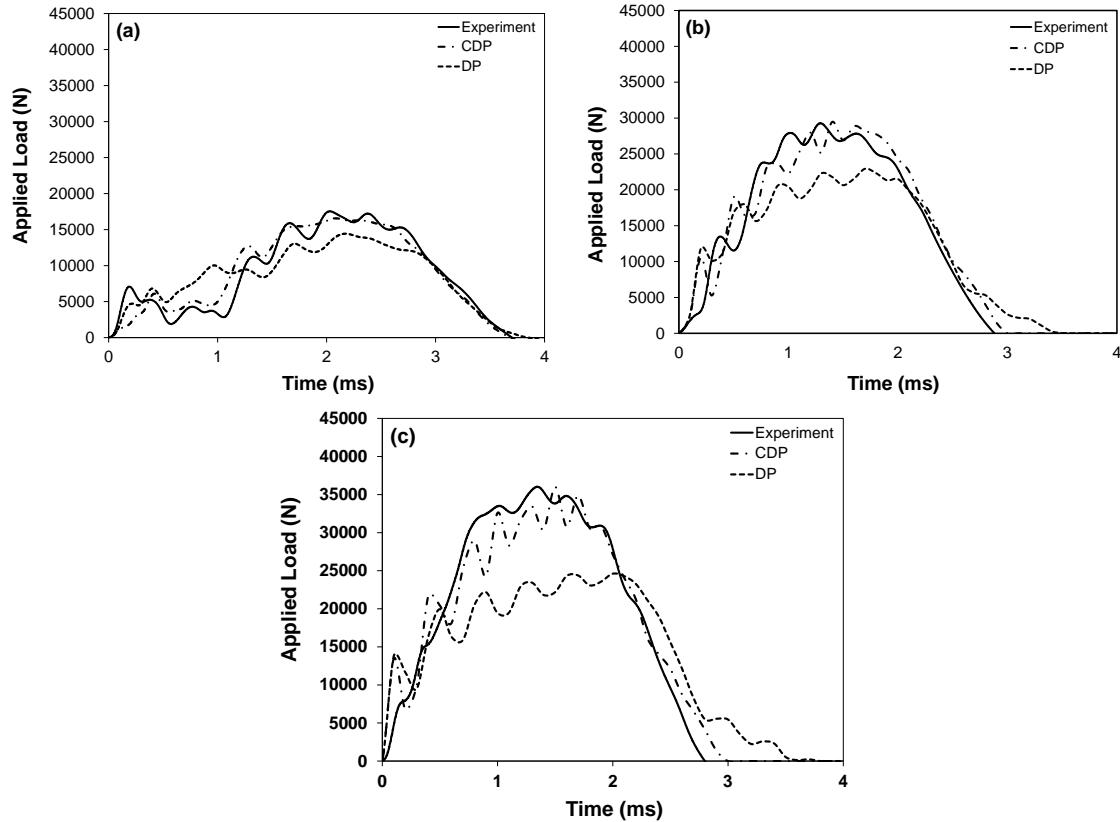


Figure 6-14: Typical impact load-time history curves for ECC specimens at different impact levels: a) 1st hit, b) 2nd hit, and c) 3rd hit.

The tolerance in the applied load estimated using the DP model was about four times that of the CDP model compared to actual experimental data. For instance, as displayed in **Fig. 6-15**, the accumulated impact load applied on the ECC2-0, ECC2-0.5, ECC2-1, and ECC2-1.5 estimated using the CDP model was 11.6%, 3.5%, 1.0%, and 2.2% lower than the corresponding experimental data, respectively, while that estimated by the DP model was 39.6%, 31.7%, 25.2%, and 26.9% lower than the experimental results, respectively. The difference in numerical accuracy can be attributed to the fact that the CDP model is constructed based on the two main failure mechanisms of concrete: tensile cracking and compressive crushing. The evolution of yield surfaces in concrete is controlled by two hardening variables, which causes failure under tensile and compressive stresses simultaneously. While, the DP model is based on the same criterion, only one of the two main failure mechanisms can be assigned for the material during the simulation, which affects its overall performance.

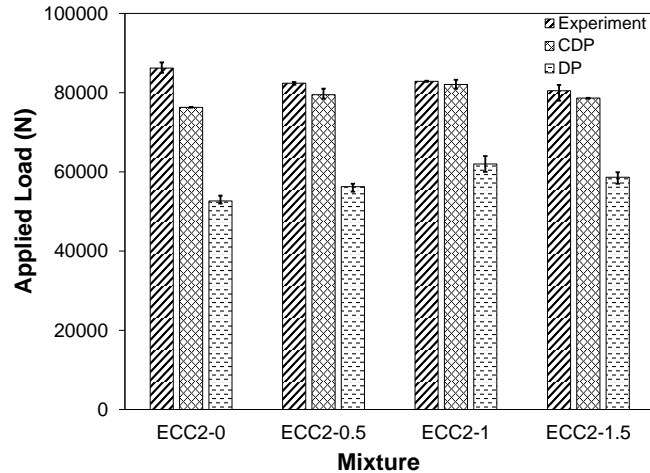
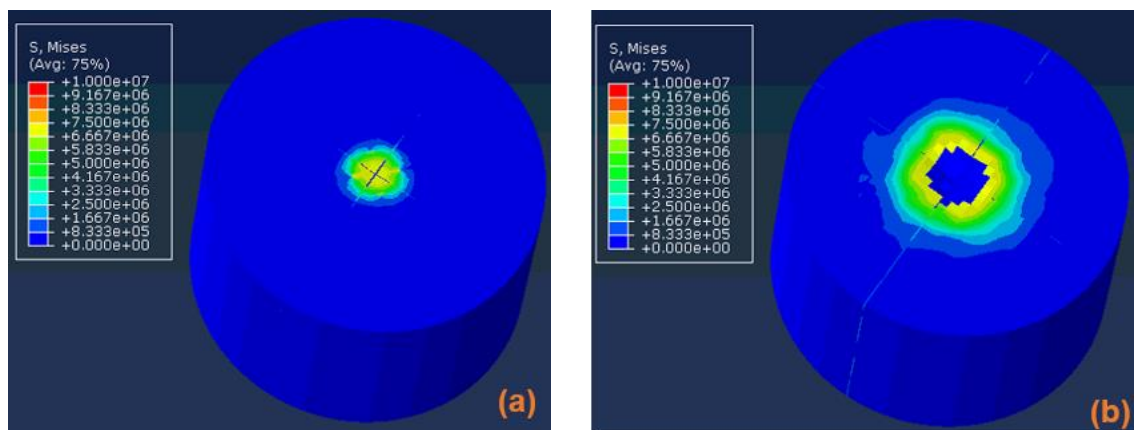


Figure 6-15: Applied impact load of different ECC specimens due to multiple impacts: a) experimental, b) CDP, and c) DP.

6.4 FAILURE CRITERION

A key benefit of the numerical simulation is the ability to capture when and where the first crack is initiated, which is experimentally more challenging. **Figures 6-16 and 6-17** display the stress distributions through the ECC specimens outlined via the numerical simulations. Maximum and minimum principal stresses were illustrated on the upper and lower surfaces of the different ECC specimens. It was observed that the stress distributions in the developed models using ductile modelling techniques such as the CDP or DP Drucker-Prager models can give realistic results of the actual crack propagation under impact loading.



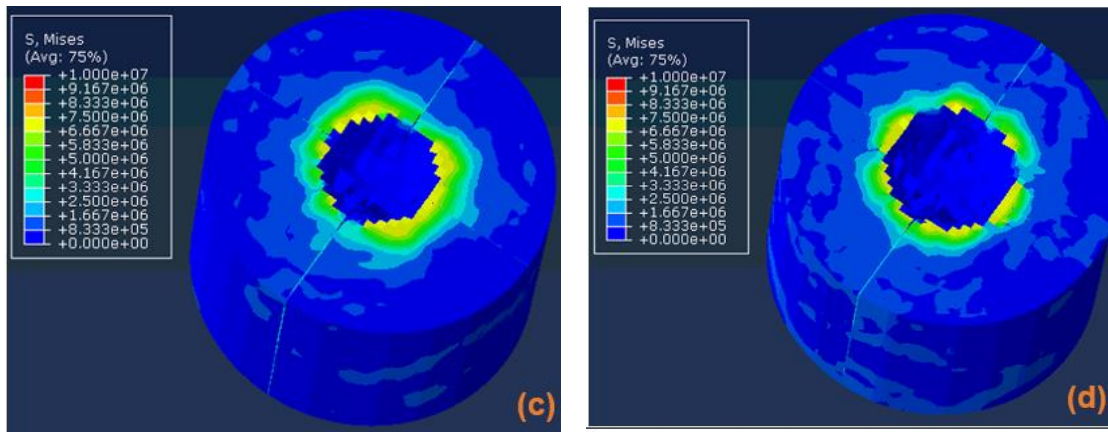


Figure 6-16: Upper surface stress distribution of ECC specimens due to impact at: a) 1 ms, b) 2 ms, c) 3 ms, and d) 4 ms.

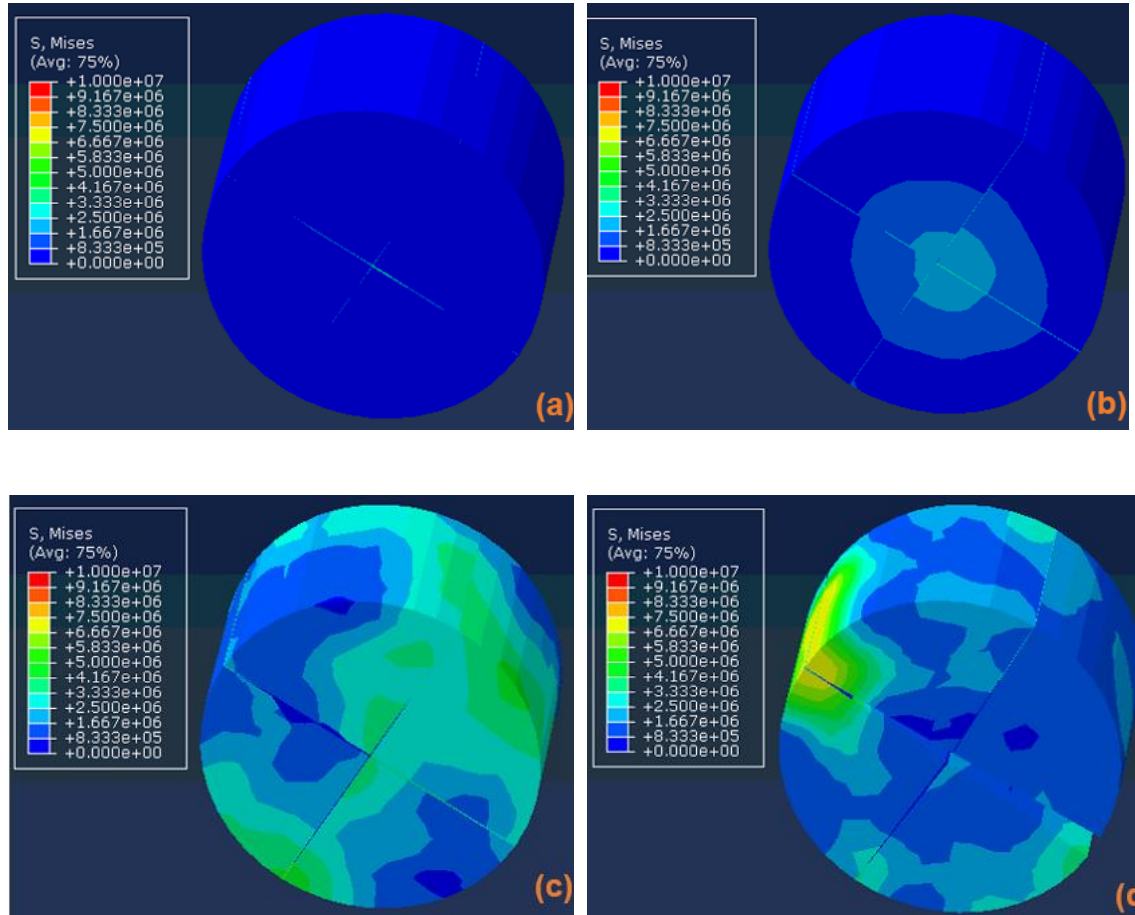


Figure 6-17: Distal face stress distribution of ECC specimens due to impact at: a) 1 ms, b) 2 ms, c) 3 ms, and d) 4 ms.

Figures 6-18 and 6-19 illustrates a comparison between the experimental and numerical simulation failure criterion of different ECC specimens under impact loading. The differences in the stress distribution between the experimentally tested and simulated specimens can generally be attributed to the fact that the tested specimens were made from a rather heterogeneous material, while a homogeneity assumption was made in the simulation process. This could lead to variation in the crack propagation path.

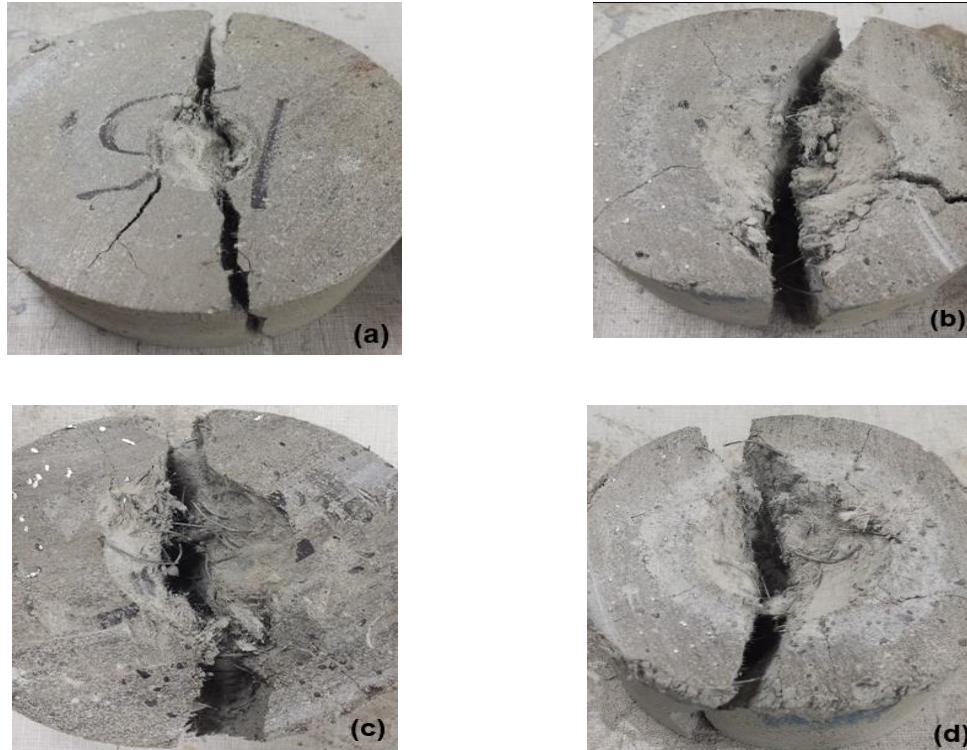


Figure 6-18: Experimental failure criterion of ECC specimens due to impact: a) ECC2-0, b) ECC2-0.5, c) ECC2-1, and d) ECC2-1.5.

The stress distribution in the ECC elements was globally distributed rather than local. This can be observed through the impulsive waves generated due to impact loading on all surfaces of the ECC specimens. Furthermore, it was observed that the tensile stresses were propagated at the upper surface of specimens around the circumferential edge of the impacting ball (**Fig. 6-19**). Yet, the compressive stresses were generated through the specimen under the impacted area. These compressive stresses were transferred into tensile

stresses when the elastic wave reflected at the distal face. Under impact loading, tensile stresses in concrete structures cannot be avoided.

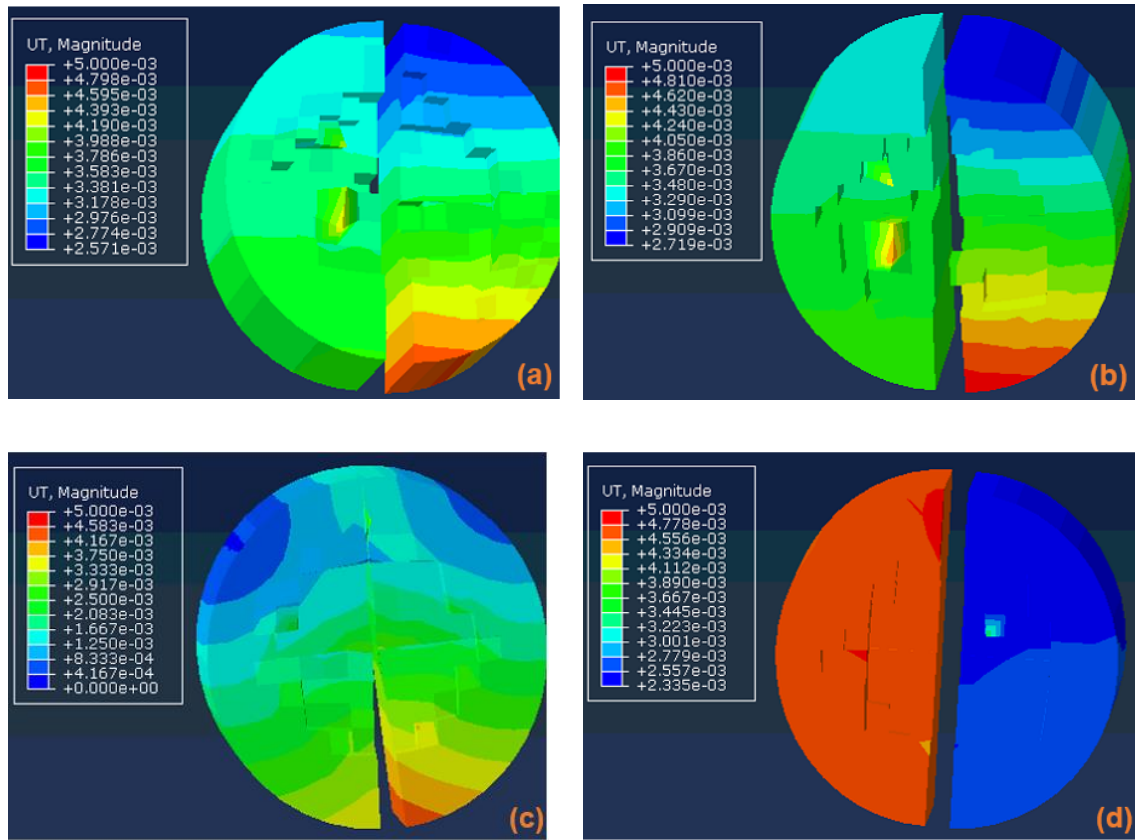


Figure 6-19: Numerical failure criterion of ECC specimens due to impact: a) ECC2-0, b) ECC2-0.5, c) ECC2-1, and d) ECC2-1.5.

6.5 VALIDATION OF NUMERICAL MODELS

The numerical models were first used to evaluate the applied impact energy required to achieve crack initiation and failure of the tested specimens and their results were subsequently compared to that experimentally acquired in chapter 5. **Figures 6-20a and b** illustrate the experimental and numerical values of the impact energy sustained until crack initiation and final fracture of the ECC specimens, respectively. It can be observed that there was reasonable agreement between the numerical predictions and experimental results. The numerically estimated results using the CDP and DP models were 18.7% and 39.2% lower than the corresponding experimental data, respectively. For instance, per the

CDP model, the sustained impact energy until first crack initiation and final fracture for the ECC2-0, ECC2-0.5, ECC2-1 and ECC2-1.5 specimens were lower than the experimental values by 15.5%, 16.2%, 18.7%, and 17.1%, and 16.3%, 17.4%, 16.7%, and 18.2%, respectively. Likewise, the sustained impact energy until first crack initiation and final fracture of the ECC2-0, ECC2-0.5, ECC2-1, and ECC2-1.5 using the DP model was lower than the experimental data by about 30.2%, 36.1%, 32.5%, and 35.5%, and 32.3%, 36.5%, 34.5%, and 39.2%, respectively. The CDP model outperformed the DP model in evaluating the fracture energy of ECC specimens under impact loading, which supports earlier discussion. Differences between the experimental and numerical results can be ascribed to the inability of the simulation to model how the fibres were pulled out along with approximations related to the definition of materials parameters.

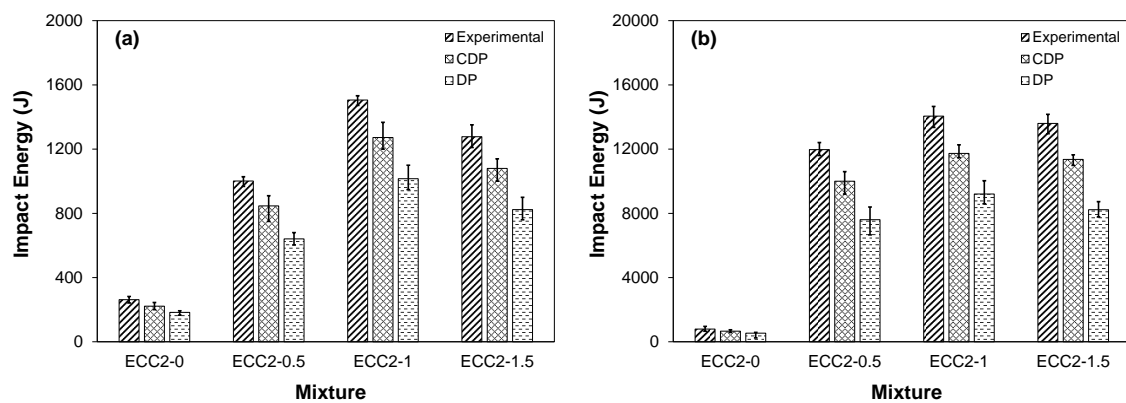


Figure 6-20: Impact energy sustained by ECC specimens: a) 1st crack, and b) failure.

The various hybrid composite HECC-SMAF specimens achieved superior impact resistance to that of the control PVA-ECC specimens. This is ascribed to the higher energy dissipation capability and pull-out resistance of SMA fibres compared to that of PVA fibres, requiring more energy before fracture of the specimens. The ECC2-1 specimen exhibited superior impact resistance compared to that of all other ECC specimens, which was observed both experimentally and numerically. Higher fibre dosage beyond 2% PVA and 1% SMA by volume fraction led to tensile strength and impact resistance degradation due to fibre clustering and increased porosity, as evidenced elsewhere by Ali *et al.* (2017).

6.6 CONCLUSIONS

Numerical simulations were carried out in the present chapter to investigate the behaviour under impact loading of PVA-ECC and HECC-SMAF composites. Numerical simulations were performed utilizing the commercial ABAQUS software. The experimental and numerical results were compared and the following conclusions were drawn:

- Generally, the impact resistance of the composite was improved owing to SMA fibre addition. Upon multiple impacts, the energy dissipation capability of the HECC-SMAF composite was increased by about 23.39%, 30.43% and 11.53% owing to SMA fibre addition of 0.5%, 1% and 1.5% by volume fraction, respectively, compared to that of the ECC specimen incorporating 2% PVA fibres alone.
- The impact penetration depth tended to decrease owing to SMA fibre addition. For instance, the ECC2-0.5, ECC2-1 and ECC2-1.5 specimens had 6.3%, 10.1% and 2.6% lower penetration depth compared to that of the control PVA-ECC specimen, respectively.
- The plasticity models implemented in the ABAQUS software, associated with the add-erosion option and maximum principal strain, were appropriate for simulating the behaviour of the ECC composite under impact loading.
- The numerical simulation results using the Concrete Damage Plasticity model showed better accuracy and closer agreement with corresponding experimental data than that of the Drucker/Prager model in terms of energy dissipation capability and maximum penetration depth.
- Generally, the stress distribution, crack propagation and failure criterion of the numerically simulated ECC specimens were in good agreement with the experimentally observed behaviour of the ECC specimens under impact loading.
- This study demonstrates the feasibility of using numerical simulation to reasonably predict the behaviour of the hybrid composite developed in this study under impact loading, which can save time, effort and cost associated with laborious experimental testing.

6.7 REFERENCES

- ABAQUS User's Manual, Version 6.12, SIMULIA, Dassault Systèmes Simulia Corp., 2012.
- ACI Standard, "Measurement of Properties of Fiber Reinforced Concrete." ACI Standard 544.2R-89, Farmington Hills, MI 48331-3439 USA, Reapproved, 2009.
- Ali, A.E.M.A., Soliman, A.M., and Nehdi, M.L., "Hybrid-fiber reinforced engineered cementitious composite under tensile and impact loading." *Materials and Design*, 117, 2017, pp. 139-149.
- Anil, O., Durucan, C., Erdem, R.T., and Yorgancilar, M.A., "Experimental and numerical investigation of reinforced concrete beams with variable material properties under impact loading." *Construction and Building Materials*, 125, 2016, pp. 94-104.
- Attrade, S., "Nonlinear finite element analysis of profiled steel deck composite slab system under monotonic loading." *MSc. dissertation*, Ryerson University, Toronto, Ontario, 2012.
- Bentur, A., and Mindess, S., "Fibre-Reinforced Cementitious Composites." 2nd edition; *New York: Taylor & Francis*, 2007, 660 p.
- Blazejowski, M., "Flexural behaviour of steel fibre reinforced concrete tunnel linings," *MSc. dissertation*, The University of Western Ontario, London, Ontario, 2012.
- Chin, L.S., "Finite element modeling of hybrid-fiber ECC targets subjected to impact and blast." *PhD dissertation*, National University of Singapore, 2006.
- El-Tehewy, E.M. and El-Sayed, M.A., "The effect of using multi layers of expanded steel mesh on penetration resistance of ferrocement slabs." *International Journal of Environment*, 4(4), 2015, pp. 300-308.
- Farnam, Y., Mohammadi, S., and Shekarchi, M., "Experimental and numerical investigations of low velocity impact behavior of high-performance fiber-

- reinforced cement based composite.” *International Journal of Impact Engineering*, 37(2), 2010, pp. 220-229.
- Li, J. and Zhang, Y.X., “Evaluation of constitutive models of hybrid-fibre engineered cementitious composites under dynamic loadings.” *Construction and Building Materials*, 30, 2012, pp. 149-160.
- Li, Q.M., Mines, R.A., and Birch, R.S., “The crush behaviour of Rohacell-51WF structural foam.” *International Journal of Solids and Structures*, 37(43), 2000, pp. 6321-6341.
- Nedal, M. and Nehdi, M., “Rational finite element assisted design of precast steel fibre reinforced steel pipes.” *Engineering Structures*, 124(1), 2016, pp. 196-206.
- Nehdi, M. and Soliman, A., “Novel Green Roofing Membrane System Made with Recycled Leftover Paint.” *Green Materials*, 1(4), 2013, pp. 231-241.
- Qian, G., Hanfeng, X., and Sidney, M., “An improved test method and numerical analysis for crack opening resistance of FRC round determinate panels.” *Wuhan University Journal of Natural Science*, 14(1), 2009, pp. 47-52.
- Tahmasebinia, F., “Numerical modelling of reinforced concrete slabs subject to impact loading.” *M.Sc. dissertation, University of Wollongong*, 2008.
- Tai, Y. and Tang, C-C., “Numerical simulation: the dynamic behavior of reinforced concrete plates under normal impact.” *Theoretical and Applied Fracture Mechanics*, 45(2), 2006, pp. 117-127.
- Teng, T-L., Chu, Y-A., Chang, F-A., Shen, B-C., and Cheng, D-S., “Development and validation of numerical model of steel fiber reinforced concrete for high-velocity impact.” *Computational Materials Science*, 42(1), 2008, pp. 90-99.
- Wu, H., Zhang, Q., Huang, F., and Jin, Q., “Experimental and numerical investigation on the dynamic tensile strength of concrete.” *International Journal of Impact Engineering*, 32(1-4), 2005, pp. 605-617.

Chapter 7

7 SUMMARY, CONCLUSIONS AND RECOMMENDATIONS

7.1 SUMMARY AND CONCLUSIONS

This study aimed at exploring the mechanical and dynamic behaviour of an innovative hybrid-fibre reinforced ECC incorporating short, randomly dispersed NiTi-SMA and PVA fibres (HECC-SMAF) with consideration of possibly using this novel composite in strengthening of key structural elements such as beams, slabs and columns to reduce its vulnerability to impact hazards.

In Chapter 3, the mechanical properties of fibreless, mono- and hybrid-ECC were investigated. Five different mixtures were tested; a fibreless ECC matrix, mono-PVA-ECC, and hybrid-ECC mixtures incorporating 2% PVA and 0.5%, 1%, and 1.5% SMA fibres by volume fraction. A slight to no increase in the compressive strength was achieved due to incorporation of fibres. Similarly, the elastic modulus and Poisson's ratio were generally decreased due to fibre addition regardless of the fibre type. Conversely, fibres addition led to improved tensile and flexural strengths. The fibre-reinforced specimens achieved ductile failure compared to the brittle one acquired by the ECC matrix. The hybrid ECC mixtures achieved highest tensile and flexural strength owing to SMA fibre addition. Moreover, strain recovery was achieved upon heat treatment owing to the shape memory effect of SMA fibres. In general, this chapter demonstrates that ECC composites incorporating SMA fibres not only have superior ductile behaviour, but could also recover strain, possibly making rehabilitation works much easier after excessive loading scenarios.

Chapter 4 expanded on the findings of Chapter 3. A series of uniaxial tensile tests were conducted on the mono- and hybrid-ECC composites. In addition, an inverse analysis was used to predict the tensile characteristics of the composite using flexural testing data. Results showed that SMA fibre addition generally improved the tensile characteristics of the composite. However, high dosages of fibres led to an overall reduction in the flexural and tensile behaviour of the composite due to fibre clustering. Among the tested mixtures, the ECC mixture incorporating 2% PVA and 1% SMA fibres by volume fraction achieved the highest tensile and flexural characteristics. The inverse method was found to be an adequate tool for estimating the tensile properties of ECC composites based on results of the simple flexural test. This chapter demonstrates that simple and cost-effective four-point bending tests can be used in combination with inverse analysis to predict the tensile behaviour of such composites, making it easier for the designer to incorporate these composites in modern smart and resilient structures that can withstand earthquake, explosive and other catastrophic loading scenarios.

In Chapter 5, the dynamic behaviour of ECC specimens was experimentally investigated under drop weight impact testing in accordance with ACI 544 recommendations. The experimental tests were conducted in four phases. First, the behaviour of the composite under impact loading was evaluated in terms of energy-penetration and load-time history relationships. Second, multiple impacts were applied to ECC specimens up to first crack initiation and fracture of specimens. Thereafter, similar heat treated ECC specimens were tested up to failure in order to investigate the shape memory effect. Finally, cracked ECC specimens were exposed to fire then tested up to failure in order to explore the effects of high temperature on the impact resistance of ECC. Results showed that fibre-reinforced ECC specimens could sustain multiple impacts up to 700 times that of control fibreless ECC. The fibres transferred the mode of failure from brittle into ductile. In addition, the ECC mixture incorporating 2% PVA and 1% SMA fibres by volume fraction achieved the highest impact resistance compared to all other mixtures. The hybrid heat-treated specimens achieved improved impact resistance owing to the local pre-stressing effect exerted by SMA fibres, despite the damage caused by the heating to the coexisting PVA fibres. Additionally, melting of PVA fibres due to fire led to general reduction in impact resistance of the mono-fibre composite. However, the presence of SMA in the hybrid

mixtures better restrained the crack propagation and led to achieving superior impact resistance compared to that of the mono-PVA-ECC, owing to the shape memory effect. This chapter highlights the potential benefits of incorporating SMA in composite materials exposed to impact loads, paving the way for possible implementation in the field of fortified structures.

Chapter 6 presented the development, calibration, and verification of a nonlinear three-dimensional finite element model of cylindrical ECC specimens under the dynamic impact test. The concrete damaged plasticity (CDP) and Drucker/Prager (DP) models, implemented in the ABAQUS software, were used to model ECC. Variability in SMA fibre dosages and its effect on the behaviour of ECC under impact loading were investigated. The models were verified using experimental data acquired in Chapter 5. Generally, the models were capable of reasonably simulating the behaviour of ECC specimens under drop weight impact testing in terms of energy-penetration and load-time history relationships. In addition, the models showed good agreement with experimentally observed behaviour of the ECC specimens in terms of the stress distribution, crack propagation and failure criterion. Additionally, the numerical simulation results using the CDP model exhibited better accuracy and closer agreement with corresponding experimental data than that of DP model in terms of energy dissipation capability and maximum penetration depth. This chapter demonstrates the feasibility of using numerical simulation to reasonably predict the behaviour of ECC composites under dynamic loading, which can save time, effort and cost associated with expensive and time consuming laboratories tests.

7.2 RECOMMENDATIONS FOR FUTURE WORK

The current research revealed that some further studies on the HECC-SMAF material would be needed as follows:

- 1) In the present thesis, the mechanical properties of tests on small-scale HECC-SMAF specimens were carried out. Therefore, utilizing HECC-SMAF in full scale structural applications should be considered in future investigations, such as beams, columns and slabs. This would result in more reliable assessment of the behaviour of the new material.

- 2) The durability performance of the HECC-SMAF material remains unexplored. Therefore, durability issues need to be investigated experimentally. Furthermore, detailed numerical analysis and service life prediction could be developed.
- 3) Due to limitations of experimental tools, the HECC-SMAF material was tested after exposure to high temperature up to 400°C. Therefore, further investigation is still required on the effect of exposure to higher temperatures and how that would affect its overall performance.
- 4) In the present thesis, numerical modelling was limited to the drop weight impact test on HECC-SMAF cylindrical specimens. Therefore, different loading techniques with various shapes of specimens may be further explored.
- 5) The numerical modelling conducted in the present study was successfully validated with experimental data. Thus, the model could be extended to the structural level through examining the behaviour of traditional RC and HECC-SMAF panels under impact loading of high-velocity projectiles.
- 6) The available CDP and DP models in ABAQUS were designed with concrete softening behaviour for post-cracking. However, ECC has a metal-like ductile behaviour. Therefore, ABAQUS concrete models should be modified to account for the post-tensioning performance of the ECC material.
- 7) Developing an individual code to portray the specific behaviour of ECC rather than those available in the ABAQUS library is an important issue for future work because it may overcome the difficulties associated with simulating ECC.

Appendices

Appendix A: Sample calculations using inverse analysis of ECC2-1.

$$\epsilon_{tu} = (0.5 * \delta_u) - 0.22$$

$$(\delta_u) \text{ at 90 days} = 4.7 \text{ mm}$$

$$\epsilon_{tu} = (0.5 * 4.7) - 0.22$$

$$\epsilon_{tu} = 2.13 \% \quad \text{(Predicted average strain)}$$

$$PD = (0.5 * SD) + 0.18$$

For SD of 0.2:

$$PD = (0.5 * 0.2) + 0.18$$

$$PD = 0.28 \quad \text{(Predicted deviation for tensile strain capacity)}$$

$$\sigma_{tl} = \frac{MOR}{(0.09 * \ln(\epsilon_{tu}) + 2.69)}$$

$$MOR \text{ at 90 days} = 12.52 \text{ MPa}$$

$$\sigma_{tl} = \frac{12.52}{(0.09 * \ln(\epsilon_{tu}) + 2.69)}$$

$$\sigma_{tl} = 4.57 \text{ MPa} \quad \text{(Predicted lower limit of effective tensile strength)}$$

$$\sigma_{tu} = \frac{MOR}{(0.14 * \ln(\epsilon_{tu}) + 2.42)}$$

$$\sigma_{tu} = \frac{12.52}{(0.14 * \ln(2.13) + 2.42)}$$

$$\sigma_{tu} = 5.019 \text{ MPa} \quad \text{(Predicted upper limit of effective tensile strength)}$$

Appendix B: Sample calculations using ANOVA of ECC2-1.5.

For $a = 4$ and $n = 3$

$$\sum_{i=1}^a \sum_{j=1}^n y_{ij}^2 = 18753.49$$

For a total number of specimens $N = 12$ and $y_n = 473.9$

$$SS_T = [\sum_{i=1}^a \sum_{j=1}^n y_{ij}^2] - [\frac{y_n^2}{N}]$$

$$SS_T = [18753.49] - [\frac{473.9^2}{12}]$$

$$SS_T = 38.39 \quad \text{(Total corrected sum of squares)}$$

For $y_i^2 = 56209$

$$[\frac{1}{n} \sum_{i=1}^a y_i^2] = \frac{1}{3} * y_i^2 = 18736.3$$

$$SS_{Treatments} = [\frac{1}{n} \sum_{i=1}^a y_i^2] - [\frac{y_n^2}{N}]$$

$$SS_{Treatments} = [18736.3] - [\frac{473.9^2}{12}]$$

$$SS_{Treatments} = 21.23 \quad \text{(Sum of squares due to using different SMA fibre reinforcement ratios)}$$

$$SS_E = SS_T - SS_{Treatments}$$

$$SS_E = 38.39 - 21.23 = 17.16 \quad \text{(Sum of squares due to error)}$$

$$MS_{Treatments} = \frac{SS_{Treatments}}{a-1}$$

$$MS_{Treatments} = \frac{21.23}{4-1}$$

$$MS_{Treatments} = 7.076 \quad (\text{Mean square due to treatments})$$

$$MS_E = \frac{SS_E}{N-a}$$

$$MS_E = \frac{17.16}{12-4}$$

$$MS_E = 2.145 \quad (\text{Mean square due to error})$$

$$F_o = \frac{MS_{Treatments}}{MS_E}$$

$$F_o = \frac{7.076}{2.145}$$

$$F_o = 3.299$$

Appendix C: Sample calculations of fibre dispersion of ECC2-0.5.

r	Ar	density	Number of fibres	Total number of fibres	Total number of fibres ²
0	2100	0.010957	0	21	441
5	2100	0.010957	26	21	441
10	2100	0.010957	59	21	441
15	2100	0.010957	122	21	441
20	2100	0.010957	163	21	441

Number of grid points	Total number of grid points	π	Percent of fibre free area
0	78	3.141593	100
36	78	3.141593	53.84615
67	78	3.141593	14.10256
78	78	3.141593	0
78	78	3.141593	0

K	K random	1-F	F	1-F random	F random
0	0	1	0	1	0
123.8095	78.53982	0.538462	0.461538	0.422925	0.577075
280.9524	314.1593	0.141026	0.858974	0.131993	0.868007
580.9524	706.8583	0	1	0.000433	0.999567
776.1905	1256.637	0	1	1.05E-06	1

Appendix D: Sample calculations of Weibull distribution of ECC2-0.

$$L_N = 1 - \frac{i-0.3}{k+0.4}$$

For $i = 1$ and $k = 3$

$$L_N = 1 - \frac{1-0.3}{3+0.4}$$

$$L_N = 0.794$$

$$\ln \left[\ln \left(\frac{1}{L_N} \right) \right] = \alpha \ln(n) - \alpha \ln(u)$$

$$\ln \left[\ln \left(\frac{1}{0.794} \right) \right] = -1.467$$

For a reliability of 0.794 at fracture:

$$u = 809.78$$

$$\alpha = 24.146$$

$$\ln \left[\ln \left(\frac{1}{L_N} \right) \right] = \alpha \ln(n) - \alpha \ln(u)$$

$$\ln \left[\ln \left(\frac{1}{0.794} \right) \right] = 24.146 * \ln(n) - 24.146 * \ln(809.78)$$

Then $n = 762.05$ J

(impact fracture energy)

Curriculum Vitae

Name: Mohamed Ali

Education

Ph.D. in Structural Engineering (2014 - 2017)

Western University, London, ON, Canada

Master of Structural Engineering (2007 - 2010)

Military Technical College, Cairo, Egypt

B. Sc. in Civil Engineering (1998 - 2003)

Military Technical College, Cairo, Egypt

Relevant Work Experience

Research & Teaching Assistant (2014- 2017)

Western University, London, ON

Structural Engineer (2011-2013)

Ministry of Defense, Cairo, Egypt

Research & Teaching Assistant (2007- 2010)

Military Technical College, Cairo, Egypt

Structural Engineer-in-Training (2004-2008)

Aggour Consultant Engineering, Cairo, Egypt

Publications

M.A.E.M. Ali, A.M. Soliman, and M.L. Nehdi, “Hybrid-Fiber Reinforced Engineered Cementitious Composite under Tensile and Impact Loading.” *Materials and Design*, 117, 2017, pp. 139-149.

M.A.E.M. Ali and M.L. Nehdi, “Innovative Crack-Healing Hybrid Fiber Reinforced Engineered Cementitious Composite.” *Construction and Building Materials*, 150, 2017, 689-702.

M.A.E.M. Ali and M.L. Nehdi, “Exploring Synergy of Engineered Cementitious Composites and Shape Memory Alloys in Creating Resilient Civil Infrastructure.” *Magazine of Concrete Research*, accepted.

M.A.E.M. Ali and M.L. Nehdi, “Tensile and Flexural Behavior of Hybrid Fiber Reinforced Engineered Cementitious Composite with Strain Recovery.” *Composites Part B*, submitted.

M.A.E.M. Ali and M.L. Nehdi, “Experimental and Numerical Investigation on Novel SMA-PVA Hybrid Fiber Reinforced Engineered Cementitious Composite under Impact Loading.” *Cement and Concrete Composites*, submitted.

M.A.E.M. Ali and M.L. Nehdi, “Experimental Investigation on Mechanical Properties of Shape Memory Alloy Fibre-Reinforced ECC Composite.” *Proceedings of the 11th International Conference on Civil and Architecture Engineering*, Cairo, Egypt, 19-21 April, 2016, 11 p.

M.A.E.M. Ali, A.M. Soliman, and M.L. Nehdi, “Behaviour of Hybrid Fibre-Reinforced ECC Composite Incorporating SMA Short Fibres under Effect of Impact Load.” *Proceedings of the 11th International Conference on Civil and Architecture Engineering*, Cairo, Egypt, 19-21 April, 2016, 11 p.

M.A.E.M. Ali and M.L. Nehdi, “Mechanical Performance of Hybrid Fibre-Reinforced Engineered Cementitious Composite Incorporating NiTi-SMA Short Fibres.” *Resilient*

Infrastructure, Proceedings of the 5th International Conference of the Canadian Society for Civil Engineering, London, ON, Canada, 1-4 June, 2016, 8 p.

M.A.E.M. Ali, A.M. Soliman, and M.L. Nehdi, “Impact Behaviour of Shape Memory Alloy Hybrid Fibre-Reinforced Engineered Cementitious Composite.” *Resilient Infrastructure, Proceedings of the 5th International Conference of the Canadian Society for Civil Engineering*, London, ON, Canada, 1-4 June, 2016, 8 p.

M.A.E.M. Ali and M.L. Nehdi, “Effect of Fire Exposure on Impact Resistance of Hybrid Fiber-Reinforced Engineered Cementitious Composites.” *Resilient Infrastructure, Proceedings of the 6th International Conference of the Canadian Society for Civil Engineering*, Vancouver, BC, Canada, 31 May-3 June, 2017, 7 p.